magnetochemistry

MDPI

Review

Lanthanoid-Anilato Complexes and Lattices †

Samia Benmansour * and Carlos J. Gómez-García *

ICMol, Departamento de Química Inorgánica, Universidad de Valencia, C/Catedrático José Beltrán 2, 46980 Paterna, Spain

* Correspondence: sam.ben@uv.es (S.B.); carlos.gomez@uv.es (C.J.G.-G.); Tel.: +34-963544423 (S.B. & C.J.G.-G.); Fax: +34-963543273 (S.B. & C.J.G.-G.)

† In memory of Prof. Roger du Wayne Willett, an enthusiastic (magneto)chemist and a very good friend.

Received: 12 November 2020; Accepted: 10 December 2020; Published: 15 December 2020

Abstract: In this review, we describe all the structurally characterized complexes containing lanthanoids (Ln, including La and group 3 metals: Y and Lu) and any anilato-type ligand (3,6-disubstituted-2,5-dihydroxy-1,4-benzoquinone dianion = $C_6O_4X_2^{2-}$). We present all the anilato-Ln compounds including those where, besides the anilato-type ligand, there is one or more coligands or solvent molecules coordinated to the lanthanoid ions. We show the different structural types observed in these compounds: from discrete monomers, dimers and tetramers to extended 1D, 2D and 3D lattices with different topologies. We also revise the magnetic properties of these Ln-anilato compounds, including single-molecule magnet (SMM) and single-ion magnet (SIM) behaviours. Finally, we show the luminescent and electrochemical properties of some of them, their gas/solvent adsorption/absorption and exchange capacity and the attempts to prepare them as thin films.

Keywords: lanthanoid; anilato; X-ray structure; magnetic properties; luminescence; single-ion magnet; single-molecule magnet; solvent exchange

1. Introduction

The field of coordination polymers (CPs) and metal organic frameworks (MOFs) with lanthanoids (Ln) is gaining interest in this decade since they may show gas and solvent exchange and adsorption/absorption and present interesting magnetic and luminescent properties and can, therefore, be used to prepare optical and magnetic sensors of gases, contaminants and different chemical species [1–3].

Among the many different ligands that can be used to construct these CPs and MOFs, anilato-type ligands (3,6-disubstituted-2,5-dihydroxy-1,4-benzoquinone dianion = $C_6O_4X_2^{2-}$, Scheme 1a) are becoming very popular since these ligands present some interesting properties: (i) They show different coordination modes as: monodentate (*1kO*), bidentate ($1k^2O,O'$), bis-bidentate ($1k^2O,O';2k^2O'',O'''$), monodentate-bidentate ($1kO;2k^2O',O''$) or even more complex coordination modes such as ($1k^2O,O';2k^2O'',O''';3kO''$) (Scheme 1c–f) [4,5]. (ii) They can act as linear bridges connecting two metal atoms (Scheme 1a) to generate many different coordination polymers [4]. (iii) They couple (antiferro)magnetically the metal centers when they are transition metal ions and the coupling can be modulated by changing X [6]. (iv) They provide a good magnetic isolation when bridging lanthanoids (as a result of the negligible overlap with the 4f orbitals), giving rise to single-molecule and single-ion magnet behaviours (SMM and SIM). (v) They can be reduced by one or two electrons to their semiquinone and cathecolate forms (Scheme 1b), resulting in an increase in the magnetic coupling and ordering temperatures [7]. (vi) They are topologically equivalent to the well-known oxalato ligand ($C_2O_4^{2-}$) and they are able to form similar monomeric complexes [8,9] as well as extended 1D, 2D and 3D lattices although with much larger cavities and channels [4,5,10,11].

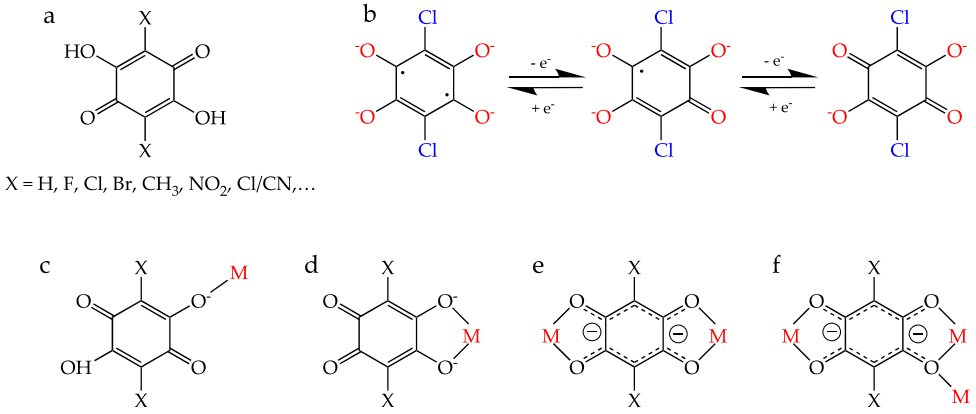

Scheme 1. (**a**) The 3,6-disubstituted anilato derivatives ($H_2C_6O_4X_2$). (**b**) Reduced forms of the chloranilato ligand (right): semiquinone (center) and cathecolate (left). (**c**–**f**) Different coordination modes of the anilato ligands. (**c**) monodentate (*1kO*), (**d**) bidentate ($1k^2O,O'$), (**e**) bis-bidentate ($1k^2O,O';2k^2O'',O'''$) and **(f)** bis-bidentate-monodentate ($1k^2O,O';2k^2O'',O''';3kO''$).

Although anilato and its derivatives (Scheme 1a) have been combined with transition metals since the 1950s [12], the use of lanthanoids with anilato ligands was not developed until the 21st century. Surprisingly, there are only three reports in the 20th century. The first one, published in 1983 by Raymon et al. [13] describes a compound with Pr(III) and chloranilate (X = Cl). The second one, published in 1987 by Robl et al. [14] presents a couple of Y(III) compounds with chloranilate and bromanilate (X = Br). The third report was published in 1996 by Robson, Abrahams et al. [15] and contains a Ce(III) compound with $dhbq^{2-}$ (X = H).

The first complete and systematic study was performed by Robson, Abrahams et al. in 2002 [16]. In this seminal article, the authors prepared and structurally characterized a total of 19 Ln-anilato compounds (and one with Sc) using $dhbq^{2-}$ (X = H) and chloranilato (X = Cl). Since then, almost 150 Ln-anilato compounds have been prepared, as we will show in this review.

The structures and properties of homometallic coordination polymers prepared with anilato ligands and transition metals (and even p- and s-block metals) were revised in a very complete study in 2002 by Kitagawa and Kawata [4]. More recently, in 2017, Mercuri et al. [17] performed a complete revision, focusing on the magnetic and conducting properties, of homo- and heterometallic complexes and coordination polymers with anilato and transition metals. Finally, we have very recently revised the heterometallic anilato-based 2D and 3D lattices with transition metals [18].

Surprisingly, as far as we know, no revision of the almost 150 prepared lanthanoid-anilato compounds has been published to date. Therefore, here we revise all the structurally characterized Ln-anilato compounds. We will show the different anilato-type ligands used (Scheme 1a) and their magnetic and luminescent properties. We will also show the gas and solvent adsorption/absorption and the solvent exchange capacity of some of them as well as the attempts to reduce the anilato bridge in some dimers. Finally, we will show the delamination of some of the layered lattices into thin films with promising properties.

This review is organized into seven different sections: In Section 1, we introduce the anilato-type ligands and their properties as well as their capacity to coordinate in a bis-bidentate way and to act as bridges connecting lanthanoid ions in coordination complexes and polymers. In Section 2, we will show and describe all the reported structures: (i) discrete monomers, dimers and tetramers; (ii) zigzag and ladder-type chains; (iii) hexagonal, rectangular and square layers; and (iv) 3D structures. In Section 3, we will show the magnetic properties of some of these compounds, focusing on their (in most cases, field-induced) single-molecule magnet (SMM) and single-ion magnet (SIM) behaviours. In Section 4, we will show their optical properties, including luminescence in the visible and NIR regions. In Section 5, we will show the porosity, gas and solvent adsorption/absorption and solvent exchange capacity of some of the layered Ln-anilato materials. In Section 6, we will show their redox

properties and, finally, in Section 7, we will show how it is possible to easily delaminate some of the layered compounds to prepare thin films with nanometric thickness.

In order to classify all the reported Ln-anilato-based compounds, we will present them in different tables grouped by type of structure and dimensionality (Tables 1 to 7), by anilato derivative ligand (Tables 8 to 12) and by Ln(III) ion (Tables 13 to 27). We hope that these tables will help in finding any compound and all those with the same Ln(III) ion, the same ligand, or the same (or related) structure.

2. Structural Classification

2.1. Discrete (0D) Complexes

As can be seen in Table 1, there are 33 reported discrete complexes containing lanthanoids and anilato ligands. There are thirty dimers (**2**-**31**), two monomers (**1** and **33**) and one tetramer (**32**). The only two reported monomers are: $[Lu(C_6O_4Cl_2)(H_2O)_4][Lu(C_6O_4Cl_2)_2(H_2O)_4]\cdot\approx 4H_2O$ (**33**) [16] and $[Co(Cp)_2][Dy(Tp)_2(C_6O_4Cl_2)]$ (**1**) (Tp^- = hydrotris(pyrazolyl)borate = $HB(pz)_3$) [19]. Compound **1** is an anionic Dy(III) complex with a terminal bidentate chloranilate and two tridentate Tp^- ligands (Figure 1a) with $[Co(Cp)_2]^+$ as counter-cations, whereas compound **33** contains the anionic $[Lu(C_6O_4Cl_2)_2(H_2O)_4]^-$ monomer with two terminal chloranilato ligands (Figure 1b). The counter cation of this monomeric anion is a cationic chain that will be described below. Although there are many known dimers, there is only one reported tetramer: $[[(Tp)(MeOH)Y)_2(\mu\text{-}B(OMe)_4)]_2(\mu\text{-}C_6O_4(CH_3)_2)_2]Cl_2$ (**32**) [20]. This compound is a Y(III) square complex with two bis-bidentante bridging methyl-anilato ligands (X = CH_3) forming two parallel sides and two $B(OMe)_4$ units forming the two other sides. The coordination sphere of the Y(III) ions is completed with one Tp^- ligand and one MeOH molecule (Figure 1c).

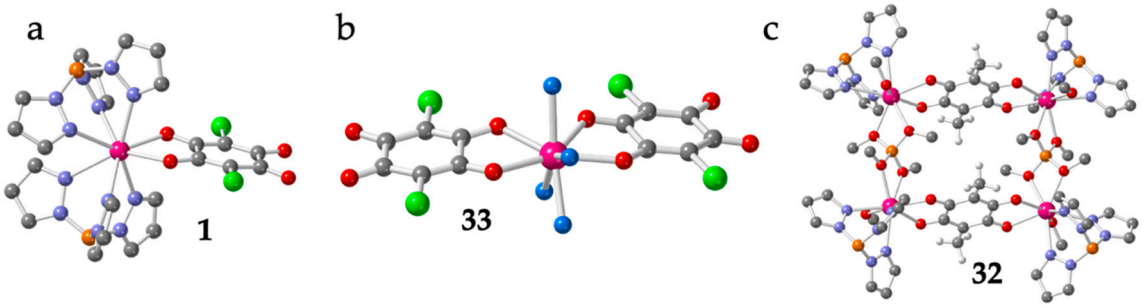

Figure 1. Structure of the only two known Ln-anilato monomers: **1** (**a**) and **33** (**b**). Structure of the unique reported Ln-anilato tetramer, **32** (**c**). Colour code: Ln = pink, Cl = green, C = grey, O = red, B = orange, N = blue and H = white. H atoms are omitted for clarity (except in the CH_3 groups in (**c**)).

Compounds $[Ln_2(C_6O_4H_2)(thf)_6Cl_4]$ with Ln = Dy (**2**) and Y (**3**) [21] constitute two unusual dimers. They are isostructural and contain a bis-bidentate bridging $dhbq^{2-}$ ligand (X = H) connecting the two Ln(III) ions. Each Ln ion completes its unusual pentagonal bipyramidal coordination geometry with two Cl and three thf coligands (Figure 2a).

Dimers $[(LnTp)_2(C_6O_4X_2)]\cdot G$ with Ln/X/G = Dy/Cl/$2CH_2Cl_2$ (**4**-**6**), Y/Cl/$2CH_2Cl_2$ (**7**-**8**), Y/Cl/$2Me_2CO$ (**9**), Y/H/- (**10**), Y/CH_3/$1.2CH_2Cl_2$ (**11**) and Y/CH_3/4.5MeOH (**12**) [19,20,22] are isostructural and contain a bridging anilato ligand (with X = H, Cl, or CH_3) connecting two Y(III) or Dy(III) ions. The octacoordination of the Ln(III) ions (with TDD-8 or SAPR-8 geometries, Table 1) is completed by two tridentate Tp^- ligands in all cases (Figure 2b). Dimers $[(LnTp)_2(C_6O_4X_2)]\cdot G$ with Ln/X/G = Dy/Br/$2CH_2Cl_2$ (**18**), Dy/F/H_2O (**19**), Y/F/H_2O (**20**) and Y/Br/$2CH_2Cl_2$ (**21**) [23] and $[(LnTp)_2(C_6O_4Cl_2)]\cdot 2CH_2Cl_2$ with Ln = Er (**22**), Ho (**23**), Tb (**24**-**25**), Gd (**26**-**27**) and Y (**28**-**29**) [19,22,24,25] are very similar to dimers **4**-**12**. They also contain a bis-bidentate anilate bridging ligand (chloranilato in all of them) connecting the two Ln(III) ions and Tp^- as capping ligands (Figure 2b) and they all show a TDD-8 coordination geometry (Table 1).

Table 1. Discrete (**1**-**33**) and 1D (**33** and **34**) Ln-anilato complexes.

#	CCDC	Structure	Ln	X	Geometry [a]	L [b]	Disposition	Reference
1	PIQFUT	Monomer	Dy	Cl	SAPR-8	Tp^-	*33*	[19]
2	DEHQUF	Dimer	Dy	H	PBPY-7	thf/Cl^-	*030/101*	[21]
3	DEHRAM	Dimer	Y	H	PBPY-7	thf/Cl^-	*030/101*	[21]
4	DEKTOF	Dimer	Dy	Cl	TDD-8	Tp^-		[20]
5	DEKTOF01	Dimer	Dy	Cl	TDD-8	Tp^-		[22]
6	DEKTOF02	Dimer	Dy	Cl	TDD-8	Tp^-		[19]
7	DEKTUL	Dimer	Y	Cl	TDD-8	Tp^-		[20]
8	DEKTUL01	Dimer	Y	Cl	TDD-8	Tp^-		[22]
9	DEKVAT	Dimer	Y	Cl	TDD-8	Tp^-		[20]
10	DEKVEX	Dimer	Y	H	SAPR-8	Tp^-		[20]
11	DEKVIB	Dimer	Y	CH_3	SAPR-8	Tp^-		[20]
12	DEKVOH	Dimer	Y	CH_3	TDD-8	Tp^-		[20]
13	EDEZAR	Dimer	Gd	NO_2	CSAPR-9	H_2O	*032*	[26]
14	EDEZEV	Dimer	Tb	NO_2	CSAPR-9	H_2O	*032*	[26]
15	EDEZIZ	Dimer	Dy	NO_2	CSAPR-9	H_2O	*032*	[26]
16	EDEZOF	Dimer	Ho	NO_2	CSAPR-9	H_2O	*032*	[26]
17	EDEZUL	Dimer	Sm	NO_2	CSAPR-9	H_2O	*032*	[26]
18	JOQSEQ	Dimer	Dy	Br	TDD-8	Tp^-		[23]
19	JOQSIU	Dimer	Dy	F	SAPR-8	Tp^-	*33*	[23]
20	JOQSOA	Dimer	Y	F	SAPR-8	Tp^-	*33*	[23]
21	JOQSUG	Dimer	Y	Br	TDD-8	Tp^-		[23]
22	KOZBEJ	Dimer	Er	Cl	TDD-8	Tp^-		[24]
23	KOZBIN	Dimer	Ho	Cl	TDD-8	Tp^-		[24]
24	LEPNIG	Dimer	Tb	Cl	TDD-8	Tp^-		[22]
25	LEPNIG01	Dimer	Tb	Cl	TDD-8	Tp^-		[24]
26	LEPNOM	Dimer	Gd	Cl	TDD-8	Tp^-		[22]
27	LEPNOM01	Dimer	Gd	Cl	TDD-8	Tp^-		[19]
28	OBIBEH	Dimer	Yb	Cl	TDD-8	Tp^-		[25]
29	OBIBEH01	Dimer	Yb	Cl	TDD-8	Tp^-		[24]
30	NOQBUT	Dimer-zz	Eu	Cl/CN	CSAPR-9	H_2O	*032*	[27]
31	NOQGEI	Dimer-zz	Eu/Dy [c]	Cl/CN	CSAPR-9	H_2O	*032*	[27]
32	DEKVUN	Tetramer	Y	CH_3	TDD-8	Tp^-/$(MeO)_4B$/MeOH		[20]
33	MIZZUQ	1D + mon	Lu	Cl	TDD-8	H_2O		[16]
34	NIGNID	1D-ladder	Er1/Er2	Cl	BTPR-8/BTPR-8	hmpa		[28]

([a]) The geometry was determined with the program SHAPE [29–36]. SAPR-8 = square antiprism, PBPY-7 = pentagonal bipyramid, TDD-8 = triangular dodecahedron, CSAPR-9 = capped square antiprism, BTPR-8 = biaugmented trigonal prism; ([b]) Tp^- = $HB(pz)_3^-$ = hydrotris(pyrazolyl)borate, thf = tetrahydrofurane, dmso = dimethyl sulfoxide, hmpa = hexamethylphosphoramide; ([c]) Eu (98%)/Dy (2%).

In contrast, dimers $[Ln_2(C_6O_4(NO_2))_3(H_2O)_{10}]\cdot 6H_2O$ with Ln = Gd (**13**), Tb (**14**), Dy (**15**), Ho (**16**) and Sm (**17**) [26] and $[Ln_2(C_6O_4(CN)Cl)_3(H_2O)_{10}]\cdot 6H_2O$ with Ln = Eu (**30**) and $Eu_{0.98}/Dy_{0.02}$ (**31**) [27] contain three anilato ligands: a bridging bis-bidentante one (as observed in all the other dimers) and a terminal bidentate one on each Ln center (in contrast with the previously described dimers). The remaining five coordination positions are occupied by water molecules. The coordination geometry is CSAPR-9 in all cases (Table 1). In dimers **13**-**17**, the two Ln(III) ions and the centers of the three anilato ligands are aligned, resulting in "linear dimers" (Figure 2c), whereas in dimers **30** and **31**, the center of the terminal anilato ligands is not aligned with the Ln···Ln axis, resulting in "zigzag dimers" (Figure 2d).

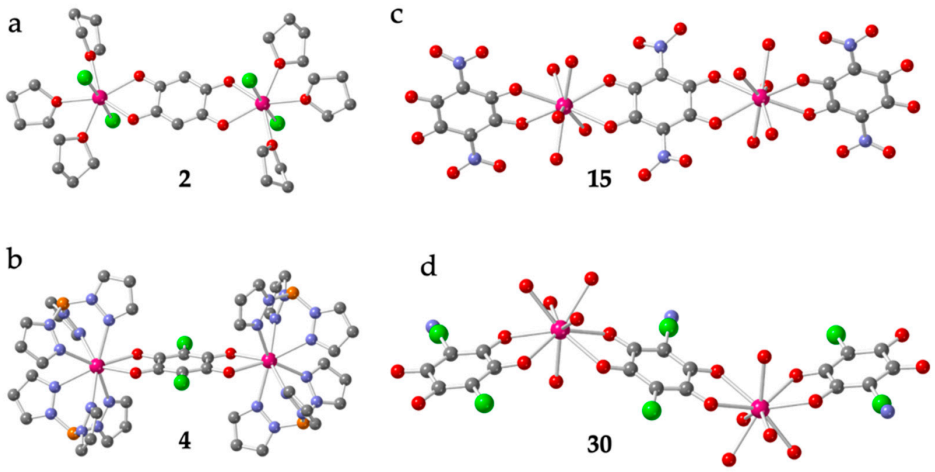

Figure 2. Structures of dimers **2** (**a**), **4** (**b**), **15** (**c**) and **30** (**d**) representative of the four types of Ln-anilato dimers. Colour code: Ln = pink, Cl = green, C = grey, O = red, B = orange and N = blue. (in **30,** there is a positional disorder between the Cl and CN groups in the anilato ring).

2.2. One Dimensional (1D) Lattices

Table 1 also shows the only two known 1D polymers containing Ln and anilato-type ligands: $[Lu(C_6O_4Cl_2)(H_2O)_4][Lu(C_6O_4Cl_2)_2(H_2O)_4]\cdot\approx 4H_2O$ (**33**) [16] and $[Er_2(C_6O_4Cl_2)_3(hmpa)(H_2O)_3]\cdot H_2O$ (**34**) (hmpa = hexamethylphosphoramide) [28]. The chains present in compound **33** are regular cationic zigzag chains formulated as $[Lu(C_6O_4Cl_2)(H_2O)_4]^+$ formed by bis-bidentate bridging chloranilato ligands connecting Lu(III) ions (Figure 3a). These chains are similar to those observed with transition metals [4] although now, the Lu(III) ions have four extra coordinated water molecules, in contrast with the transition metals, that only have two. Interestingly, the counter-anions of these cationic chains are also unique since they are the anionic monomers $[Lu(C_6O_4Cl_2)_2(H_2O)_4]^-$ described above (Figure 1b). Although the full crystal structure was not reported, Robson et al. also prepared the Yb(III) derivative of compound **33** [16].

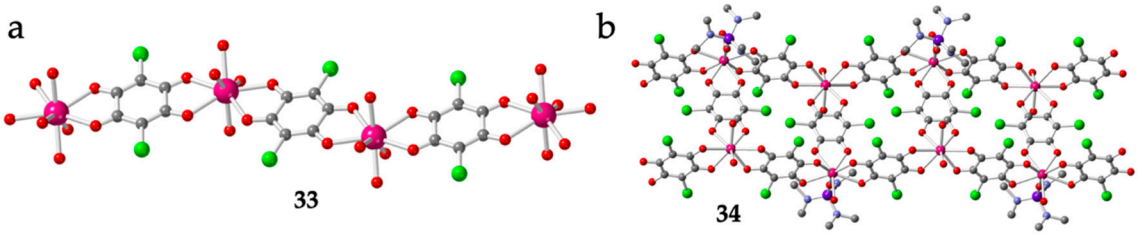

Figure 3. (**a**) View of the anionic zigzag chain in **33**. (**b**) Structure of the zigzag ladder type chain in **34**. Colour code: Ln = pink, Cl = green, C = grey, O = red, P = purple and N = blue. H atoms are omitted for clarity.

The other chain compound, $[Er_2(C_6O_4Cl_2)_3(hmpa)(H_2O)_3]\cdot H_2O$ (**34**), is an example of the important role played by the size and shape of the coordinating solvents (L) in determining the final structure and the dimensionality [28]. In this compound, the presence of a very bulky coordinating solvent (hexamethylphosphoramide) precludes the growth of the coordination polymer in two or three dimensions, in contrast with the observed behaviour in other related polymers with smaller coordinating solvent molecules (see below). Compound **33**, the only known example of Ln-anilato compound with a ladder chain structure, presents a (3,4) topology where both the side rail and the rungs are formed by bridging bis-bidentate chloranilato ligands (Figure 3b). There are two unique Er(III) ions, both with an unusual biaugmented trigonal prism geometry (BTPR-8) due to the steric hindrance of the bulky coordinated hexamethylphosphoramide molecule [28].

2.3. Two-Dimensional (2D) Lattices

Two-dimensional lattices are, by far, the most common ones in the Ln-anilato family of compounds, with more than one hundred known examples (Tables 2 to 6). In order to rationalize these 2D lattices, we have classified them according to their topology and shape of the rings forming the layers. As can be seen in Tables 2 to 6, the most recurrent ones are the hexagonal 3,6-gon and square 4,4-gon topologies.

The 3,6-gon topology is, by far, the most abundant one, with more than 90 reported examples (Tables 2 to 5). In this topology, each Ln(III) is connected to three other Ln(III) ions through anilato bridges giving rise to regular (Figure 4a and Table 2) or distorted (Figure 4b and Table 3) hexagonal rings with the typical honey comb hexagonal structure. In some of these lattices the hexagons are so distorted that they look like rectangles (with two Ln-Ln-Ln angles close to 180°). These rectangular six-membered rings may adopt a brick-wall structure (Figure 4c and Table 4) or a herringbone one (Figure 4d and Table 5).

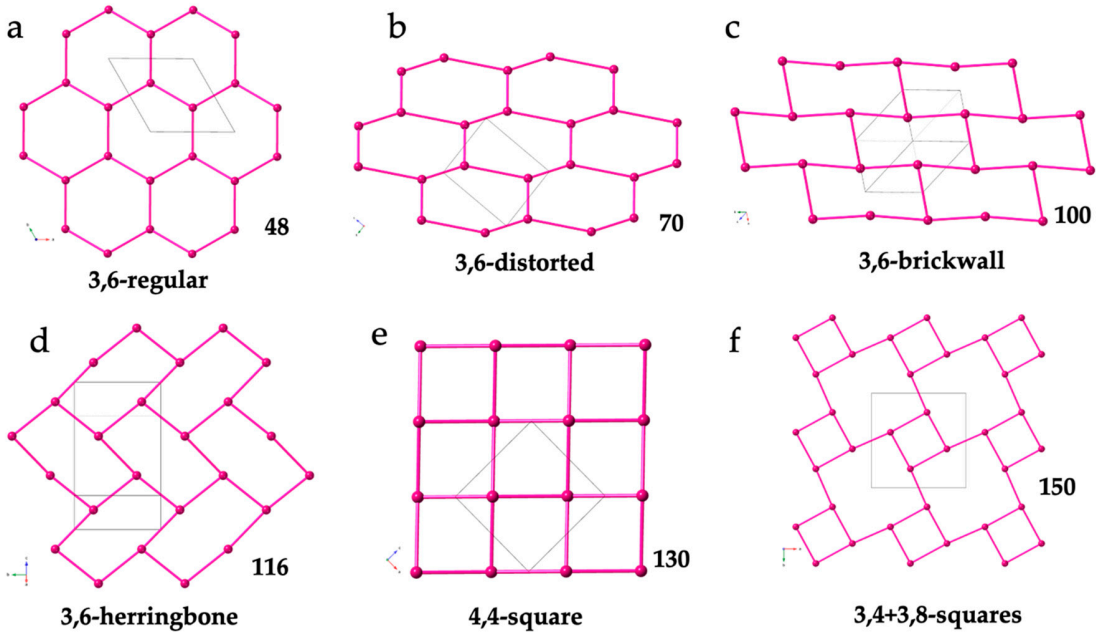

Figure 4. Schematic views of the different 2D lattices found in Ln-anilato compounds: (**a**) View of the (3,6) lattice with regular hexagons in **48**. (**b**) View of the (3,6) lattice with distorted hexagons in **70**. (**c**) View of the (3,6) lattice with rectangular rings in a brick-wall structure in **100**. (**d**) View of the (3,6) lattice with rectangular rings in a herringbone structure in **116**. (**e**) View of the (4,4) lattice in **130**. (**f**) View of the (3,4)+(3,8) lattice in **150**. Only the Ln(III) ions are displayed for clarity. The pink bonds represent the anilato bridges.

The 4,4-gon topology (Figure 4e) is observed in a total of twenty compounds (**130-149**, Table 6). In these 2D lattices, each Ln(III) is connected to four Ln(III) ions by anilato bridges giving rise to square rings that form a chessboard square structure.

Only three compounds show different 2D lattices: $[La_2(C_6O_4Cl_2)_3(H_2O)_6]\cdot\approx 7H_2O$ (**129**) [16], that shows a 3,4 topology (see below) and $[Ln_2(C_6O_4ClCN)_3(dmso)_6]\cdot nH_2O$ with Ln/n = Er/0 (**150**) and Dy/7 (**151**), that show a (3,4)+(3,8) topology (Figure 4f and Table 6) [37,38].

As observed by Robson, Abrahams et al. in their seminal work in 2002 [16], the distortions of the hexagonal rings are due to the differences in the spatial orientations of the anilato ligands around the Ln(III) ions, which, in turn, depend on the coordination geometry and on the position occupied of the two or three coordinated solvent molecules (L). As we will see below, the size of the Ln(III) ion and the size and shape of the coordinated solvent molecules also play a key role in the final structure. The different orientations result in different angles between the anilato rings and the average plane

of the layer. Thus, in the regular hexagons, the anilato rings appear tilted ca. 45° with respect to the layer (Figure 5a), whereas in the distorted hexagons, there are two possible dispositions: four anilato with their rings almost parallel to the layer (*face-on, FO*) and two rings almost perpendicular to it (*edge-on, EO*) (Figure 5b) or the opposite (i.e., 2 *FO* + 4 *EO*, Figure 5c). In the rectangular layers, there are two *FO* and four *EO* ones (Figure 5d). As can be seen in Figure 5, the diagonals of the regular hexagons are around 16.6 Å, whereas in the distorted hexagons, the diagonals are of ca. 15, 17 and 19 Å (depending on the distortions). Finally, the rectangular rings show two large distances (of ca. 18–20 Å) and a much shorter one (of ca. 7 Å).

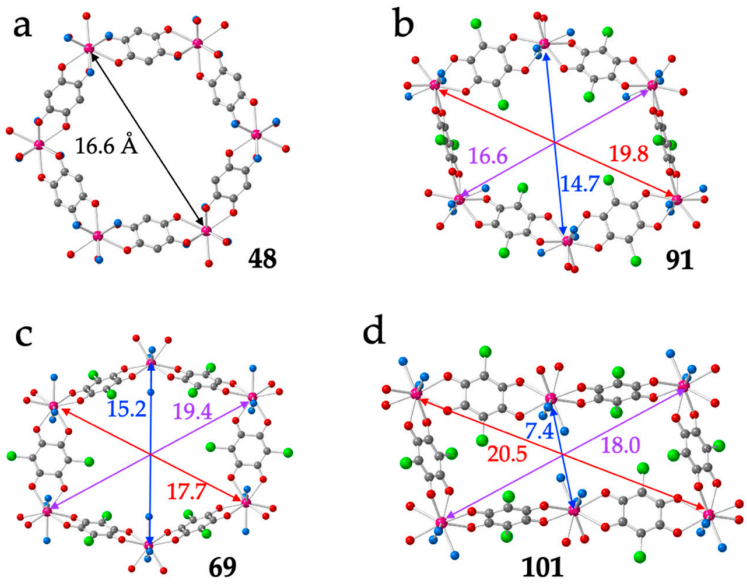

Figure 5. (**a**) Regular hexagonal ring in compound **48** showing the orientation of the anilato rings with respect to the mean plane of the ring. (**b**) Distorted hexagonal ring in compound **91** showing four *face-on* (*FO*) and two *edge-on* (*EO*) anilato rings. (**c**) Distorted hexagonal ring in compound **69** showing the two *FO* and four *EO* anilato rings. (**d**) Rectangular ring in compound **101** showing the two *FO* and four *EO* anilato rings. The distances corresponding to the different diagonals are in Å. Colour code: Ln = pink, C = grey, Cl = green, $O_{anilato}$ = red and $O_{solvent}$ = blue.

Two important aspects of these 2D lattice are: (i) the planarity (or lack of planarity) of the four-, six-, or eight-membered rings and (ii) the relative disposition of two consecutive layers along the direction perpendicular to the layers (eclipsed or alternated). The eclipsed disposition implies the formation of channels (hexagonal or rectangular) that may contain crystallization solvent molecules that might be removed and/or exchanged, as we will show below.

2.3.1. Two-Dimensional Regular Hexagonal Lattices

The most common 2D structural type is the hexagonal honey comb lattice (Table 2 and Figure 4a), where each Ln(III) ion is connected to three other through bis-bidentate anilato bridges, also observed with transition metals [39,40]. The main difference is that due to their higher ionic radii, the coordination numbers of the Ln(III) ions are higher (usually eight or nine) and there are two or three coordination positions occupied by other ligands (L). These additional coligands are, in most cases, H_2O or a solvent with a high capacity to coordinate Ln(III) ions such as dimethyl sulfoxide (dmso), dimethylformamide (dmf), or dimethylacetamide (dma) [41,42]. The most important consequences of this increase in the coordination number are (i) the lack of planarity of the hexagonal rings (and, therefore, of the honey comb layers) and/or (ii) the presence of distortions in the hexagonal rings.

The lack of planarity was observed in the series of compounds reported by Robson, Abrahams et al. with $dhbq^{2-}$ (X = H) formulated as $[Ln_2(dhbq)_3(H_2O)_6]\cdot 18H_2O$ with Ln(III) = La (**36**), Gd (**37**),

Yb (**38**), Lu (**39**), Y (**40**) and Ce (**42**) [15,16], later enlarged by Ohkoshi et al. with Ho(III) (**35**) [43], by Chainok et al. with Er (**41**) [44] and recently completed by us [45] with Pr (**43**), Nd (**44**), Sm (**45**), Eu (**46**), Tb (**47**), Dy (**48**) and Tm (**49**) (Table 2). In this series of isostructural compounds, the hexagons are very regular but they are not planar. They show three equal Ln···Ln distances of ca. 16.6 Å along the diagonals of the hexagons (Figure 5a) and show a chair conformation (Figure 6a) with Ln-Ln-Ln angles (°) close to those of a tetrahedron (Table 2).

As noted by Robson et al. [16], this lack of planarity is due to the coordination of three water molecules that occupy one triangular face of the tricapped trigonal prismatic (TCTPR-9) coordination geometry of the Ln(III) ions (Figure 6b). We call this distribution as *300* in Table 2 to indicate that there are three solvent molecules on the upper triangular face of the trigonal prism (*3*–) and no solvent molecules on the central (*-0-*) nor lower (*–0*) positions (of course, the *300* disposition is equivalent to the *003* one since the trigonal prism can be upside down). Each of the three $dhbq^{2-}$ ligands occupies a central capping position (*-1-*) and one vertex of the lower triangular face (*–1*) (therefore, each anilato is coordinated at the *011* positions). This disposition results in a propeller-like orientation of the anilato ligands, giving rise to corrugated hexagonal layers (Figure 6c). These layers are packed in an alternated way, preventing the formation of hexagonal channels perpendicular to the layer. Interestingly, the water molecules in this layered structure form a $Ln_2(H_2O)_{18}$ cage with six coordinated water molecules and twelve crystallization ones (Figure 6d). These cages connect two nonconsecutive layers and cross the hexagonal hole of the layer in between them. As we will show below, the 12 crystallization water molecules can be easily removed in a reversible way and even exchanged with other different solvents such as MeOH, EtOH, dmf, HCOOH and CH_3COOH.

Table 2. Ln-anilato compounds with regular hexagonal 2D structures.

#	CCDC	Ln	X	Geometry [a]	L [b]	Disposition	α (°) [c]	Pk [d]	Reference
35	KUYKIZ	Ho	H	TCTPR-9	H_2O	*300*	107.7	AL	[43]
36	MIZXAU	La	H	TCTPR-9	H_2O	*300*	107.2	AL	[16]
37	MIZXEY	Gd	H	TCTPR-9	H_2O	*300*	107.6	AL	[16]
38	MIZXIC	Yb	H	TCTPR-9	H_2O	*300*	107.8	AL	[16]
39	MIZXOI	Lu	H	TCTPR-9	H_2O	*300*	107.7	AL	[16]
40	MIZXUO	Y	H	TCTPR-9	H_2O	*300*	107.7	AL	[16]
41	PIVKAJ	Er	H	TCTPR-9	H_2O	*300*	107.7	AL	[44]
42	ZOTTAD	Ce	H	TCTPR-9	H_2O	*300*	107.3	AL	[15]
43	1944109	Pr	H	TCTPR-9	H_2O	*300*	107.3	AL	[45]
44	1944110	Nd	H	TCTPR-9	H_2O	*300*	107.4	AL	[45]
45	1944111	Sm	H	TCTPR-9	H_2O	*300*	107.4	AL	[45]
46	1944112	Eu	H	TCTPR-9	H_2O	*300*	107.5	AL	[45]
47	1944113	Tb	H	TCTPR-9	H_2O	*300*	107.6	AL	[45]
48	1944114	Dy	H	TCTPR-9	H_2O	*300*	107.6	AL	[45]
49	1944117	Tm	H	TCTPR-9	H_2O	*300*	107.7	AL	[45]
50	DIFLEM	Ce	Cl/CN	CSAPR-9	dmf	*021*	99.6	AL	[46]
51	WOTWIO	Dy	Cl/CN	CSAPR-9	dmf	*021*	102.0	AL	[47]
52	WOTWOU	Ho	Cl/CN	CSAPR-9	dmf	*021*	102.2	AL	[47]
53	XIKNOX	Nd	Cl/CN	CSAPR-9	dmf	*021*	101.3	AL	[48]
54	XIKPAL	Er	Cl/CN	CSAPR-9	dmf	*021*	103.0	AL	[48]
55	XOYTEN	Dy	Cl/CN	CSAPR-9	dmf	*021*	101.8	AL	[38]
56	NIGNUP	Er	Cl	CSAPR-9	fma	*021*	127.2	AL	[28]

([a]) The geometry was determined with the program SHAPE [29–36]. TCTPR-9 = tri-capped trigonal prism, CSAPR-9 = capped square antiprism; ([b]) dmf = dimethylformamide, fma = formamide; ([c]) largest Ln-Ln-Ln angle in the hexagon. ([d]) packing: EC = eclipsed, AL = alternated.

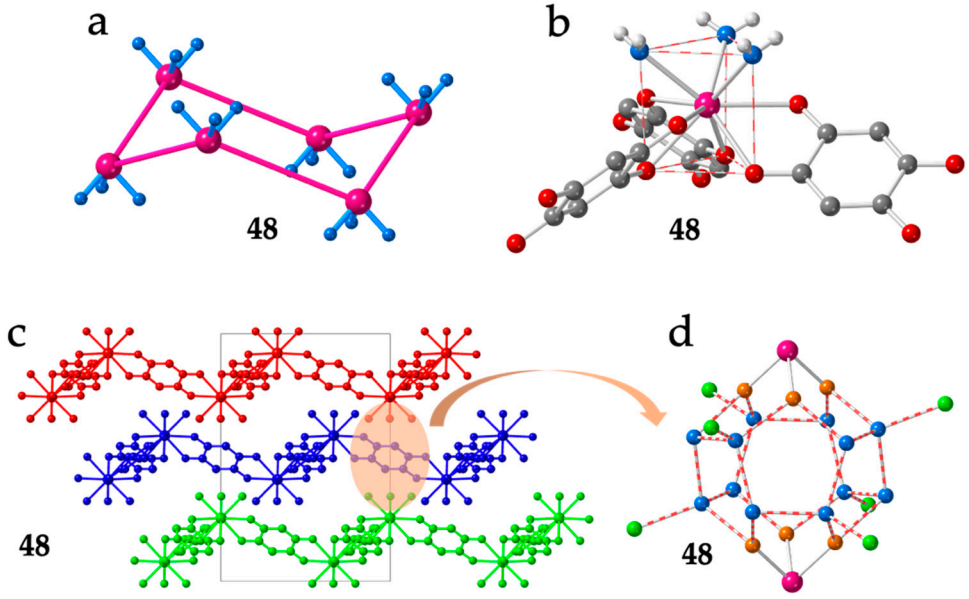

Figure 6. Structure of compound **48**. (**a**) Side view of one hexagonal ring. (**b**) View of the coordination environment of the Dy(III) ions. (**c**) View of three consecutive layers. (**d**) View of the $Dy_2(H_2O)_{18}$ cluster connecting two nonconsecutive layers. Orange atoms are the coordinated water molecules. Blue (and green) atoms are the crystallization water molecules belonging (or not) to the cluster. Colour code: Ln = pink, C = grey, $O_{anilato}$ = red and O_{water} = blue/green/orange.

A similar structure with regular hexagonal rings is also observed in the series of compounds $[Ln_2(C_6O_4ClCN)_3(dmf)_6]\cdot nG$ with G = H_2O and CH_2Cl_2 and Ln = Ce (**50**), Dy (**51**), Ho (**52**), Nd (**53**), Er (**54**) and Dy (**55**). This series contain the asymmetric chlorocyananilato (X = Cl and CN) ligand and dimethylformamide (dmf) instead of water as additional coligand [38,46–48].

The hexagonal rings are even more bent than in the $dhbq^{2-}$ series (Figure 7a), resulting in smaller Ln-Ln-Ln angles (around 100°, see Table 2) and in more corrugated layers (Figure 7b). The lack of planarity in this series is also attributed to the spatial disposition of the chlorocyananilato ligands around the Ln(III) ions, although now, the coordination geometry is a distorted capped square antiprism (CSAPR-9, Figure 7c) with the solvent molecules occupying two positions of the capped square face and one in the other square face, (*021* in our notation, Table 2). One of the anilato ligands occupies the capped position and one position in the upper square face (*110*), a second anilato ligand occupies one position on each of the two square faces (*011*) and the third anilato ligand occupies two positions in the lower square face (*002*) (Figure 7c). As in the previous series, the layers are packed in an alternated way.

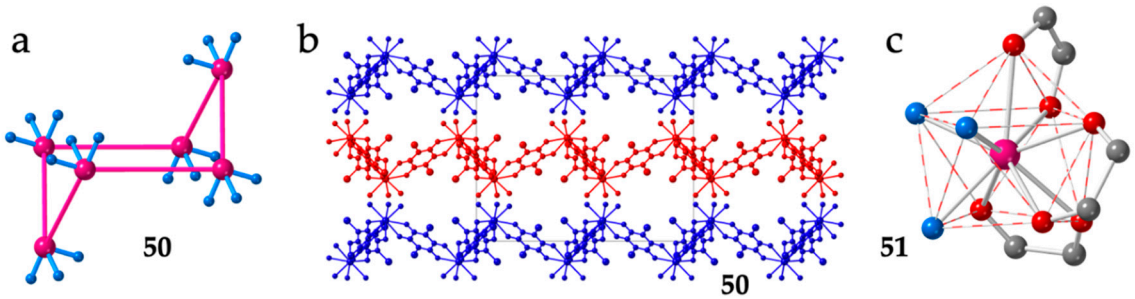

Figure 7. (**a**) Side view of one hexagonal ring in compound **50**. (**b**) View of three consecutive layers in compound **50**. The solvent molecules have been omitted for clarity. (**c**) View of the coordination environment of the Dy(III) ion in compound **51**. Colour code: Ln = pink, C = grey, $O_{anilato}$ = red and O_{dmf} = blue.

Finally, there is an additional example of regular hexagonal rings with chloranilato, Er(III) and formamide (fma) as coligand: $[Er_2(C_6O_4Cl_2)_3(fma)_6]\cdot 4fma\cdot 2H_2O$ (**56**) (Figure 8a) [28]. The coordination geometry around the Er(III) ion is also a distorted CSAPR-9 with the solvent molecules showing a *021* disposition (Figure 8b), although now they are not located on the same triangular face, as observed in the $[Ln_2(C_6O_4ClCN)_3(dmf)_6]\cdot nG$ series (Figure 7c). The three anilato ligands show the same distribution (*110*, *011* and *002*) although, of course, cannot occupy the same positions. Interestingly, as a result of this change in the disposition of the solvent molecules and the anilato ligands, the hexagonal rings are now almost planar (Figure 8c), the Ln-Ln-Ln angles are close to the ideal value of 120° (Table 2) and the layers are much flatter (Figure 8d) although are also packed in an alternated way.

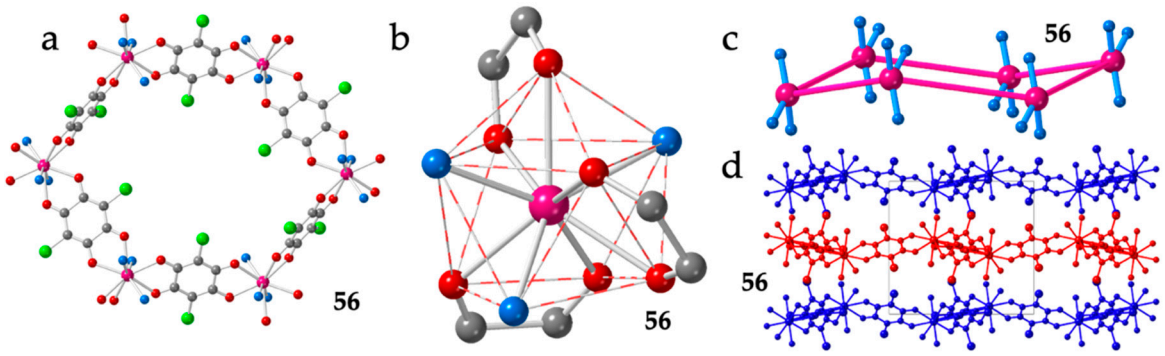

Figure 8. Structure of compound **56**. (**a**) View of one hexagonal ring. (**b**) View of the CSAPR-9 coordination geometry around the Er(III) ion. (**c**) Side view of one hexagonal ring showing the position of the three oxygen atoms of the fma molecules coordinated to each Er(III) ion. (**d**) View of three consecutive layers. Colour code in (**a**–**c**): Ln = pink, C = grey, $O_{anilato}$ = red and $O_{solvent}$ = blue.

2.3.2. Two-Dimensional Distorted Hexagonal Lattices

The second effect of the increase in the coordination number of the Ln(III) ions is the distortion observed in the hexagonal rings (Figure 4b). The main consequence of this distortion implies an increase of two opposite Ln-Ln-Ln angles, which are now in the range of 133–150° (Table 3). These distortions were already observed by Robson, Abrahams et al. in the series of chloranilato-based compounds formulated as $[Ln_2(C_6O_4Cl_2)_3(H_2O)_6]\cdot nH_2O$ with Ln(III) = Pr (**58**), Nd (**59**), Tb (**60**), Ce (**61** and **62**), Y (**63**), Gd (**64**) and Eu (**65**) [15,16], later enlarged with a EtOH solvate of the Gd(III) derivative: $[Gd_2(C_6O_4Cl_2)_3(H_2O)_6]\cdot 2EtOH$ (**57**) by Zucchi et al. [49] and recently completed by us [28,45] with Ln(III) = Er (**66**), La (**67**), Sm (**68**), Dy (**69**) and Ho (**70**) (Table 3). Interestingly, in this series of compounds, Robson et al. found different structural types (phases) depending on the size of the Ln(III) ion and the number of crystallization water molecules (n):

Type I structure corresponds to a coordination number of ten and is only observed for the largest ion, La(III), with n = 7. This phase is not a (3,6)-phase, but a double (3,4) one, and will be described below (compound **128**).

Type II structure is formed when the coordination number is nine. It is observed for most of the intermediate Ln(III) ions. There are three different type **II** structures:

Type IIa is originally found for the large lanthanoids, i.e., Ce (**61** and **62**), Pr (**58**), Nd (**59**) and, surprisingly, for the smaller Tb (**60**) ion (Table 3). This structure has ≈ 12 crystallization water molecules and shows distorted hexagonal rings with two *FO* and four *EO* anilato rings (Figure 9a). The Ln(III) ions present a TCTPR-9 geometry with the coordinated water molecules occupying one vertex of each of the triangular faces and one of the capping positions (disposition *111*) (Figure 9b). The three anilato ligands show dispositions of the type *200*, *011* and *011*. Interestingly, the Ce(III) derivative shows a single-crystal to single-crystal phase transition from a monoclinic *C2/m* phase (**61**) to a triclinic *P*-1 one (**62**) upon losing a small amount of crystallization water [16]. The monoclinic phase also presents a similar distorted hexagonal lattice and a similar TCTPR-9 coordination geometry with a *111*

disposition of the coordinated water molecules (Table 3). Interestingly, the Gd(III) derivative has also been obtained as both, the monoclinic *C2/m* phase in a EtOH solvate (**57**) [49] and as the triclinic *P*-1 phase with water as crystallization solvent (**64**) [16].

Type IIb structure was originally obtained for Y (**63**), Gd (**64**) and Eu (**65**) with n ≈ 10 (Table 3) and is very similar to type **IIa**. The main difference is the presence of four *FO* and two *EO* anilato rings in the distorted hexagonal cavities (Figure 9c) instead of two *FO* and four *EO*, as in type **IIa**. This difference is due to the different positions of the solvent molecules around the Ln(III) ions that now are located on the triangular faces (two in one face and one in the other in a *201* disposition, compared to the *111* disposition found in phase **IIa**). The anilato ligands show dispositions of the type *110*, *011* and *011* (Figure 9d).

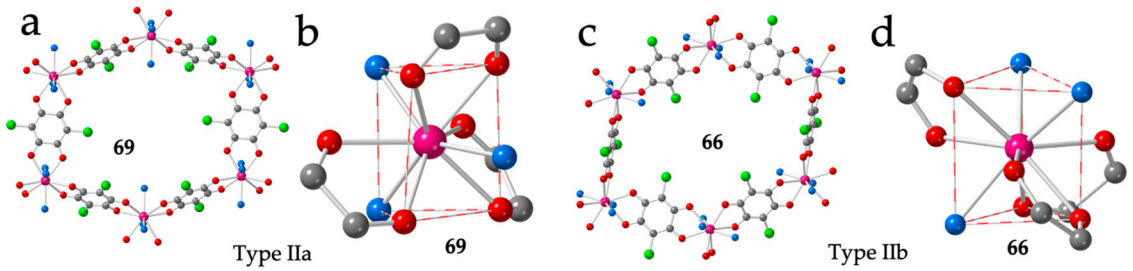

Figure 9. (**a**) View of one hexagonal ring in compound **69** showing the two *face-on* and four *edge-on* anilato rings. (**b**) View of the coordination environment of the Dy(III) ion in compound **69**. (**c**) View of one hexagonal ring in compound **66** showing the four *face-on* and two *edge-on* anilato rings. (**d**) View of the coordination environment of the Er(III) ion in compound **66**. Colour code: Ln = pink, C = grey, $O_{anilato}$ = red, Cl = green and $O_{solvent}$ = blue.

Finally, Robson et al. also noted that there is a third type II phase that they called **Type IIc** that had only been observed in less hydrated compounds such as $[Pr_2(C_6O_4Cl_2)_3(EtOH)_6]\cdot 2EtOH$ (**96**) [13] and $[Y_2(C_6O_4Cl_2)_3(H_2O)_6]\cdot \approx 6H_2O$ (**97**) [14]. This phase has later been observed in other compounds with small lanthanoids and chloranilato or bromanilato as ligands (see Table 4). It shows very distorted hexagonal cavities that can be considered as rectangles and will be described in the next section with the rectangular 3,6 lattices.

As already noted by Robson et al. [16], the number of crystallization water molecules in these series is not easy to determine. Furthermore, the exact number may depend on the storage conditions of the single crystals. In order to shed some light on this matter, we have recently completed the $[Ln_2(C_6O_4Cl_2)_3(H_2O)_6]\cdot nH_2O$ series and performed a study of the crystal structures of all the members of the series [45]. This study showed that if the single crystals are taken directly from the mother liquor and covered with grease to prevent any solvent loss, then the series $[Ln_2(C_6O_4Cl_2)_3(H_2O)_6]\cdot nH_2O$ presents up to four different water contents: (i) n = 14, for the four largest ions (La to Nd); (ii) n = 12, for the intermediate ion (Sm to Ho); (iii) n = 10, for Er and (iii) n = 8, for the two smallest ions (Yb and Tm). Compounds with n = 14 and 12 (from La to Ho) are isostructural and their structure corresponds to the structural type **IIa** described by Robson et al. [16]. The only known example with n = 10 (Ln = Er) shows different unit cell parameters and, therefore, is a different crystalline phase (not a solvate). This phase corresponds to the structural type **IIb** described by Robson et al. [16]. Finally, for n = 8 (Ln = Tm and Yb), the structure shows more important changes since now, the coordinated water molecules occupy different positions (two on one triangular face and one on the other, with a *201* disposition) and the hexagonal rings are so distorted that they look like rectangles. This phase corresponds to the ones reported by Robl for $[Y_2(C_6O_4X_2)_3(H_2O)_6]\cdot nH_2O$ with X/n = Cl/6.6 (**97**) and Br/6 (**101**) [14] and will be described with the rectangular phases in the next section.

Table 3. Reported Ln-anilato compounds with distorted hexagonal 2D structures.

	CCDC	Ln	X	Geometry [a]	L [b]	Disposition	Type	α (°) [c]	Pk [d]	Reference
57	GEQBAH [e]	Gd	Cl	TCTPR-9	H_2O	*111*	IIa	138.0	AL	[49]
58	MIZYID	Pr	Cl	TCTPR-9	H_2O	*111*	IIa	134.9	AL	[16]
59	MIZYOJ	Nd	Cl	TCTPR-9	H_2O		IIa	–	AL	[16]
60	MIZYUP	Tb	Cl	TCTPR-9	H_2O	*111*	IIa	135.8	AL	[16]
61	MIZZAW [e]	Ce	Cl	TCTPR-9	H_2O	*111*	IIa	133.7	AL	[16]
62	MIZZAW01	Ce	Cl	TCTPR-9	H_2O	*111*	IIa	134.6	AL	[16]
63	MIZZEA	Y	Cl	TCTPR-9	H_2O	*111*	IIa	136.1	AL	[16]
64	MIZZIE	Gd	Cl	TCTPR-9	H_2O	*111*	IIb	136.2	AL	[16]
65	MIZZOK	Eu	Cl	TCTPR-9	H_2O		IIb	–	AL	[16]
66	NIGNEZ	Er	Cl	TCTPR-9	H_2O	*201*	IIb	136.6	AL	[28]
67	1944118	La	Cl	TCTPR-9	H_2O	*111*	IIa	133.4	AL	[45]
68	1944120	Sm	Cl	TCTPR-9	H_2O	*111*	IIa	135.0	AL	[45]
69	1944123	Dy	Cl	TCTPR-9	H_2O	*111*	IIa	135.7	AL	[45]
70	1944124	Ho	Cl	TCTPR-9	H_2O	*111*	IIa	136.0	AL	[45]
71	XAWZUT	Er	Br	TCTPR-9	H_2O	*111*	IIa	138.4	AL	[50]
72	1565271	La	Br	TCTPR-9	H_2O	*111*	IIa	135.0	AL	[45]
73	1565272	Ce	Br	TCTPR-9	H_2O	*111*	IIa	136.2	AL	[45]
74	1565273	Pr	Br	TCTPR-9	H_2O	*111*	IIa	137.8	AL	[45]
75	1565274	Nd	Br	TCTPR-9	H_2O	*111*	IIa	136.9	AL	[45]
76	1565275	Sm	Br	TCTPR-9	H_2O	*111*	IIa	137.7	AL	[45]
77	1565276	Eu	Br	TCTPR-9	H_2O	*111*	IIa	137.4	AL	[45]
78	1565277	Gd	Br	TCTPR-9	H_2O	*111*	IIa	137.7	AL	[45]
79	1565278	Tb	Br	TCTPR-9	H_2O	*111*	IIa	138.3	AL	[45]
80	1565279	Dy	Br	TCTPR-9	H_2O	*111*	IIa	138.1	AL	[45]
81	1565280	Ho	Br	TCTPR-9	H_2O	*111*	IIa	138.3	AL	[45]
82	NIDFOY	Tb	Br	TDD-8	dmso	*trans*	IIb	141.0	AL	[51]
83	NIDFUE	Dy	Br	TDD-8	dmso	*trans*	IIb	140.7	AL	[51]
84	NIDGAL	Ho	Br	TDD-8	dmso	*trans*	IIb	141.4	AL	[51]
85	XAXBAC	Er	Br	TDD-8	dmso	*trans*	IIb	140.7	AL	[50]
86	NIDGEP	Yb	Br	TDD-8	dmso	*trans*	IIb	141.3	AL	[51]
87	DIFLUC	Yb	Cl/CN	TDD-8	dmso	*trans*	IIb	150.0	AL	[46]
88	POMTUJ	Yb	Cl/CN	TDD-8	dmso	*trans*	IIb	144.8	AL	[37]
89	POMVAR	Yb/Er	Cl/CN	TDD-8	dmso	*trans*	IIb	145.2	AL	[37]
90	NIGQIG	Er	Cl	TDD-8	dmso	*trans*	IIb	141.0	AL	[28]
91	NIGNOJ	Er	Cl	TDD-8	dmso	*trans*	IIb	142.3	AL	[28]
92	KUVBIP	La	*t*-Bu	TDD-8	dma	*cis*	IIb	138.3	EC	[52]
93	KUVBOV	Pr	*t*-Bu	TDD-8	dma	*cis*	IIb	136.6	EC	[52]
94	KUVBUB	Nd	*t*-Bu	TDD-8	dma	*cis*	IIb	135.8	EC	[52]
95	LEBGEG	Gd	H	SAPR-8	thf/Cl^-	*20*	–	140.8	AL	[53]

([a]) The geometry was determined with the program SHAPE [29–36]. TCTPR-9 = tricapped trigonal prism, TDD-8 = triangular dodecahedron, SAPR-8 = square antiprism; ([b]) dmso = dimethyl sulfoxide, dma = dimethylacetamide, thf = tetrahydrofurane; ([c]) largest Ln-Ln-Ln angle in the hexagon; ([d]) packing: EC = eclipsed, AL = alternated. ([e]) monoclinic *C*2/*m* phase.

Given the important structural changes (from regular hexagons to distorted ones and even rectangles) observed when the ligand $dhbq^{2-}$ (X = H) is replaced by chloranilato (X = Cl), we decided to synthesize and structurally characterize the same series with bromanilato (X = Br). The complete bromanilato series can be formulated as: $[Ln_2(C_6O_4Br_2)_3(H_2O)_6]\cdot nH_2O$ with Ln/n = La/9 (**72**), Ce/8 (**73**), Pr/11 (**74**), Nd/7 (**75**), Sm/10 (**76**), Eu/6 (**77**), Gd/8 (**78**), Tb/10 (**79**), Dy/8 (**80**), Ho/10 (**81**), Er/7 (**71**), Tm/5.5 (**102**) and Yb/3.5 (**103**) (Tables 3 and 4) [45]. Although the general trend is that the number of crystallization water molecules decreases as the size of the Ln(III) decreases, there are some exceptions. These exceptions can be explained by the fact that the solvent molecules occupy the interlayer space and the inner space in the distorted hexagonal cavities and the exact number can change easily (as observed in the series with chloranilato). Despite the many different water contents, we only observe three different crystal phases along the series. The two largest ions (La and Ce) show a structure very similar to type **IIa** observed for chloranilato, with the same distorted hexagonal rings (Figure 10a) and with the same *111* disposition of the coordinated water molecules and *200*, *011* and *011* dispositions for the anilato ligands (Figure 10b).

The intermediate Ln(III) ions (from Pr to Er) show a second type of unit cell parameters and a structure very similar to that of La and Ce (type **IIa** structure with distorted hexagonal rings, Figure 10c) and the same distribution of the coordinated water molecules around the Ln(III) ion (Figure 10d). Finally, the two smallest Ln(III) ions (Tm and Yb) present a completely different structure with less crystallization water molecules and rectangular rings, similar to those observed with chloranilato (Table 4). These rectangular lattices will be described in the next section.

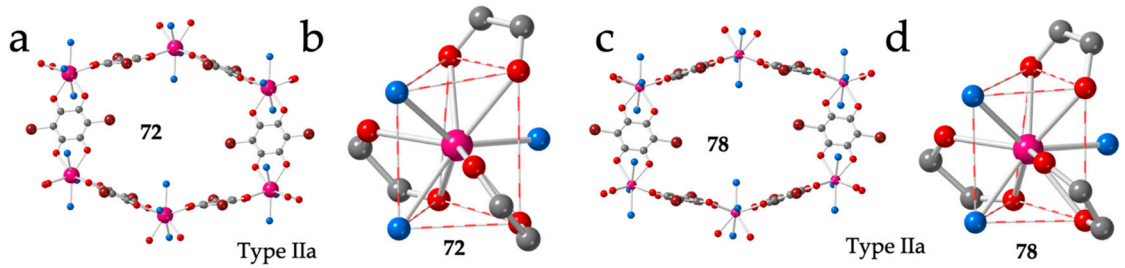

Figure 10. (**a**) View of one hexagonal ring in compound **72** showing the two *face-on* and four *edge-on* anilato rings. (**b**) View of the coordination environment of the La(III) ion in compound **72**. (**c**) View of one hexagonal ring in compound **78** showing the two *face-on* and four *edge-on* anilato rings. (**d**) View of the coordination environment of the Gd(III) ion in compound **78**. Colour code: Ln = pink, C = grey, $O_{anilato}$ = red, Br = brown and $O_{solvent}$ = blue.

A third series showing a distorted honey comb structure with four *FO* and two *EO* anilato ligands (type **IIb**) was obtained for the small lanthanoids (from Tb to Yb) using dimethyl sulfoxide (dmso) as solvent: $[Ln_2(C_6O_4Br_2)_3(dmso)_4]\cdot 2dmso\cdot 2H_2O$ with Ln = Tb (**82**), Dy (**83**), Ho (**84**), Er (**85**) and Yb (**86**) (Figure 11a and Table 3) [50,51]. In this series, the Ln(III) ions are octacoordinated due to the large size of the coordinated solvent (dmso) and small size of the Ln(III) ions. This role of the size of the Ln(III) ion is clearly demonstrated by the fact that the large lanthanoids (from La to Gd) coordinate a third dmso molecule and form rectangular layers that will be described in the next section. The coordination geometry in compounds **82-86** is a triangular dodecahedron (TDD-8) and the two dmso molecules are coordinated in *trans* positions with O-Ln-O bond angles of ca. 150°, in order to reduce the steric hindrance of the bulky dmso molecules (Figure 11b). A similar structure with the same coordination geometry around the Ln(III) ions is also observed in three closely related compounds prepared with the asymmetric ligand chlorocyananilato (X = Cl and CN) and Yb(III) or a 1:1 mixture of Yb/Er: $[Yb_2(C_6O_4ClCN)_3(dmso)_4]\cdot 2H_2O$ (**87**) [46], $[Yb_2(C_6O_4ClCN)_3(dmso)_4]\cdot dmso$ (**88**) and $[YbEr(C_6O_4ClCN)_3(dmso)_4]\cdot dmso$ (**89**) [37] and in two related compounds with chloranilato and Er(III) with dmso and dimethylacetamide (dma) as solvents: $[Er_2(C_6O_4Cl_2)_3(dmso)_4]\cdot 2dmso\cdot 2H_2O$ (**90**) [28] and $[Er_2(C_6O_4Cl_2)_3(dma)_4]$ (**91**) (Table 3) [28].

There are three very recently reported distorted hexagonal lattices prepared with *tert*-butyl-anilato (X = *t*-Bu) and dma, formulated as: $[Ln_2(C_6O_4(t\text{-}Bu)_2)_3(dma)_4]$ with Ln = La (**92**), Pr (**93**) and Nd (**94**) (Figure 11c and Table 3) [52]. The coordination geometry is also a TDD-8 but in contrast to compounds **82-91**, in **92-94** the two dma ligands occupy *cis* positions with O-Ln-O angles of ca. 83° (Figure 11d). The smaller steric hindrance of dma compared to dmso may be at the origin of this different disposition. A second difference is the distortion of the hexagonal cavities, much more pronounced in compounds **92-94** (Figure 11c) probably due to the steric effect of the bulky *tert*-butyl groups in the anilato ligands.

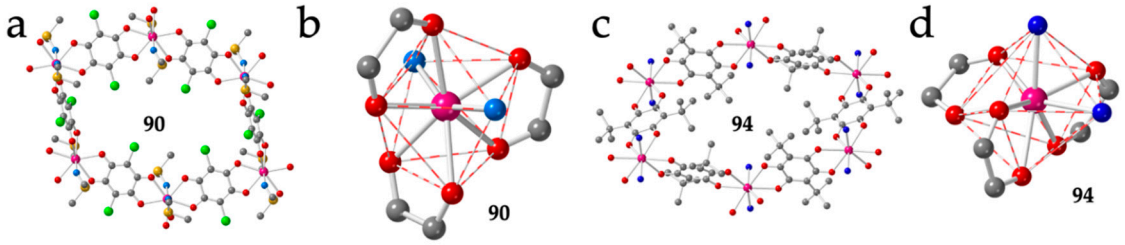

Figure 11. (**a**) View of a distorted hexagonal ring in compound **90** showing the four *FO* and two *EO* anilato rings. (**b**) View of the coordination environment of the Er(III) ion in compound **90**. (**c**) View of a distorted hexagonal ring in compound **94** with four *FO* and two *EO* anilato rings. (**d**) View of the coordination environment of the Nd ion in compound **94**. Colour code: Ln = pink, C = grey, $O_{anilato}$ = red, Cl = green, S = yellow and $O_{solvent}$ = blue.

There is a final example formulated as [Gd(dhbq)Cl(thf)$_2$] (**95**) that shows a quite original distorted hexagonal lattice where one of the anilato bridges is replaced by a double Cl^- one [53]. This change implies that two of the six sides of the hexagons are much shorter than the other four (4.49 vs. 8.63 Å and 8.64 Å, Figure 12a). In this compound, each Gd(III) ion is coordinated to two bis-bidentate bridging $dhbq^{2-}$ ligands, two bridging Cl^- ligands and two thf molecules (Figure 12b) in a very distorted square antiprism geometry (SAPR-8, Table 3). The two Cl^- ligands occupy *cis* positions on the same square face of the square antiprism (*20*), whereas the thf molecules are located one on each square face (*11*) and the two $dhbq^{2-}$ ligands are located with *11* and *02* dispositions (Figure 12b). This spatial orientation gives rise to very distorted but almost planar hexagonal rings with the coordinated thf molecules pointing almost perpendicular to the ring plane (Figure 12c).

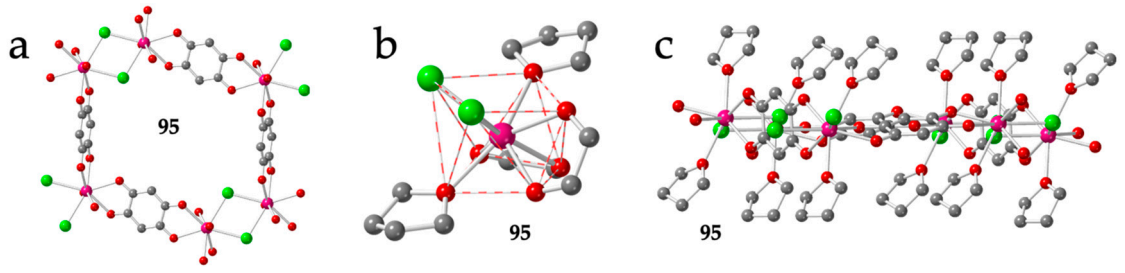

Figure 12. (**a**) View of a distorted hexagonal ring in compound **95** showing the two short sides corresponding to the double Cl^- bridges (only the O atom of the thf molecules is shown for clarity). (**b**) View of the coordination environment of the Gd(III) ion in compounds **95**. (**c**) Side view of the hexagonal ring in **95**. Colour code: Ln = pink, C = grey, O = red and Cl = green.

2.3.3. 2D Rectangular Lattices

When the distortion of the hexagons becomes more important, the largest Ln-Ln-Ln angles increase and reach values in the range ca. 160-170°. The hexagonal cavities look like rectangles, although keeping the same 3,6 topology (Figure 4c,d). As can be seen in Tables 4 and 5, these large distortions are common and, in fact, were already observed in $[Pr_2(C_6O_4Cl_2)_3(EtOH)_6]\cdot 2EtOH$ (**96**), the first Ln-anilato compound reported in 1983 by Raymond et al. [13].

The rectangular rings may adopt two possible structures: (i) a brick-wall one where the long axis of all the rectangles are parallel (Figure 4c) and (ii) spike-like or herringbone, where the long axis of the rectangles of neighbouring rows are almost orthogonal (Figure 4d).

Table 4. Reported Ln-anilato compounds with a rectangular 2D structure and a brick-wall structure.

#	CCDC	Ln	X	Geometry [a]	L [b]	Disposition	α (°)[c]	Pk [d]	Reference
96	CAZZAE	Pr	Cl	TCTPR-9	EtOH	*201*	162.1	AL	[13]
97	GASMUI	Y	Cl	TCTPR-9	H_2O	*201*	169.9	AL	[14]
98	JOGJAT	Er	Cl	CSAPR-9	H_2O	*030*	166.4	AL	[54]
99	1944126	Tm	Cl	TCTPR-9	H_2O	*210*	171.5	AL	[45]
100	1944127	Yb	Cl	TCTPR-9	H_2O	*210*	171.3	AL	[45]
101	GASMOC	Y	Br	TCTPR-9	H_2O	*210*	169.5	AL	[14]
102	1565282	Tm	Br	TCTPR-9	H_2O	*210*	169.0	AL	[45]
103	LUTRIE	Yb	Br	TCTPR-9	H_2O	*210*	168.8	AL	[55]
104	DIFLOW	Pr	Cl/CN	CSAPR-9	dmso	*030*	164.0	EC	[46]
105	NOQGAE	Eu/Dy	Cl/CN	CSAPR-9	dmso	*030*	163.2	EC	[27]
106	WOTWUA	Ce	Cl/CN	CSAPR-9	dmso	*030*	164.4	EC	[47]
107	WOTXAH	Nd	Cl/CN	CSAPR-9	dmso	*030*	163.8	EC	[47]
108	XOYTUD	Dy	Cl/CN	CSAPR-9	dmso	*030*	162.6	EC	[38]
109	WOTWEK	Nd	Cl/CN	CSAPR-9	dmf	*012*	157.9	EC	[47]
110	GEPZUY	Eu	Cl	TCTPR-9	bipym/H_2O	*110/100*	172.7	EC	[49]
111	QOVJUJ	Yb1/Yb2	Cl/CN	TDD-8/TDD-8	dmso/dobdc^{2-}	*trans*	144.4/165.1	AL	[56]
112	QOVJOD	Yb	Cl/CN	TDD-8	dmso/F_4bdc^{2-}	–	158.4	AL	[56]

([a]) The geometry was determined with the program SHAPE [29–36]. TCTPR-9 = tri-capped trigonal prism, CSAPR-9 = capped square antiprism, TDD-8 = triangular dodecahedron; ([b]) dmso = dimthylsulfoxide, dmf = dimethylformamide, bipym = 2,2′-bipyrimidine, H_2dobdc = 2,5-dihydroxybenzene-1,4-dicarboxylic acid, H_2F_4bdc = 2,3,5,6-tetrafluorobenzene-1,4-dicarboxylic acid; ([c]) largest Ln-Ln-Ln angle in the hexagon; ([d]) packing: EC = eclipsed, AL = alternated.

The brick-wall structure has been observed in five compounds with chloranilato: $[Pr_2(C_6O_4Cl_2)_3(EtOH)_6]\cdot 2EtOH$ (**96**) [13], $[Ln_2(C_6O_4Cl_2)_3(H_2O)_6]\cdot nH_2O$ with Ln/n = Y/6.6 (**97**), Tm/8 (**99**) and Yb/8 (**100**) [14,45] and $[Er_2(C_6O_4Cl_2)_3(H_2O)_6]\cdot 2H_2O\cdot 1.5CH_3COCH_3$ (**98**) [54] as well as in three related compounds with bromanilato: $[Y_2(C_6O_4Br_2)_3(H_2O)_6]\cdot 6H_2O$ (**101**) [14], $[Ln_2(C_6O_4Br_2)_3(H_2O)_6]\cdot nH_2O$ with Ln/n = Tm/5.5 (**102**) [45] and Yb/3.5 (**103**) [55] (Table 4). Except for compound **98**, that shows a capped square antiprism (CSAPR-9) geometry, the coordination geometry around the Ln(III) ions is tricapped trigonal prism (TCTPR-9) with the coordinated water molecules in *210* disposition and the anilato ligands in positions *110*, *011* and *002* (Figure 13a). Compound **96** has EtOH instead of water and shows a *201* disposition of the solvent molecules (with the anilato ligands in *110*, *011* and *011* positions (Figure 13b). This difference may be due to the larger size of the EtOH molecules compared to H_2O. As mentioned above, compound **98** is the only one in these series with a CSAPR-9. The water molecules are coordinated in *030* disposition and the anilato ligands in *110*, *002* and *002* (Figure 13c). This surprising result might be due to the templating effect of the NMe_4^+ or NBu_4^+ cations used during the synthesis of compound **98**, in contrast to that of the NEt_4^+ cations, that produce anionic 3D lattices, as we will see below [54].

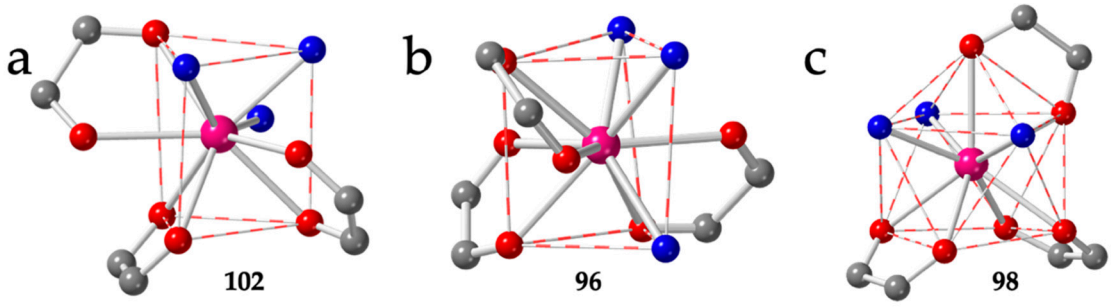

Figure 13. (**a**) View of the coordination environment of the Tm(III) ion in compound **102**. (**b**) View of the coordination environment of the Pr(III) ion in compound **96**. (**c**) View of the coordination environment of the Er(III) ion in compound **98**. Colour code: Ln = pink, C = grey, $O_{anilato}$ = red and $O_{solvent}$ = blue.

A second series of compounds showing the brick-wall structure is the series prepared with the asymmetric chlorocyananilato ligand (X = Cl and CN) with dmso as solvent formulated as $[Ln_2(C_6O_4ClCN)_3(dmso)_6]\cdot G$ with Ln = Pr (**104**) [46], Eu/Dy (**105**) [27], Ce (**106**) [47], Nd (**107**) [47] and Dy (**108**) [38]. In this series, the Ln(III) ions show a CSAPR-9 geometry with the three dmso molecules occupying three vertices of the capped square face (*030*) and the chlorocyananilato ligands in *110*, *002* and *002* dispositions (Figure 14a). Interestingly, if we replace the dmso by dmf in the Nd(III) derivative, the obtained compound, formulated as $[Nd_2(C_6O_4ClCN)_3(dmf)_6]$ (**109**) [47] also shows the brick-wall structure in the layers and a CSAPR-9 geometry, but the disposition of the solvent molecules (dmf) is different since now they occupy one position on the capped square face and two on the bottom one (*012*). The chlorocyananilato ligands show *110*, *011* and *011* dispositions (Figure 14b).

There are three more compounds with a brick-wall lattice and different coligands such as 2,2'-bipyrimidine (bipym): $[Eu_2(C_6O_4Cl_2)_3(bipym)_2]\cdot 4EtOH$ (**110**) [49], the dianion of 2,5-dihydroxybenzene-1,4-dicarboxylic acid (H_2dobdc): $[Yb_4(C_6O_4(CN)Cl)_5(dobdc)(dmso)_{10}]\cdot 2dmso$ (**111**) [56] and the dianion of 2,3,5,6-tetrafluorobenzene-1,4-dicarboxylic acid (H_2F_4bdc): $[Yb_2(C_6O_4(CN)Cl)_2(F_4bdc)(dmso)_6]$ (**112**) [56]. Compound **110** presents a TCTPR-9 geometry with *110* and *100* dispositions of the bidentate bipym and H_2O coligands, respectively. The three chloranilato ligands show *110*, *011* and *002* dispositions (Figure 14c).

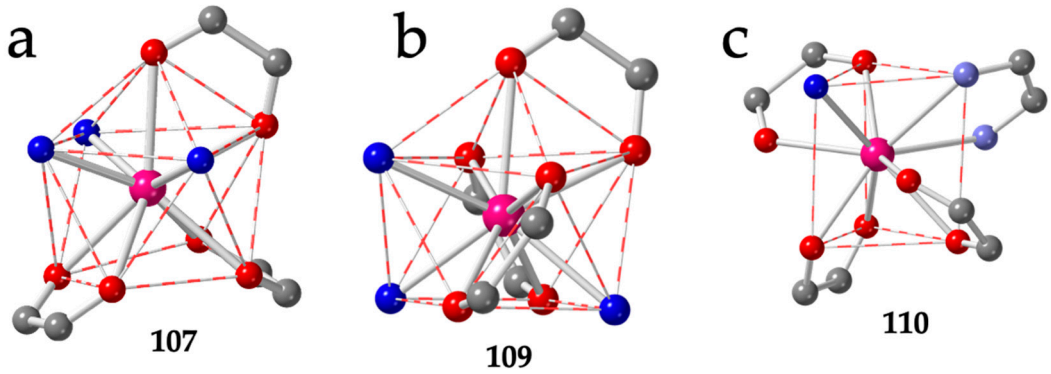

Figure 14. (**a**) View of the coordination environment of the Nd(III) ion in compound **107**. (**b**) View of the coordination environment of the Nd(III) ion in compound **109**. (**c**) View of the coordination environment of the Eu(III) ion in compound **110**. Colour code: Ln = pink, C = grey, $O_{anilato}$ = red, $O_{solvent}$ = blue and N_{bipym} = light blue.

Compound **111** shows two independent Yb ions, both with TDD-8 geometry, although with different coordination environments: Yb1 is coordinated to three bidentate anilato ligand and two *trans*

dmso molecules (Figure 15a), whereas Yb2 is coordinated to two bidentate anilato ligands, three dmso molecules and one dobdc^{2-} monodentate ligand (Figure 15b).

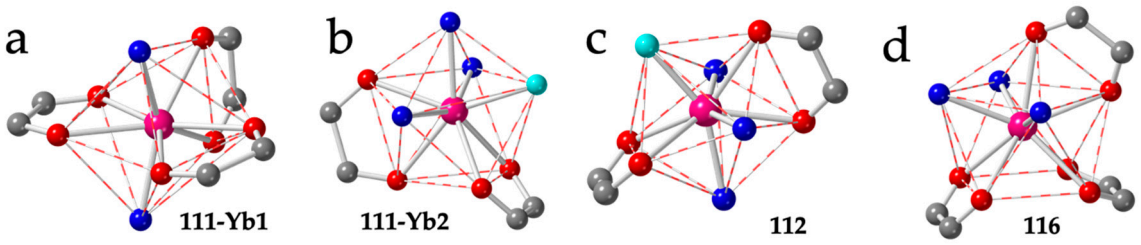

Figure 15. Coordination environment of the Yb1 (**a**) and Yb2 (**b**) ions in compound **111**. (**c**) Coordination environment of the Yb(III) ion in compound **112**. (**d**) Coordination environment of the La ion in compound **116**. Colour code: Ln = pink, C = grey, $O_{anilato}$ = red, $O_{solvent}$ = blue and $O_{coligand}$ = light blue.

The layers in compound **111** are formed by distorted hexagons with six anilato ligands (with a maximum Ln-Ln-Ln angle of 144.4°) alternating with rectangles containing four anilato and two dobdc^{2-} ligands (with a maximum Ln-Ln-Ln angle of 165.1°). The directions of both largest Ln-Ln-Ln angles are parallel, resulting in a brick-wall structure of the distorted hexagons and the rectangles [56]. Finally compound **112** also has a TDD-8 geometry with two bidentante anilato ligands, three dmso molecules and one monodentate F_4bdc^{2-} ligand (Figure 15c), very similar to Yb2 in **111**. The rectangles in the layers in compound **112** contain four anilato and two F_4bdc^{2-} ligands [56].

The other structural type found in the rectangular cavities is the so-called herringbone or spike-like structure (Figure 4d). In this structure, the rectangles are also arranged in parallel rows but the rectangles of consecutive rows are tilted ca. 90°. This structure has been found in a total of fifteen compounds with lanthanoids and anilato ligands (Table 5). In all cases, the coordination geometry around the Ln(III) ion is capped square antiprism (CSAPR-9) and the three solvent molecules are located in three vertices of the capped face (*030* disposition) (Figure 15d). With chloranilato, this herringbone structure has only been found in three compounds: two with water, $[Gd_2(C_6O_4Cl_2)_3(H_2O)_6]\cdot 2bipym\cdot 6H_2O$ (**113**) [49] and $[Ce_2(C_6O_4Cl_2)_3(H_2O)_6]\cdot 2H_2O\cdot 3C_3H_6O$ (**114**) [54] and one with dmf: $[Er_2(C_6O_4Cl_2)_3(dmf)_6]$ (**115**) [28]. In contrast, with bromanilato, the herringbone structure is more common and has been found in eight compounds with dmso: $[Ln_2(C_6O_4Br_2)_3(dmso)_6]\cdot 2dmso$ [51], with Ln = La (**116**), Ce (**117**), Pr (**118**), Nd (**119**), Sm (**120**), Eu (**121**), Gd (**122**) and also in the Dy-doped Eu derivative: $[Dy_{0.04}Eu_{1.96}(C_6O_4Br_2)_3(dmso)_6]\cdot 2dmso$ (**123**) [27]. As mentioned above, this series shows the key role that plays the size of the Ln(III) ion on the coordination number, coordination geometry and final structure. Thus, for the smaller Ln(III) ions (from Tb to Yb, **82–86**), the coordination number is eight, the geometry is TDD-8 and the structure is a distorted hexagonal lattice (Table 3), whereas for the larger Ln(III) ions (from La to Gd, **116-122**), the coordination number is nine, the geometry is CSAPR-9 and the structure is a rectangular herringbone lattice [27].

The herringbone structure has also been found in four compounds with dmf, two with bromanilato: $[Ln_2(C_6O_4Br_2)_3(dmf)_6]$; Ln = Er (**124**) [50] and Dy (**125**) [55] and two with the asymmetric chlorocyananilato ligand: $[Ln_2(C_6O_4(CN)Cl)_3(dmf)_6]$; Ln = Pr (**126**) [46] and Yb (**127**) [48].

Table 5. Reported Ln-anilato compounds with a rectangular 2D structure and a herringbone structure.

#	CCDC	Ln	X	Geometry [a]	L [b]	Disposition	α (°) [c]	Pk [d]	Reference
113	GEQBEL	Gd	Cl	CSAPR-9	H_2O	*030*	159.9	EC	[49]
114	JOGHAR	Ce	Cl	CSAPR-9	H_2O	*030*	164.5	AL	[54]
115	NIGPAX	Er	Cl	CSAPR-9	dmf	*030*	160.3	EC	[28]
116	NIDLIY	La	Br	CSAPR-9	dmso	*030*	165.5	EC	[51]
117	NIDLOE	Ce	Br	CSAPR-9	dmso	*030*	165.4	EC	[51]
118	NIDLUK	Pr	Br	CSAPR-9	dmso	*030*	165.5	EC	[51]
119	NIDMAR	Nd	Br	CSAPR-9	dmso	*030*	164.0	EC	[51]
120	NIDMEV	Sm	Br	CSAPR-9	dmso	*030*	164.0	EC	[51]
121	NIDFEO	Eu	Br	CSAPR-9	dmso	*030*	163.8	EC	[51]
122	NIDFIS	Gd	Br	CSAPR-9	dmso	*030*	163.7	EC	[51]
123	NOQBON	Eu/Dy [e]	Br	CSAPR-9	dmso	*030*	163.9	EC	[27]
124	XAXBEG	Er	Br	CSAPR-9	dmf	*030*	159.0	EC	[50]
125	LUTROK	Dy	Br	CSAPR-9	dmf	*030*	158.9	EC	[55]
126	DIFLIQ	Pr	Cl/CN	CSAPR-9	dmf	*030*	170.7	EC	[46]
127	XIKNUD	Yb	Cl/CN	CSAPR-9	dmf	*030*	167.0	EC	[48]

([a]) The geometry was determined with the program SHAPE [29–36]. CSAPR-9 = capped square antiprism; ([b]) dmf = dimethylformamide, dmso = dimethyl sulfoxide, ([c]) largest Ln-Ln-Ln angle in the hexagon; ([d]) packing: EC = eclipsed, AL = alternated; ([e]) Eu (98%)/Dy (2%).

2.3.4. Other 2D (Square) Lattices

As mentioned above, besides the 3,6-gon topology, although less common, there are also some 2D lattices with (3,4)-, (4,4)- and even mixed (3,4)+(3,8)-topologies (Table 6). The only reported example with the (3,4) topology is also the only known example with a coordination number of ten: $[La_2(C_6O_4Cl_2)_3(H_2O)_6]\cdot\approx 7H_2O$ (**128**) [16]. Although this compound has the general formula $[Ln_2(anilato)_3(L)_n]\cdot mG$, in fact, the structure is very original since the La(III) ions are coordinated to three bidentate chloranilato ligands, two terminal water molecules and two bridging water molecules connecting two La(III) ions (Figure 16a). The coordination geometry of the La(III) ions is a sphenocorona (JSPC-10) [36] and the structure is formed by large squares containing four La(III) centers connected by bis-bidentate anilato ligands (as in other 4,4-lattices) and small rectangles with two anilato bridges and two double aquo-bridges (Figure 16d).

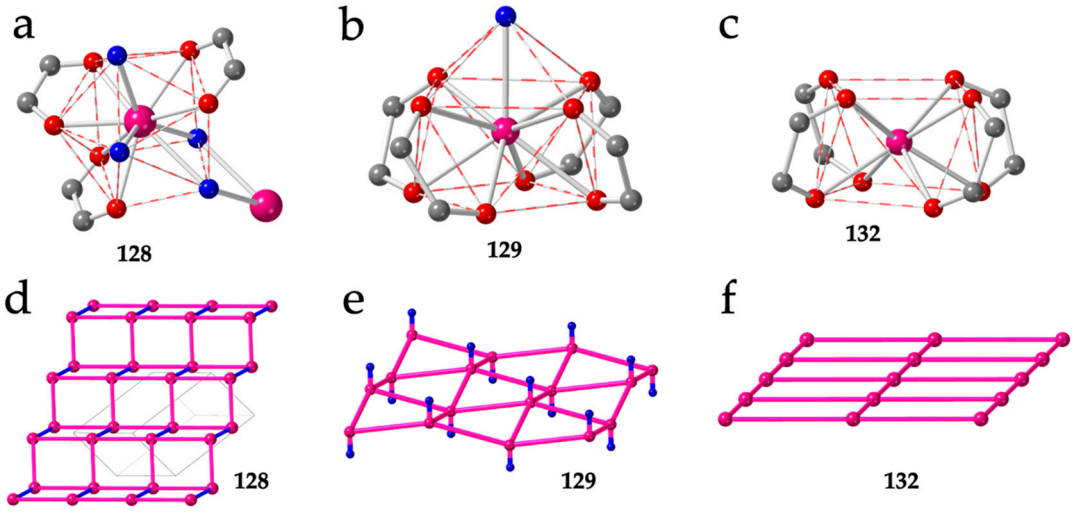

Figure 16. (**a**) Coordination environment of the La(III) ions in compound **128**. (**b**) Coordination environment of the Dy(III) ions in compound **129.** (**c**) Coordination environment of the Dy(III) ions in compound **132**. (**d**) Schematic view of the layered structure in compound **128**. (**e**) Schematic view of the corrugated layers in compound **129**. (**f**) Schematic view of the planar layers in compound **132**. Pink and blue lines represent the anilato and double aquo bridges, respectively. Colour code: Ln = pink, C = grey, $O_{anilato}$ = red and O_{water} = blue.

Although there are already twenty reported Ln-anilato compounds with the 4,4 topology (Table 6), the first compound with this topology, $(H_3O)[Dy(C_6O_4(CN)Cl)_2(H_2O)]\cdot 4H_2O$ (**129**), was not reported until 2018 [46]. In this compound, the Dy(III) ions show a capped square antiprism (CSAPR-9) geometry with a water molecule in the capped position and four chlorocyananilato ligands occupying the closest positions of both square faces (Figure 16b). Accordingly, the four anilato ligands extend along four orthogonal directions, giving rise to a chessboard-like square lattice (Figure 4e) although it is not planar given the pushing effect of the water molecule (Figure 16e). The same structure has also been recently reported with the same ligand, but with $NEt_2H_2^+$ instead of H_3O^+ as cation, in $(NEt_2H_2)[Dy(C_6O_4(CN)Cl)_2]\cdot 2dmf\cdot 2.5H_2O$ (**130**) [38]. In contrast with all the 3,6 lattices of the type $[Ln_2(anilato)_3(L)_n]$, which are neutral, the 4,4 lattices are anionic since they are formed by two dianionic anilato ligands and one Ln(III) ion: $[Ln(anilato)_2]^-$. The presence of cations in the structure represents an additional factor that may play a role in determining the final structure as we will see below. Although in compounds **129** and **130,** the cations are H_3O^+ and $NEt_2H_2^+$, respectively, Robson et al. [57] have recently reported a large series with NEt_4^+ cations and chloranilato formulated as: $(NEt_4)[Ln(C_6O_4Cl_2)_2]\cdot nG$ with Ln/n/G = Y/1.43/CS_2 (**131**), Y/0/- (**132**), Y/1.87/I_2 (**133**), Y/0.91/Br_2 (**134**), Dy/1.5/C_2H_6O (**135**), Gd/1/C_2H_6O (**136**), Yb/1/C_2H_6O (**137**), Er/1/C_2H_6O (**138**), Y/1/C_2H_6O (**139**), Tb/1.5/C_2H_6O (**140**), Lu/1.5/C_2H_6O (**141**) and Ho/1.5/C_2H_6O (**142**). This series was later enlarged by Harris et al. [58] with the Nd/0/- (**143**), Eu/0/- (**144**) and Sm/0/- (**145**) members and also with the Ce, La and Nd derivatives (see below) (Table 6). In this series, the coordination geometry is square antiprism (SAPR-8) with the Ln(III) ion coordinated by four bidentate anilato ligands that also occupy the closest positions of both square faces and extend along four orthogonal directions (Figure 16c) giving rise to a planar square lattice (Figure 16f) since now there is no additional water molecule. The role of the lanthanoid size is again evidenced in this series. Thus, for large lanthanoids such as La, Ce and Nd, there is room for an extra water molecule coordinated to the Ln(III) ions resulting in the series $(NEt_4)[Ln(C_6O_4Cl_2)_2(H_2O)]$ with Ln = Ce (**146**), La (**147**) and Nd (**148**) [58]. In this series, the coordination geometry is capped square antiprism (CSAPR-9), as observed in compounds **129** and **130**, with the water molecule located on the capped position (Figure 16b). An additional interesting aspect of this series is the single-crystal to single-crystal transformation observed in the Nd(III) derivative upon removal of the coordinated water molecule [58].

Table 6. Reported Ln-anilato complexes with 2D-(4,4), 2D-(3,4) and 2D-(3,4)+(3,8) structures.

#	CCDC	Structure	Ln	X	Geometry [a]	A^+	L [b]	Disposition	α (°) [c]	Pk [d]	Reference
128	MIZYAV	3,4	La	Cl	JSPC-10	–	H_2O	–	121.3	EC	[16]
129	DIFMAJ	4,4	Dy	Cl/CN	CSAPR-9	H_3O^+	H_2O	*100*	89.2	EC	[46]
130	XOYVAL	4,4	Dy	Cl/CN	CSAPR-9	$NEt_2H_2^+$	H_2O	*100*	94.1	EC	[38]
131	QOFBAR	4,4	Y	Cl	SAPR-8	NEt_4^+	–	–	90.0	EC	[57]
132	QOFBOF	4,4	Y	Cl	SAPR-8	NEt_4^+	–	–	90.0	EC	[57]
133	QOFBUL	4,4	Y	Cl	SAPR-8	NEt_4^+	–	–	90.0	EC	[57]
134	QOFCAS	4,4	Y	Cl	SAPR-8	NEt_4^+	–	–	90.0	EC	[57]
135	QOFCEW	4,4	Dy	Cl	SAPR-8	NEt_4^+	–	–	90.0	EC	[57]
136	QOFNAD	4,4	Gd	Cl	SAPR-8	NEt_4^+	–	–	90.0	EC	[57]
137	QOFNEH	4,4	Yb	Cl	SAPR-8	NEt_4^+	–	–	90.0	EC	[57]
138	QOFNOR	4,4	Er	Cl	SAPR-8	NEt_4^+	–	–	90.0	EC	[57]
139	QOFNUX	4,4	Y	Cl	SAPR-8	NEt_4^+	–	–	90.0	EC	[57]
140	QOFPAF	4,4	Tb	Cl	SAPR-8	NEt_4^+	–	–	90.0	EC	[57]
141	QOFPEJ	4,4	Lu	Cl	SAPR-8	NEt_4^+	–	–	90.0	EC	[57]
142	QOFPIN	4,4	Ho	Cl	SAPR-8	NEt_4^+	–	–	90.0	EC	[57]
143	WOXTIP	4,4	Nd	Cl	SAPR-8	NEt_4^+	–	–	90.0	EC	[58]
144	WOXTOV	4,4	Eu	Cl	SAPR-8	NEt_4^+	–	–	90.0	EC	[58]
145	WOXTUB	4,4	Sm	Cl	SAPR-8	NEt_4^+	–	–	90.0	EC	[58]
146	WOXVEN	4,4	Ce	Cl	CSAPR-9	NEt_4^+	H_2O	*100*	90.0	EC	[58]
147	WOXVIR	4,4	La	Cl	CSAPR-9	NEt_4^+	H_2O	*100*	90.0	EC	[58]
148	WOXVOX	4,4	Nd	Cl	CSAPR-9	NEt_4^+	H_2O	*100*	90.0	EC	[58]
149	POMVIZ	(3,4) (3,8)	Er	Cl/CN	CSAPR-9		dmso	*030*	175.0 90.0	AL	[37]
150	XOYVEP	(3,4) (3,8)	Dy	Cl/CN	CSAPR-9		dmso	*030*	171.8 90.0	AL	[38]

([a]) The geometry was determined with the program SHAPE [29–36]. JSPC-10 = sphenocorona, CSAPR-9 = capped square antiprism, SAPR-8 = square antiprism; ([b]) dmso = dimthylsulfoxide; ([c]) largest Ln-Ln-Ln angle in the square; ([d]) packing: EC = eclipsed, AL = alternated.

Finally, there are two original 2D structures with (3,4)-(3,8) lattices (Figures 4f and 17a), formulated as $[Ln_2(C_6O_4(CN)Cl)_3(dmso)_6]\cdot nH_2O$, with Ln/n = Er/0 (**149**) [37] and Dy/7 (**150**) [38]. In these (3,4)+(3,8) lattices, each Ln is connected to three other Ln through anilato bridges that extend in three orthogonal directions with a T-shape, generating eight-membered rings with four *face-on (FO)* and four *edge-on (EO)* anilato ligands together with four-membered rings with four *EO* anilato ligands (Figure 17a) [37,38]. The coordination geometry around the Ln(III) ions is also a CSAPR-9 with the solvent molecules occupying three vertices of the capped square face (*030*) and the anilato ligands with *110*, *002* and *002* dispositions (Table 6 and Figure 17b).

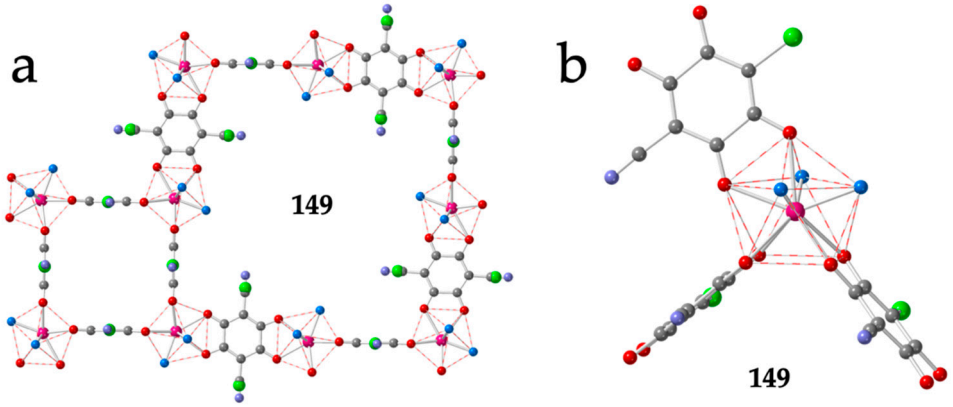

Figure 17. (**a**) View of a four-membered ring and an eight membered ring of the (3,4)+(3,8) layer in compound **149**. (**b**) SCAPR-9 Coordination environment of the Er(III) ions in compound **149** showing the orthogonal orientation of the three anilato bridges. Colour code: Ln = pink, C = grey, Cl = green, N = light blue, $O_{anilato}$ = red and $O_{solvent}$ = blue.

2.4. Three Dimensional (3D) Lattices

As can be seen in Table 7, there are only seven reported 3D Ln-anilato compounds, all with chloranilato and six of them reported in 2019. Except compounds **156** and **157**, they all show the well-known adamantane lattice (Figure 18a), although with large distortions. Most of the reported 3D lattices have been reported in a recent interesting study by Hua and Bondaruk [54] regarding the role of the geometry and size of the counter-cations on these anionic 3D lattices. Interestingly, the 3D-diamond lattice has the same basic formula as the 2D 4,4-lattices: $[Ln(anilato)_2]^-$ and, therefore, it also needs a charge-balancing cation. The study of Hua and Bondaruk shows that the cation plays a key role in determining the dimensionality and the final topology since the cations establish, besides the electrostatic interactions with the anionic lattice, many different interactions such as H-bonds, π-π, Cl-π, halogen-H and CH-π interactions [54].

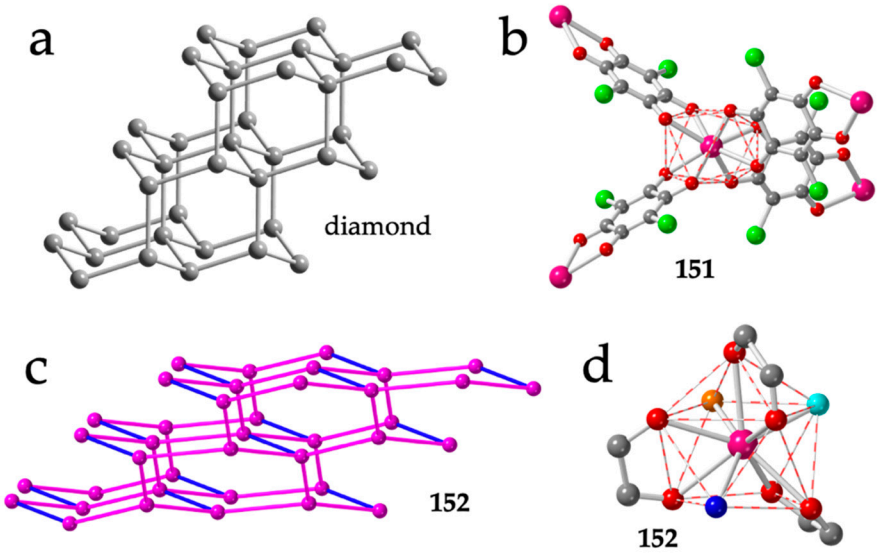

Figure 18. (**a**) Structure of diamond. (**b**) Tetrahedral disposition of the four anilato ligands around the Y(III) ions in compound **151**. (**c**) Distorted adamantane structure in compound **152**. Pink and blue lines represent the anilato and formate bridges, respectively. (**d**) Coordination geometry around the Tb(III) ion in compound **152**. Colour code: Ln = pink, Cl = green, C = grey, $O_{anilato}$ = red, O_{water} = dark blue, O_{dmf} = orange and $O_{formate}$ = light blue.

The first known 3D structure in the Ln-anilato family: $(H_3O)[Y(C_6O_4Cl_2)_2]\cdot 8MeOH$ (**151**), was also reported by Robson, Abrahams et al. in their seminal work in 2002 [16], although a preliminary report had been published in 2000 [59]. This compound shows the typical adamantane structure although with distortions in the tetrahedral environment, that appears elongated along its C_2 axis. The coordination geometry around the Y atom is distorted TDD-8 (Figure 18b). In this compound, the presence of H_3O^+ as counterion is proposed based on the lack of other cations and on charge-balance arguments [16].

Compound (NMe2H2)[Tb2($C_6O_4Cl_2$)3(dmf)2(H2O)2(HCOO)] (**152**) presents three long chloranilato bridges and a short formate one, resulting in a very distorted adamantane structure (Figure 18c) [60]. The Tb(III) ions in compound **152** are coordinated by three chloranilato ligands, one formate, one dmf and one water molecule in a CSAPR-9 coordination geometry (Figure 18d). The formate ion and the dmf molecule occupy two *cis* positions in the capped square face (*010*) and the water molecule occupies one vertex of the other square face (*001*), whereas the chloranilato ligands show *110*, *011* and *002* dispositions (Figure 18d).

Table 7. Reported Ln-anilato complexes with 3D lattices.

#	CCDC	Structure	Ln	X	Geometry [a]	A^+	L [b]	Disposition	Reference
151	MOBBIO	3D-diam	Y	Cl	TDD-8	H_3O^+	–	–	[16]
152	EFOXUV	3D-diam	Tb	Cl	CSAPR-9	$NMe_2H_2^+$	H_2O/dmf/$HCOO^-$	*001/010/010*	[60]
153	JOGHEV	3D-diam	Er	Cl	SAPR-8	$DPMP^+$	–	–	[54]
154	JOGHIZ	3D-diam	Ce	Cl	CSAPR-9	$DPMP^+$	H_2O	*010*	[54]
155	JOGHOF	3D-diam	Ce	Cl	TCTPR-9	PPh_4^+	H_2O	*010*	[54]
156	JOGHUL	3D-noq	Ce1 Ce2 Ce3	Cl	CSAPR-9 CSAPR-9 TCTPR-9/MUFF	PPh_3Me^+	H_2O H_2O H_2O	*010* *001* *100*	[54]
157	JOGJEX	3D-4,4-c	Er1/Er2	Cl	CSAPR-9/TDD-8	PPh_3Me^+	H_2O/-	*010*/-	[54]

([a]) The geometry was determined with the program SHAPE [29–36]. TDD-8 = triangular dodecahedron, CSAPR-9 = capped square antiprism, SAPR-8 = square antiprism, TCTPR-9 = tri-capped trigonal prism; MUFF = muffin ([b]) dmf = dimethylformamide.

The diamond net is also observed in the closely related compounds: $(DPMP)[Er(C_6O_4Cl_2)_2]$ (**153**), $(DPMP)[Ce(C_6O_4Cl_2)_2(H_2O)]\cdot H_2O\cdot C_3H_6O$ (**154**) and $(PPh_4)[Ce(C_6O_4Cl_2)_2(H_2O)]$ (**155**) (DPMP = 1-(diphenylmethyl)-pyridinium) [54]. These three compounds show the effect of the cation and of the size of the Ln(III) ion in the coordination geometry. Thus, the small Er(III) ion in compound **153** can only accommodate four chloranilato ligands in a square antiprism geometry (Figure 19a), giving rise to a quite regular diamond net (Figure 19b). In contrast, the larger Ce(III) ion in compounds **154** and **155** allows the coordination of an additional water molecule, resulting in a distorted CSAPR-9 in **154** (with a *010* disposition for the water molecule, Figure 19c) and in a distorted TCTPR-9 in **155** (with a *100* disposition for the water molecule, Figure 19d). Interestingly, the coordination of the additional water molecule does not change the diamond net topology but increases the distortions of the lattice. Another interesting point of this series is the change in the coordination geometry (CSAPR-9 in **154** vs. TCTPR-9 in **155**). This change can be attributed to the different symmetry and shape of the cations used to prepare both compounds: $DPMP^+$ in **154** and PPh_4^+ in **155**. A similar effect of the symmetry and shape of closely related cations of the type NR_4^+ and PR_4^+ was observed in a series of tris-anilato-metalate complexes with transition metals [9].

A remarkable fact is that compounds $(NEt_4)[Y(C_6O_4Cl_2)_3]$ (**132**) and $(H_3O)[Y(C_6O_4Cl_2)_2]\cdot 8MeOH$ (**151**) show the same coordination environment around the Y(III) ions (four bidentante chloranilato ligands) but the geometries are different: SAPR-8 in **132** (Figure 16c) vs. TDD-8 in **151** (Figure 18b). This simple difference in the coordination geometry gives rise to different spatial orientations of the anilato ligands (square in **132** and tetrahedral in **151**) that originate two very different structures (a 2D 4,4-square lattice in **132** vs. a 3D diamond net in **151**). Since the ligand and the Ln(III) ion are the same

in both compounds, these differences might be only attributed to the different counter-cation in each lattice: NEt_4^+ in **131** vs. H_3O^+ in **151**.

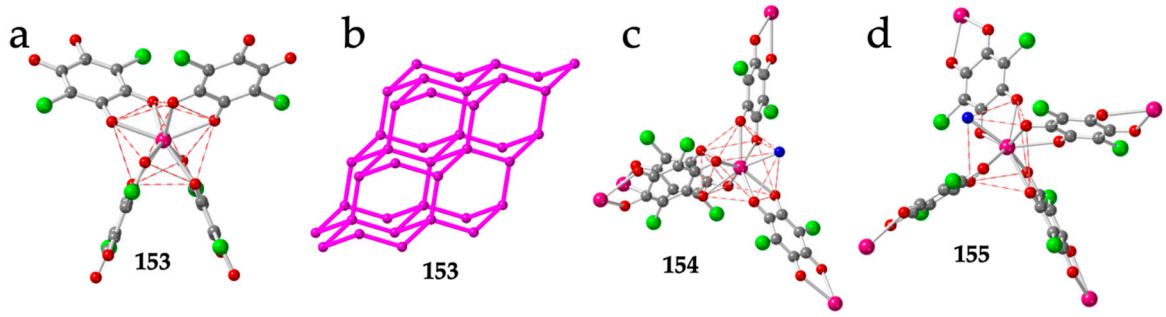

Figure 19. (**a**) Coordination environment of the Er(III) ion in compound **153**. (**b**) Distorted adamantane structure in compound **153** showing only the Er(III) ions. Pink lines represent the anilato bridges. (**c**) Coordination environment of the Ce(III) ion in compound **154**. (**d**) Coordination environment of the Ce(III) ion in compound **155**. Colour code: Ln = pink, Cl = green, C = grey, $O_{anilato}$ = red and O_{water} = blue.

Besides the five mentioned examples of diamond 3D lattices, there are two more examples of Ln-anilato 3D lattices: compound $(PPh_3Me)[Ce(C_6O_4Cl_2)_2(H_2O)]$ (**156**) shows a very original 3D structure with three unique Ce(III) ions nonacoordinated by four bidentate chloranilato ligands and a water molecule [54]. Ce1 and Ce2 show both a CSAPR-9 geometry although the water molecule is located on the capped square face in Ce1 (*010*, Figure 20a) or in the basal square face in Ce2 (*001*, Figure 20b). In contrast, Ce3 presents a geometry in between TCTPR-9 and MFF (Muffin) [35] with the water molecule coordinated on one of the triangular faces (*100*, Figure 20c). The structure can be described as a 3D-noq anionic lattice formed by three-, four- and five-membered rings with PPh_3Me^+ cations inserted in the larger cavities (Figure 20d).

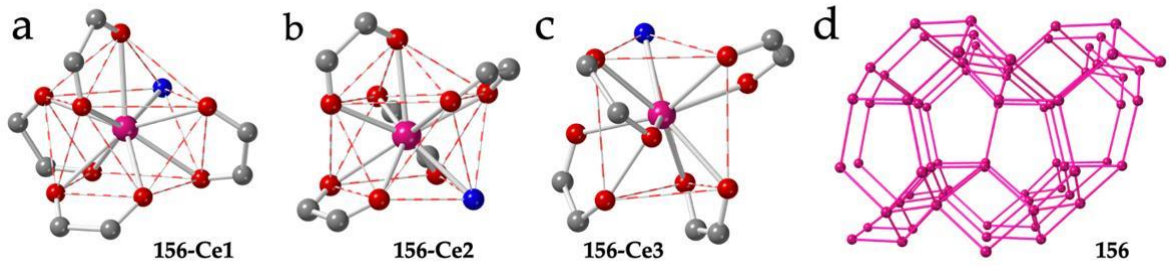

Figure 20. (**a**–**c**) Coordination environments of the Ce1, Ce2 and C3 ions, respectively, in compound **156**. (**d**) Perspective view of the structure of compound **156**. Pink lines represent the anilato bridges. Colour code: Ln = pink, C = grey, $O_{anilato}$ = red and O_{water} = blue.

Finally, compound $(PPh_3Me)[Er(C_6O_4Cl_2)_2]\cdot 1/2H_2O$ (**157**) shows a unique 3D 4,4′-c structure with four- and five-membered rings (Figure 21a) and net point symbol $\{4.5^2.7^3\}\{4.5^3.7^2\}$ with PPh_3Me^+ cations located in the five-membered rings [54]. In this compound, there are two unique Er(III) ions with different coordination geometries. Er1 ion is surrounded by four chloranilato ligands and a water molecule in a CSAPR-9 geometry with the water molecule located on the capped square face (*010*, Figure 21b), whereas Er2 is surrounded by four chloranilato ligands in a TDD-8 geometry without any additional coligand (Figure 21c).

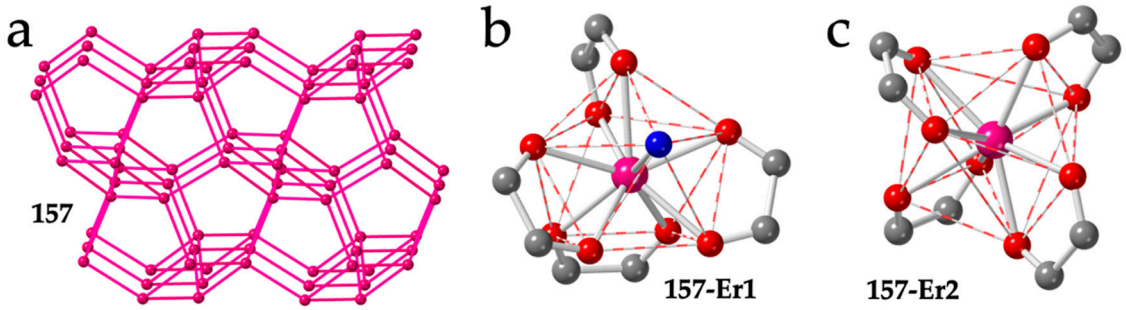

Figure 21. (**a**) View of the structure of compound **157**. Only the Er(III) ions are shown. Pink lines connecting the Er atoms represent the anilato bridges. (**b**) Coordination environment of the Er1 ion in compound **157**. (**c**) Coordination environment of the Er2 ion in compound **157**. Colour code: Ln = pink, C = grey, $O_{anilato}$ = red and O_{water} = blue.

2.5. Anilato-Type Ligands

A second way to classify the above Ln-anilato compounds is based on the anilato-type ligand. With this criterion, we can see that there are nineteen compounds with lanthanoids and the ligand $dhbq^{2-}$ (Table 8). Among these nineteen compounds, three are dimers, one shows a distorted hexagonal 2D lattice and the remaining fifteen compounds present a regular hexagonal 2D lattice.

Table 8. Structurally characterized Ln compounds with $dhbq^{2-}$.

#	CCDC	Structure	Ln	X	L [a]	Reference
2	DEHQUF	Dimer	Dy	H	thf/Cl^-	[21]
3	DEHRAM	Dimer	Y	H	thf/Cl^-	[21]
10	DEKVEX	Dimer	Y	H	Tp^-	[20]
35	KUYKIZ	2D-hex	Ho	H	H_2O	[43]
36	MIZXAU	2D-hex	La	H	H_2O	[16]
37	MIZXEY	2D-hex	Gd	H	H_2O	[16]
38	MIZXIC	2D-hex	Yb	H	H_2O	[16]
39	MIZXOI	2D-hex	Lu	H	H_2O	[16]
40	MIZXUO	2D-hex	Y	H	H_2O	[16]
41	PIVKAJ	2D-hex	Er	H	H_2O	[44]
42	ZOTTAD	2D-hex	Ce	H	H_2O	[15]
43	1944109	2D-hex	Pr	H	H_2O	[45]
44	1944110	2D-hex	Nd	H	H_2O	[45]
45	1944111	2D-hex	Sm	H	H_2O	[45]
46	1944112	2D-hex	Eu	H	H_2O	[45]
47	1944113	2D-hex	Tb	H	H_2O	[45]
48	1944114	2D-hex	Dy	H	H_2O	[45]
49	1944117	2D-hex	Tm	H	H_2O	[45]
95	LEBGEG	2D-dist.hex	Gd	H	thf/Cl^-	[53]

([a]) thf = tetrahydrofurane, Tp^- = $HB(pz)_3^-$ = hydrotris(pyrazolyl)borate.

By far, the most used anilato ligand with lanthanoids is chloranilato (X = Cl), with a total of 63 structurally characterized compounds (Table 9) with all the dimensionalities (0D, 1D, 2D and 3D). Among these 63 compounds, there is one monomer, one compound formed by a monomer and a chain,

eight dimers, one ladder chain, one regular hexagonal 2D lattice, sixteen distorted hexagonal layers, six rectangular brick-wall 2D lattices, three rectangular herringbone layers, one 2D-3,4 lattice, eighteen 2D-4,4 square layers, five adamantane 3D structures, one 3D-noq and one 3D-4,4-c lattice.

Table 9. Structurally characterized Ln compounds with chloranilato.

#	CCDC	Structure	Ln	X	L [a]	A^{+b}	Reference
1	PIQFUT	Monomer	Dy	Cl	Tp^-	–	[19]
4	DEKTOF	Dimer	Dy	Cl	Tp^-	–	[20]
5	DEKTOF01	Dimer	Dy	Cl	Tp^-	–	[22]
6	DEKTOF02	Dimer	Dy	Cl	Tp^-	–	[19]
7	DEKTUL	Dimer	Y	Cl	Tp^-	–	[20]
8	DEKTUL01	Dimer	Y	Cl	Tp^-	–	[22]
9	DEKVAT	Dimer	Y	Cl	Tp^-	–	[20]
22	KOZBEJ	Dimer	Er	Cl	Tp^-	–	[24]
23	KOZBIN	Dimer	Ho	Cl	Tp^-	–	[24]
24	LEPNIG	Dimer	Tb	Cl	Tp^-	–	[22]
25	LEPNIG01	Dimer	Tb	Cl	Tp^-	–	[24]
26	LEPNOM	Dimer	Gd	Cl	Tp^-	–	[22]
27	LEPNOM01	Dimer	Gd	Cl	Tp^-	–	[19]
28	OBIBEH	Dimer	Yb	Cl	Tp^-	–	[25]
29	OBIBEH01	Dimer	Yb	Cl	Tp^-	–	[24]
33	MIZZUQ	1D + mon	Lu	Cl	H_2O	–	[16]
34	NIGNID	1D-ladder	Er	Cl	hmpa	–	[28]
56	NIGNUP	2D-hex	Er	Cl	fma	–	[28]
57	GEQBAH	2D-dist.hex	Gd	Cl	H_2O	–	[49]
58	MIZYID	2D-dist.hex	Pr	Cl	H_2O	–	[16]
59	MIZYOJ	2D-dist.hex	Nd	Cl	H_2O	–	[16]
60	MIZYUP	2D-dist.hex	Tb	Cl	H_2O	–	[16]
61	MIZZAW	2D-dist.hex	Ce	Cl	H_2O	–	[16]
62	MIZZAW01	2D-dist.hex	Ce	Cl	H_2O	–	[16]
63	MIZZEA	2D-dist.hex	Y	Cl	H_2O	–	[16]
64	MIZZIE	2D-dist.hex	Gd	Cl	H_2O	–	[16]
65	MIZZOK	2D-dist.hex	Eu	Cl	H_2O	–	[16]
66	NIGNEZ	2D-dist.hex	Er	Cl	H_2O	–	[28]
67	1944118	2D-dist.hex	La	Cl	H_2O	–	[45]
68	1944120	2D-dist.hex	Sm	Cl	H_2O	–	[45]
69	1944123	2D-dist.hex	Dy	Cl	H_2O	–	[45]
70	1944124	2D-dist.hex	Ho	Cl	H_2O	–	[45]
90	NIGQIG	2D-dist.hex	Er	Cl	dmso	–	[28]
91	NIGNOJ	2D-dist.hex	Er	Cl	dma	–	[28]
96	CAZZAE	2D-brickwall	Pr	Cl	EtOH	–	[13]
97	GASMUI	2D-brickwall	Y	Cl	H_2O	–	[14]
98	JOGJAT	2D-brickwall	Er	Cl	H_2O	–	[54]

Table 9. *Cont.*

#	CCDC	Structure	Ln	X	L [a]	A^{+b}	Reference
99	1944126	2D-brickwall	Tm	Cl	H_2O	–	[45]
100	1944127	2D-brickwall	Yb	Cl	H_2O	–	[45]
110	GEPZUY	2D-brickwall	Eu	Cl	bipym/H_2O	–	[49]
113	GEQBEL	2D-herringbone	Gd	Cl	H_2O	–	[49]
114	JOGHAR	2D-herringbone	Ce	Cl	H_2O	–	[54]
115	NIGPAX	2D-herringbone	Er	Cl	dmf	–	[28]
128	MIZYAV	2D-3,4	La	Cl	H_2O	–	[16]
131	QOFBAR	2D-4,4	Y	Cl	–	NEt_4^+	[57]
132	QOFBOF	2D-4,4	Y	Cl	–	NEt_4^+	[57]
133	QOFBUL	2D-4,4	Y	Cl	–	NEt_4^+	[57]
134	QOFCAS	2D-4,4	Y	Cl	–	NEt_4^+	[57]
135	QOFCEW	2D-4,4	Dy	Cl	–	NEt_4^+	[57]
136	QOFNAD	2D-4,4	Gd	Cl	–	NEt_4^+	[57]
137	QOFNEH	2D-4,4	Yb	Cl	–	NEt_4^+	[57]
138	QOFNOR	2D-4,4	Er	Cl	–	NEt_4^+	[57]
139	QOFNUX	2D-4,4	Y	Cl	–	NEt_4^+	[57]
140	QOFPAF	2D-4,4	Tb	Cl	–	NEt_4^+	[57]
141	QOFPEJ	2D-4,4	Lu	Cl	–	NEt_4^+	[57]
142	QOFPIN	2D-4,4	Ho	Cl	–	NEt_4^+	[57]
143	WOXTIP	2D-4,4	Nd	Cl	–	NEt_4^+	[58]
144	WOXTOV	2D-4,4	Eu	Cl	–	NEt_4^+	[58]
145	WOXTUB	2D-4,4	Sm	Cl	–	NEt_4^+	[58]
146	WOXVEN	2D-4,4	Ce	Cl	H_2O	NEt_4^+	[58]
147	WOXVIR	2D-4,4	La	Cl	H_2O	NEt_4^+	[58]
148	WOXVOX	2D-4,4	Nd	Cl	H_2O	NEt_4^+	[58]
151	MOBBIO	3D-diam	Y	Cl	–	H_3O^+	[16]
152	EFOXUV	3D-diam	Tb	Cl	H_2O/dmf/$HCOO^-$	$NMe_2H_2^+$	[60]
153	JOGHEV	3D-diam	Er	Cl	–	$DPMP^+$	[54]
154	JOGHIZ	3D-diam	Ce	Cl	H_2O	$DPMP^+$	[54]
155	JOGHOF	3D-diam	Ce	Cl	H_2O	PPh_4^+	[54]
156	JOGHUL	3D-noq	Ce	Cl	H_2O	PPh_3Me^+	[54]
157	JOGJEX	3D-4,4-c	Er1	Cl	H_2O	PPh_3Me^+	[54]

([a]) Tp^- = $HB(pz)_3^-$ = hydrotris(pyrazolyl)borate, hmpa = hexamethylphosphoramide, fma = formamide, dmso = dimthylsulfoxide, dma = dimethylacetamide, bipym = 2,2′-bipyrimidine, dmf = dimethylformamide; ([b]) $DPMP^+$ = 1-(diphenylmethyl)-pyridinium.

With the ligand bromanilato (X = Br), there are 31 compounds (Table 10): two dimers, sixteen distorted hexagonal layers, three rectangular brick-wall layers and ten rectangular herringbone ones.

Table 10. Structurally characterized Ln compounds with bromanilato.

#	CCDC	Structure	Ln	X	L [a]	Reference
18	JOQSEQ	Dimer	Dy	Br	Tp^-	[23]
21	JOQSUG	Dimer	Y	Br	Tp^-	[23]
71	XAWZUT	2D-dist.hex	Er	Br	H_2O	[50]
72	1565271	2D-dist.hex	La	Br	H_2O	[45]
73	1565272	2D-dist.hex	Ce	Br	H_2O	[45]
74	1565273	2D-dist.hex	Pr	Br	H_2O	[45]
75	1565274	2D-dist.hex	Nd	Br	H_2O	[45]
76	1565275	2D-dist.hex	Sm	Br	H_2O	[45]
77	1565276	2D-dist.hex	Eu	Br	H_2O	[45]
78	1565277	2D-dist.hex	Gd	Br	H_2O	[45]
79	1565278	2D-dist.hex	Tb	Br	H_2O	[45]
80	1565279	2D-dist.hex	Dy	Br	H_2O	[45]
81	1565280	2D-dist.hex	Ho	Br	H_2O	[45]
82	NIDFOY	2D-dist.hex	Tb	Br	dmso	[51]
83	NIDFUE	2D-dist.hex	Dy	Br	dmso	[51]
84	NIDGAL	2D-dist.hex	Ho	Br	dmso	[51]
85	XAXBAC	2D-dist.hex	Er	Br	dmso	[50]
86	NIDGEP	2D-dist.hex	Yb	Br	dmso	[51]
101	GASMOC	2D-brickwall	Y	Br	H_2O	[14]
102	1565282	2D-brickwall	Tm	Br	H_2O	[45]
103	LUTRIE	2D-brickwall	Yb	Br	H_2O	[55]
116	NIDLIY	2D-herringbone	La	Br	dmso	[51]
117	NIDLOE	2D-herringbone	Ce	Br	dmso	[51]
118	NIDLUK	2D-herringbone	Pr	Br	dmso	[51]
119	NIDMAR	2D-herringbone	Nd	Br	dmso	[51]
120	NIDMEV	2D-herringbone	Sm	Br	dmso	[51]
121	NIDFEO	2D-herringbone	Eu	Br	dmso	[51]
122	NIDFIS	2D-herringbone	Gd	Br	dmso	[51]
123	NOQBON	2D-herringbone	Eu/Dy	Br	dmso	[27]
124	XAXBEG	2D-herringbone	Er	Br	dmf	[50]
125	LUTROK	2D-herringbone	Dy	Br	dmf	[55]

([a]) dmso = dimthylsulfoxide, dmf = dimethylformamide.

With the asymmetric ligand chlorocyananilato (X = Cl/CN), there is a total of 25 reported compounds (Table 11). Among these 25 compounds, two are zigzag dimers, six are 2D regular hexagonal layers, three are distorted hexagonal lattices, eight are rectangular brick-wall lattices, two are rectangular herringbone lattices, two are square 4,4 layers and the remaining two are (3,4)+(3,8) layers.

Table 11. Structurally characterized Ln compounds with chlorocyananilato.

#	CCDC	Structure	Ln	X	L [a]	A^+	Reference
30	NOQBUT	Dimer-zz	Eu	Cl/CN	H_2O	–	[27]
31	NOQGEI	Dimer-zz	Eu/Dy [b]	Cl/CN	H_2O	–	[27]
50	DIFLEM	2D-hex	Ce	Cl/CN	dmf	–	[46]
51	WOTWIO	2D-hex	Dy	Cl/CN	dmf	–	[47]
52	WOTWOU	2D-hex	Ho	Cl/CN	dmf	–	[47]
53	XIKNOX	2D-hex	Nd	Cl/CN	dmf	–	[48]
54	XIKPAL	2D-hex	Er	Cl/CN	dmf	–	[48]
55	XOYTEN	2D-hex	Dy	Cl/CN	dmf	–	[38]
87	DIFLUC	2D-dist.hex	Yb	Cl/CN	dmso	–	[46]
88	POMTUJ	2D-dist.hex	Yb	Cl/CN	dmso	–	[37]
89	POMVAR	2D-dist.hex	Yb/Er	Cl/CN	dmso	–	[37]
104	DIFLOW	2D-brickwall	Pr	Cl/CN	dmso	–	[46]
105	NOQGAE	2D-brickwall	Eu/Dy	Cl/CN	dmso	–	[27]
106	WOTWUA	2D-brickwall	Ce	Cl/CN	dmso	–	[47]
107	WOTXAH	2D-brickwall	Nd	Cl/CN	dmso	–	[47]
108	XOYTUD	2D-brickwall	Dy	Cl/CN	dmso	–	[38]
109	WOTWEK	2D-brickwall	Nd	Cl/CN	dmf	–	[47]
111	QOVJUJ	2D-brickwall	Yb1	Cl/CN	dmso/$dobdc^{2-}$	–	[56]
112	QOVJOD	2D-brickwall	Yb	Cl/CN	dmso/F_4bdc^{2-}	–	[56]
126	DIFLIQ	2D-herringbone	Pr	Cl/CN	dmf	–	[46]
127	XIKNUD	2D-herringbone	Yb	Cl/CN	dmf	–	[48]
129	DIFMAJ	2D-4,4	Dy	Cl/CN	H_2O	H_3O^+	[46]
130	XOYVAL	2D-4,4	Dy	Cl/CN	H_2O	$NEt_2H_2^+$	[38]
149	POMVIZ	2D-(3,4)+(3,8)	Er	Cl/CN	dmso	–	[37]
150	XOYVEP	2D-(3,4)+(3,8)	Dy	Cl/CN	dmso	–	[38]

([a]) dmf = dimethylformamide, dmso = dimthylsulfoxide, H_2dobdc = 2,5-dihydroxybenzene-1,4-dicarboxylic acid, H_2F_4bdc = 2,3,5,6-tetrafluorobenzene-1,4-dicarboxylic acid; ([b]) Eu (98%)/Dy (2%).

Finally, there are a few reported compounds with lanthanoids and other anilato ligands (Table 12) such as: methylanilato (X = CH_3), with three reported examples [20], nitranilato (X = NO_2), with five reported compounds [26], fluoranilato (X = F), with two reported compounds [23] and *tert*-butylanilato (X = *t*-Bu), with three very recently reported examples [52].

Table 12. Structurally characterized Ln compounds with other anilato-type ligands.

#	CCDC	Structure	Ln	X	L [a]	Reference
11	DEKVIB	Dimer	Y	CH_3	Tp^-	[20]
12	DEKVOH	Dimer	Y	CH_3	Tp^-	[20]
32	DEKVUN	Tetramer	Y	CH_3	$Tp^-/(MeO)_4B/MeOH$	[20]
13	EDEZAR	Dimer	Gd	NO_2	H_2O	[26]
14	EDEZEV	Dimer	Tb	NO_2	H_2O	[26]
15	EDEZIZ	Dimer	Dy	NO_2	H_2O	[26]
16	EDEZOF	Dimer	Ho	NO_2	H_2O	[26]
17	EDEZUL	Dimer	Sm	NO_2	H_2O	[26]
19	JOQSIU	Dimer	Dy	F	Tp^-	[23]
20	JOQSOA	Dimer	Y	F	Tp^-	[23]
92	KUVBIP	2D-dist.hex	La	*t*-Bu	dma	[52]
93	KUVBOV	2D-dist.hex	Pr	*t*-Bu	dma	[52]
94	KUVBUB	2D-dist.hex	Nd	*t*-Bu	dma	[52]

([a]) Tp^- = $HB(pz)_3^-$ = hydrotris(pyrazolyl)borate, dma = dimethylacetamide.

2.6. Lanthanoid Metal Ions

If we classify all the Ln-anilato compounds based on the lanthanoid metal ion, we can see that there are eighteen compounds with Y(III) (Table 13), seven with La(III) (Table 14), twelve with Ce(III) (Table 15), eight with Pr(III) (Table 16), ten with Nd(III) (Table 17), six with Sm(III) (Table 18), ten with Eu(III) (including three Dy-doped compounds, Table 19), ten with Gd(III) (Table 20), eight with Tb(III) (Table 21), eighteen with Dy(III) (Table 22), eight with Ho(III) (Table 23), eighteen with Er(III) (including one Er/Yb (1:1) compound, Table 24), three with Tm(III) (Table 25), twelve with Yb(III) (including one Er/Yb (1:1) compound, Table 26) and three with Lu(III) (Table 27).

Table 13. Structurally characterized Y(III) compounds with anilato ligands.

#	CCDC	Structure	Ln	X	L	A^+	Reference
3	DEHRAM	Dimer	Y	H	thf/Cl^-	–	[21]
7	DEKTUL	Dimer	Y	Cl	Tp^-	–	[20]
8	DEKTUL01	Dimer	Y	Cl	Tp^-	–	[22]
9	DEKVAT	Dimer	Y	Cl	Tp^-	–	[20]
10	DEKVEX	Dimer	Y	H	Tp^-	–	[20]
11	DEKVIB	Dimer	Y	CH_3	Tp^-	–	[20]
12	DEKVOH	Dimer	Y	CH_3	Tp^-	–	[20]
20	JOQSOA	Dimer	Y	F	Tp^-	–	[23]
21	JOQSUG	Dimer	Y	Br	Tp^-	–	[23]
32	DEKVUN	Tetramer	Y	CH_3	Tp^-/$(MeO)_4B$/MeOH	–	[20]
40	MIZXUO	2D-hex	Y	H	H_2O	–	[16]
63	MIZZEA	2D-dist.hex	Y	Cl	H_2O	–	[16]
97	GASMUI	2D-brickwall	Y	Cl	H_2O	–	[14]
101	GASMOC	2D-brickwall	Y	Br	H_2O	–	[14]
132	QOFBOF	2D-4,4	Y	Cl	–	NEt_4^+	[57]
133	QOFBUL	2D-4,4	Y	Cl	–	NEt_4^+	[57]
134	QOFCAS	2D-4,4	Y	Cl	–	NEt_4^+	[57]
139	QOFNUX	2D-4,4	Y	Cl	–	NEt_4^+	[57]
151	MOBBIO	3D-diam	Y	Cl	–	H_3O^+	[16]

Table 14. Structurally characterized La(III) compounds with anilato ligands.

#	CCDC	Structure	Ln	X	L	A^+	Reference
36	MIZXAU	2D-hex	La	H	H_2O	–	[16]
67	1944118	2D-dist.hex	La	Cl	H_2O	–	[45]
72	1565271	2D-dist.hex	La	Br	H_2O	–	[45]
92	KUVBIP	2D-dist.hex	La	*t*-Bu	dma	–	[52]
116	NIDLIY	2D-herringbone	La	Br	dmso	–	[51]
128	MIZYAV	2D-3,4	La	Cl	H_2O	–	[16]
147	WOXVIR	2D-4,4	La	Cl	H_2O	NEt_4^+	[58]

Table 15. Structurally characterized Ce(III) compounds with anilato ligands.

#	CCDC	Structure	Ln	X	L	A^+	Reference
42	ZOTTAD	2D-hex	Ce	H	H_2O	–	[15]
50	DIFLEM	2D-hex	Ce	Cl/CN	dmf	–	[46]
61	MIZZAW	2D-dist.hex	Ce	Cl	H_2O	–	[16]
62	MIZZAW01	2D-dist.hex	Ce	Cl	H_2O	–	[16]
73	1565272	2D-dist.hex	Ce	Br	H_2O	–	[45]
106	WOTWUA	2D-brickwall	Ce	Cl/CN	dmso	–	[47]
114	JOGHAR	2D-herringbone	Ce	Cl	H_2O	–	[54]
117	NIDLOE	2D-herringbone	Ce	Br	dmso	–	[51]
146	WOXVEN	2D-4,4	Ce	Cl	H_2O	NEt_4^+	[58]
154	JOGHIZ	3D-diam	Ce	Cl	H_2O	$DPMP^+$	[54]
155	JOGHOF	3D-diam	Ce	Cl	H_2O	PPh_4^+	[54]
156	JOGHUL	3D-noq	Ce	Cl	H_2O	PPh_3Me^+	[54]

Table 16. Structurally characterized Pr(III) compounds with anilato ligands.

#	CCDC	Structure	Ln	X	L	Reference
43	1944109	2D-hex	Pr	H	H_2O	[45]
58	MIZYID	2D-dist.hex	Pr	Cl	H_2O	[16]
74	1565273	2D-dist.hex	Pr	Br	H_2O	[45]
93	KUVBOV	2D-dist.hex	Pr	*t*-Bu	Dma	[52]
96	CAZZAE	2D-brickwall	Pr	Cl	EtOH	[13]
104	DIFLOW	2D-brickwall	Pr	Cl/CN	dmso	[46]
118	NIDLUK	2D-herringbone	Pr	Br	dmso	[51]
126	DIFLIQ	2D-herringbone	Pr	Cl/CN	Dmf	[46]

Table 17. Structurally characterized Nd(III) compounds with anilato ligands.

#	CCDC	Structure	Ln	X	L	A^+	Reference
44	1944110	2D-hex	Nd	H	H_2O	–	[45]
53	XIKNOX	2D-hex	Nd	Cl/CN	dmf	–	[48]
59	MIZYOJ	2D-dist.hex	Nd	Cl	H_2O	–	[16]
75	1565274	2D-dist.hex	Nd	Br	H_2O	–	[45]
94	KUVBUB	2D-dist.hex	Nd	t-Bu	dma	–	[52]
107	WOTXAH	2D-brickwall	Nd	Cl/CN	dmso	–	[47]
109	WOTWEK	2D-brickwall	Nd	Cl/CN	dmf	–	[47]
119	NIDMAR	2D-herringbone	Nd	Br	dmso	–	[51]
143	WOXTIP	2D-4,4	Nd	Cl	–	NEt_4^+	[58]
148	WOXVOX	2D-4,4	Nd	Cl	H_2O	NEt_4^+	[58]

Table 18. Structurally characterized Sm(III) compounds with anilato ligands.

#	CCDC	Structure	Ln	X	L	A^+	Reference
17	EDEZUL	Dimer	Sm	NO_2	H_2O	–	[26]
45	1944111	2D-hex	Sm	H	H_2O	–	[45]
68	1944120	2D-dist.hex	Sm	Cl	H_2O	–	[45]
76	1565275	2D-dist.hex	Sm	Br	H_2O	–	[45]
120	NIDMEV	2D-herringbone	Sm	Br	dmso	–	[51]
145	WOXTUB	2D-4,4	Sm	Cl	–	NEt_4^+	[58]

Table 19. Structurally characterized Eu(III) compounds with anilato ligands.

#	CCDC	Structure	Ln	X	L	A^+	Reference
30	NOQBUT	Dimer-zz	Eu	Cl/CN	H_2O	–	[27]
31	NOQGEI	Dimer-zz	Eu/Dy	Cl/CN	H_2O	–	[27]
46	1944112	2D-hex	Eu	H	H_2O	–	[45]
65	MIZZOK	2D-dist.hex	Eu	Cl	H_2O	–	[16]
77	1565276	2D-dist.hex	Eu	Br	H_2O	–	[45]
105	NOQGAE	2D-brickwall	Eu/Dy	Cl/CN	dmso	–	[27]
110	GEPZUY	2D-brickwall	Eu	Cl	bipym/H_2O	–	[49]
121	NIDFEO	2D-herringbone	Eu	Br	dmso	–	[51]
123	NOQBON	2D-herringbone	Eu/Dy	Br	dmso	–	[27]
144	WOXTOV	2D-4,4	Eu	Cl	–	NEt_4^+	[58]

Table 20. Structurally characterized Gd(III) compounds with anilato ligands.

#	CCDC	Structure	Ln	X	L	A^+	Reference
13	EDEZAR	Dimer	Gd	NO_2	H_2O	–	[26]
26	LEPNOM	Dimer	Gd	Cl	Tp^-	–	[22]
27	LEPNOM01	Dimer	Gd	Cl	Tp^-	–	[19]
37	MIZXEY	2D-hex	Gd	H	H_2O	–	[16]
57	GEQBAH	2D-dist.hex	Gd	Cl	H_2O	–	[49]
64	MIZZIE	2D-dist.hex	Gd	Cl	H_2O	–	[16]
78	1565277	2D-dist.hex	Gd	Br	H_2O	–	[45]
95	LEBGEG	2D-dist.hex	Gd	H	thf/Cl^-	–	[53]
113	GEQBEL	2D-herringbone	Gd	Cl	H_2O	–	[49]
122	NIDFIS	2D-herringbone	Gd	Br	dmso	–	[51]
136	QOFNAD	2D-4,4	Gd	Cl	–	NEt_4^+	[57]

Table 21. Structurally characterized Tb(III) compounds with anilato ligands.

#	CCDC	Structure	Ln	X	L	A^+	Reference
14	EDEZEV	Dimer	Tb	NO_2	H_2O	–	[26]
24	LEPNIG	Dimer	Tb	Cl	Tp^-	–	[22]
25	LEPNIG01	Dimer	Tb	Cl	Tp^-	–	[24]
47	1944113	2D-hex	Tb	H	H_2O	–	[45]
60	MIZYUP	2D-dist.hex	Tb	Cl	H_2O	–	[16]
79	1565278	2D-dist.hex	Tb	Br	H_2O	–	[45]
82	NIDFOY	2D-dist.hex	Tb	Br	dmso	–	[51]
140	QOFPAF	2D-4,4	Tb	Cl	–	NEt_4^+	[57]
152	EFOXUV	3D-diam	Tb	Cl	H_2O/dmf/$HCOO^-$	$NMe_2H_2^+$	[60]

Table 22. Structurally characterized Dy(III) compounds with anilato ligands.

#	CCDC	Structure	Ln	X	L	A^+	Reference
1	PIQFUT	Monomer	Dy	Cl	Tp^-	–	[19]
2	DEHQUF	Dimer	Dy	H	thf/Cl^-	–	[21]
4	DEKTOF	Dimer	Dy	Cl	Tp^-	–	[20]
5	DEKTOF01	Dimer	Dy	Cl	Tp^-	–	[22]
6	DEKTOF02	Dimer	Dy	Cl	Tp^-	–	[19]
15	EDEZIZ	Dimer	Dy	NO_2	H_2O	–	[26]
18	JOQSEQ	Dimer	Dy	Br	Tp^-	–	[23]
19	JOQSIU	Dimer	Dy	F	Tp^-	–	[23]
48	1944114	2D-hex	Dy	H	H_2O	–	[45]
51	WOTWIO	2D-hex	Dy	Cl/CN	dmf	–	[47]
55	XOYTEN	2D-hex	Dy	Cl/CN	dmf	–	[38]
69	1944123	2D-dist.hex	Dy	Cl	H_2O	–	[45]
80	1565279	2D-dist.hex	Dy	Br	H_2O	–	[45]
83	NIDFUE	2D-dist.hex	Dy	Br	dmso	–	[51]
108	XOYTUD	2D-brickwall	Dy	Cl/CN	dmso	–	[38]
125	LUTROK	2D-herringbone	Dy	Br	dmf	–	[55]
129	DIFMAJ	2D-4,4	Dy	Cl/CN	H_2O	H_3O^+	[46]
130	XOYVAL	2D-4,4	Dy	Cl/CN	H_2O	$NEt_2H_2^+$	[38]
135	QOFCEW	2D-4,4	Dy	Cl	–	NEt_4^+	[57]
150	XOYVEP	2D-(3,4)+(3,8)	Dy	Cl/CN	dmso	–	[38]

Table 23. Structurally characterized Ho(III) compounds with anilato ligands.

#	CCDC	Structure	Ln	X	L	A^+	Reference
16	EDEZOF	Dimer	Ho	NO_2	H_2O	–	[26]
23	KOZBIN	Dimer	Ho	Cl	Tp^-	–	[24]
35	KUYKIZ	2D-hex	Ho	H	H_2O	–	[43]
52	WOTWOU	2D-hex	Ho	Cl/CN	dmf	–	[47]
70	1944124	2D-dist.hex	Ho	Cl	H_2O	–	[45]
81	1565280	2D-dist.hex	Ho	Br	H_2O	–	[45]
84	NIDGAL	2D-dist.hex	Ho	Br	dmso	–	[51]
142	QOFPIN	2D-4,4	Ho	Cl	–	NEt_4^+	[57]

Table 24. Structurally characterized Er(III) compounds with anilato ligands.

#	CCDC	Structure	Ln	X	L	A^+	Reference
22	KOZBEJ	Dimer	Er	Cl	Tp^-	–	[24]
34	NIGNID	1D-ladder	Er	Cl	hmpa	–	[28]
41	PIVKAJ	2D-hex	Er	H	H_2O	–	[44]
54	XIKPAL	2D-hex	Er	Cl/CN	dmf	–	[48]
56	NIGNUP	2D-hex	Er	Cl	fma	–	[28]
66	NIGNEZ	2D-dist.hex	Er	Cl	H_2O	–	[28]
71	XAWZUT	2D-dist.hex	Er	Br	H_2O	–	[50]
85	XAXBAC	2D-dist.hex	Er	Br	dmso	–	[50]
89	POMVAR	2D-dist.hex	Yb/Er	Cl/CN	dmso	–	[37]
90	NIGQIG	2D-dist.hex	Er	Cl	dmso	–	[28]
91	NIGNOJ	2D-dist.hex	Er	Cl	dma	–	[28]
98	JOGJAT	2D-brickwall	Er	Cl	H_2O	–	[53]
115	NIGPAX	2D-herringbone	Er	Cl	dmf	–	[28]
124	XAXBEG	2D-herringbone	Er	Br	dmf	–	[50]
138	QOFNOR	2D-4,4	Er	Cl	–	NEt_4^+	[57]
149	POMVIZ	2D-(3,4)+(3,8)	Er	Cl/CN	dmso	–	[37]
153	JOGHEV	3D-diam	Er	Cl	–	$DPMP^+$	[54]
157	JOGJEX	3D-4,4-c	Er	Cl	H_2O	PPh_3Me^+	[54]

Table 25. Structurally characterized Tm(III) compounds with anilato ligands.

#	CCDC	Structure	Ln	X	L	Reference
49	1944117	2D-hex	Tm	H	H_2O	[45]
99	1944126	2D-brickwall	Tm	Cl	H_2O	[45]
102	1565282	2D-brickwall	Tm	Br	H_2O	[45]

Table 26. Structurally characterized Yb(III) compounds with anilato ligands.

#	CCDC	Structure	Ln	X	L	A^+	Reference
28	OBIBEH	Dimer	Yb	Cl	Tp^-	–	[25]
29	OBIBEH01	Dimer	Yb	Cl	Tp^-	–	[24]
38	MIZXIC	2D-hex	Yb	H	H_2O	–	[16]
86	NIDGEP	2D-dist.hex	Yb	Br	dmso	–	[51]
87	DIFLUC	2D-dist.hex	Yb	Cl/CN	dmso	–	[46]
88	POMTUJ	2D-dist.hex	Yb	Cl/CN	dmso	–	[37]
89	POMVAR	2D-dist.hex	Yb/Er	Cl/CN	dmso	–	[37]
100	1944127	2D-brickwall	Yb	Cl	H_2O	–	[45]
103	LUTRIE	2D-brickwall	Yb	Br	H_2O	–	[55]
111	QOVJUJ	2D-brickwall	Yb	Cl/CN	dmso/$dobdc^{2-}$	–	[56]
112	QOVJOD	2D-brickwall	Yb	Cl/CN	dmso/F_4bdc^{2-}	–	[56]
127	XIKNUD	2D-herringbone	Yb	Cl/CN	dmf	–	[48]
137	QOFNEH	2D-4,4	Yb	Cl	–	NEt_4^+	[57]

Table 27. Structurally characterized Lu(III) compounds with anilato ligands.

#	CCDC	Structure	Ln	X	L	A^+	Reference
33	MIZZUQ	1D + mon	Lu	Cl	H_2O	–	[16]
39	MIZXOI	2D-hex	Lu	H	H_2O	–	[16]
141	QOFPEJ	2D-4,4	Lu	Cl	–	NEt_4^+	[57]

3. Magnetic Properties

Single-Molecule and Single-Ion Magnets

Most of the magnetically characterized Ln-anilato compounds show the expected magnetic properties of isolated Ln(III) ions with the corresponding decrease in the $\chi_m T$ product when the temperature is decreased as a result of the depopulation of the excited levels that appear due to the ligand field. This behaviour confirms the absence of noticeable magnetic interactions through the anilato bridges when connecting Ln(III) ions. In fact, only when connecting transition metals, anilato bridges show weak antiferromagnetic interactions (that can be modulated by the X group) [6,61]. Although this lack of magnetic interactions may appear as a disadvantage from the magnetic point of view, the good magnetic isolation provided by the anilato ligands precludes the fast relaxation of the magnetization and allows the synthesis of Ln-anilato complexes and coordination polymers behaving as single-molecule magnets (SMMs) and single-ion magnets (SIMs) with slow relaxation of the magnetization. SMMs and SIMs are attracting many interest recently since they present memory effects and quantum phenomena that may find applications in data storage, quantum computing and spintronics [62–64]. SMMs and SIMs retain their spin orientation and show a slow relaxation of the magnetization at low temperatures that may follow different mechanisms such as: (i) Orbach (O), (ii) Raman (R), (iii) direct (D) and (iv) quantum tunnelling (QT). The O, R and D mechanisms are temperature dependent and the D and QT mechanisms are field dependent [62–64]. Usually, when several mechanisms are operative, the relaxation time is determined by the faster process and, thus, QT is operative at low temperatures (when no DC field is applied), whereas Orbach mechanism is the dominant one at high temperatures. In some cases, the application of a DC field (usually below 3000 Oe) suppress the fast relaxation through the QT mechanism. In these compounds, called field-induced-SMM of field induced-SIM (FI-SMM or FI-SIM), the application of a DC field is required to observe the slow relaxation of the magnetization and the direct mechanism may contribute to the

relaxation of the magnetization. The equation used to reproduce the relaxation rate (the inverse of the relaxation times, τ) as a function of the temperature and/or DC field includes the O, R, D and QT mechanisms as follow [62–64]:

$$\tau^{-1} = \tau_0^{-1} exp\left(\frac{-U_{eff}}{k_B T}\right) + CT^n + AH^2T + \tau_{QTM}^{-1}. \quad (1)$$

Surprisingly, the possibility to prepare Ln-anilato-based SMMs and SIMs has not been exploited until very recently (Table 28). Thus, the first Ln-anilato complexes showing SMM behaviour were reported in 2017 by Boskovic et al. in two closely related Dy(III) dimers $[(Tp)_2Dy_2(C_6O_4Cl_2)]\cdot 2CH_2Cl_2$ (**4**) and $[(Tp)_2Dy_2(C_6O_4(CH_3)_2)]\cdot 1.1CH_2Cl_2$ (**4′**) (Tp^- = hydrotris(pyrazolyl)borate = $HB(pz)_3$) [20]. Although only the structure of compound **4** was reported, compound **4′** is isostructural to the Y analogue $[(Tp)_2Y_2(C_6O_4(CH_3)_2)]\cdot 1.2CH_2Cl_2$ (**11**) [20]. Compound **4′** shows an almost temperature independent slow relaxation of the magnetization that follows a quantum tunnelling mechanism when no DC field is applied at low temperatures and when a DC field of 1600 Oe is applied, both compounds (**4** and **4′**) show slow relaxation of the magnetizations with an Orbach relaxation mechanism for **4′** with U_{eff} = 47 K and Orbach and Raman mechanisms for **4** with U_{eff} = 24 K [20].

Compound $[(Tp)_2Dy_2(C_6O_4Cl_2)]\cdot 2CH_2Cl_2$ (**4**) was almost simultaneously reported twice more (compounds **5** and **6** in Table 28) by Slageren et al. [22] and by Ishikawa et al. [19]. Both reports confirm the FI-SMM behaviour of compound **4** and complete the magnetic studies with different applied DC fields and temperature ranges. Furthermore, Slageren et al. [22] showed that when the chloranilato bridge is chemically reduced using cobaltocene, the Dy and Tb dimers (**4** and **24**, respectively) behave as SMM even with no applied DC field. Slageren also showed that when a DC field of 1000 Oe is applied, the reduced Dy derivative shows two different relaxation processes [22]. The energy barriers obtained by Slageren et al., even when the choranilato bridge was reduced, are similar to those obtained by Boskovic et al. [20] (Table 28). The third study, made by Ishikawa et al. [19], was performed with a DC field of 950 Oe and also showed a similar energy barrier for the high temperature data although now the relaxation times was fit to a model including only Raman and Direct mechanisms [19]. In this study, Ishikawa et al. also reported the monomer $[Co(Cp)_2][Dy(Tp)_2(C_6O_4Cl_2)]$ (**1**), that also behaves as a FI-SMM with an energy barrier of 49.4 K when a DC field of 1500 Oe is applied. Under this DC field, the relaxation of the magnetization of compound **1** follows Raman and Direct mechanisms [19].

Boskovic et al. [23] reported in 2019 a similar dimer to compound **4** but prepared with bromanilato instead of chloranilato: $[(Tp)_2Dy_2(C_6O_4Br_2)]$ (**18**). Compound **18** is also a FI-SMM and presents a low energy barrier of 7 K when a DC field of 390 Oe is applied. As observed in dimer **4**, when the bromanilato bridge in dimer **18** is reduced, the compound behaves as a SMM with zero applied DC field. The reduced dimer **18** also shows low energy barriers of 10.4 and 10.6 K for DC fields of 0 and 380 Oe, respectively. In all cases, the relaxation of the magnetization follows Orbach, Raman and direct mechanisms [23].

In addition, in 2019, Ishikawa et al. [24] reported the Er and Yb derivatives with chloranilato (compounds **22** and **29**, respectively, Table 28). Both compounds behave as FI-SMM and show energy barriers of 25.9 and 22.3 K, respectively, when a DC field of 1000 Oe is applied. In both cases, the relaxation times can be very well reproduced using Orbach and Raman mechanisms [24].

As can be seen in Table 28, all the above-mentioned SMM and FI-SMM complexes contain the coligand (Tp^- = hydrotris(pyrazolyl)borate = $HB(pz)_3$). The only reported dimer with SMM behaviour without the Tp^- coligand is compound $[Eu_{1.96}Dy_{0.04}(C_6O_4(CN)Cl)_3(H_2O)_{10}]\cdot 6H_2O$ (**31**) [27]. This dimer shows a zigzag structure (Figure 2d) and contains a bridging chlorocyananilato ligand. Compound **31** is also the only doped dimer with SMM behaviour (contains Eu doped with 2% of Dy) and is also the only Ln-anilato dimer showing SMM without applying a DC field or reducing the bridging anilato ligand. This compound presents an energy barrier of 25.3 K and the relaxation of the magnetization could be fit to an Orbach and Direct mechanisms, although in this case, the frequency maxima appear at high frequencies and could not be observed [27].

Besides these discrete complexes (nine dimers and one monomer, Table 28), there are also six Ln-anilato 2D lattices showing FI-SMM or even SMM (in one case). Two of these six 2D lattices are isostructural 4,4-nets showing FI-SMM behaviour: $(NEt_4)[Dy(C_6O_4Cl_2)_2]$ (**135**) and $(NEt_4)[Gd(C_6O_4Cl_2)_2]$ (**136**) [57]. In both cases, the measurements were performed with a DC field of 1000 Oe, although no analysis of the relaxation mechanisms nor the energy barrier was reported [57]. The observation of slow relaxation in compound **136** is very surprising since Gd(III) is an isotropic ion and is very unusual to observe SMM or FI-SMM behaviour in Gd(III) complexes [65]. The exact mechanism to explain this unusual behaviour is not clear yet.

The four remaining 2D lattices showing slow relaxation of the magnetization are 3,6-networks (Table 28). Three of them contain Dy(III) and bromanilato: $[Dy_2(C_6O_4Br_2)_3(H_2O)_6]\cdot 8H_2O$ (**80**) [45,55], $[Dy_2(C_6O_4Br_2)_3(dmso)_4]\cdot 2dmso\cdot 2H_2O$ (**83**) [51,55] and $[Dy_2(C_6O_4Br_2)_3(dmf)_6]$ (**125**) [55], whereas the fourth one contains Eu doped with Dy: $[Dy_{0.04}Eu_{1.96}(C_6O_4Br_2)_3(dmso)_6]\cdot 2dmso$ (**123**) [27]. Compounds **80**, **83** and **125** are three closely related compounds that, in fact, show reversible interconversion upon solvent exchange (see below) [55]. Compounds **80** and **83** show distorted hexagonal 2D lattices whereas compound **125** shows a rectangular herringbone 2D structure. Compounds **80** and **83** show slow relaxation of the magnetization under a DC field of 1000 Oe (Figure 22a), with energy barriers of 9.6 and 22.8 K, respectively (Figure 22b).

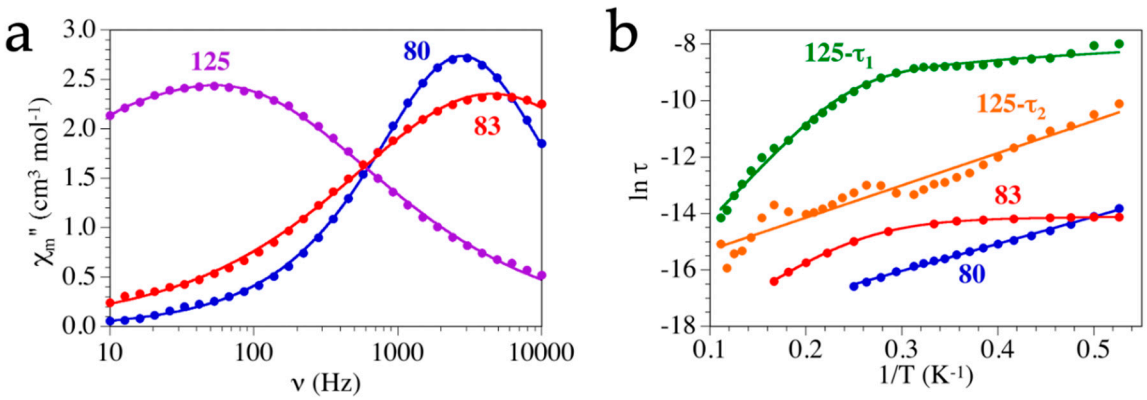

Figure 22. (**a**) Frequency dependence of χ_m'' for compounds **80**, **83** and **125** at 1.9 K with a DC field of 1000 Oe. Solid lines are the fit to the Debye model with one (in **80** and **83**) or two (in **125**) relaxation processes. (**b**) Arrhenius plot with the relaxation time for compounds **80**, **83** and **125** with a DC field of 1000 Oe. Solid lines are the fit to the general model with Orbach mechanism in **80** and the fast process (τ_2) in **125**; Orbach and direct mechanisms in the slow process (τ_1) in **125** and Orbach, direct and quantum tunnelling in **83**.

The relaxation of the magnetization follows an Orbach mechanism in compound **80**, whereas in compound **83** it follows Orbach, direct and quantum tunnelling mechanisms. Since both compounds show the same structure, Ln(III) ion and ligand, we can attribute these differences to the changes in the coordination geometry of the Dy(III) ions (TCTPR-9 in **80** vs. TDD-8 in **83**). These changes in the coordination number and geometry are due to the different sizes of the coligands (H_2O in **80** vs. dmso in **83**). Despite showing a different structure, compound **125** is closely related to compounds **80** and **83** (the only difference is that it contains dmf as coligand, instead of H_2O or dmso). Compound **125** also shows slow relaxation of the magnetization when a DC field of 1000 Oe is applied (Figure 22a), although now there are two different relaxation processes: (i) a slow relaxation process (SR) with an energy barrier of 36 K and a relaxation following Orbach and direct mechanisms and (ii) a fast relaxation (FR) process with an energy barrier of 11.4 K that relaxes following an Orbach mechanism (Figure 22b) [55]. Finally, compound **123** is the only 2D lattice showing slow relaxation of the magnetization with zero applied DC field. This compound shows an energy barrier of 40.9 K [27].

Table 28. Ln-anilato compounds with slow relaxation of the magnetization.

#	CCDC	Structure	Ln	X	Geometry[a]	A^+	L [b]	H (Oe)	U_{eff} (K)	Rel. Mec. [c]	Reference
1	PIQFUT	Mon.	Dy	Cl	SAPR-8	–	Tp^-	1500	49.4	R/D	[19]
4	DEKTOF	Dimer	Dy	Cl	TDD-8	–	Tp^-	1600	24	O/R	[20]
4′	-	Dimer	Dy	CH_3	TDD-8	–	Tp^-	1600	47	O	[20]
5	DEKTOF01	Dimer	Dy	Cl	TDD-8	–	Tp^-	1000 1000 0	39 31 [e] SMM [e]	O O O	[22]
6	DEKTOF02	Dimer	Dy	Cl	TDD-8	–	Tp^-	950	44.7	R/D	[19]
18	JOQSEQ	Dimer	Dy	Br	TDD-8	–	Tp^-	390 0 380	7 10.4 [e] 10.6 [e]	O/R/D O/R/D O/R/D	[23]
22	KOZBEJ	Dimer	Er	Cl	TDD-8	–	Tp^-	1000	25.9	O/R	[24]
24	LEPNIG	Dimer	Tb	Cl	TDD-8	–	Tp^-	0	SMM [e]	–	[22]
29	OBIBEH01	Dimer	Yb	Cl	TDD-8	–	Tp^-	1000	22.3	O/R	[24]
31	NOQGEI	Dimer-zz	Eu/Dy [d]	Cl/CN	CSAPR-9	–	H_2O	0	25.3	O/D	[27]
80	1565279	2D-hex	Dy	Br	TCTPR-9	–	H_2O	1000	9.6	O	[45,55]
83	NIDFUE	2D-hex	Dy	Br	TDD-8	–	dmso	1000	22.8	O/D/QT	[51,55]
123	NOQBON	2D-herr	Eu/Dy [d]	Br	CSAPR-9	–	dmso	0	40.9	O/D	[27]
125	LUTROK	2D-herr	Dy	Br	CSAPR-9	–	dmf	1000	11.4 (FR) 36 (SR)	O O/D	[55]
135	QOFCEW	2D-4,4	Dy	Cl	SAPR-8	NEt_4^+	–	SMM	–	–	[57]
136	QOFNAD	2D-4,4	Gd	Cl	SAPR-8	NEt_4^+	–	SMM	–	–	[57]

([a]) The geometry was determined with the program SHAPE [29–36]. SAPR-8 = square antiprism, TDD-8 = triangular dodecahedron, CSAPR-9 = capped square antiprism; ([b]) Tp^- = $HB(pz)_3^-$ = hydrotris(pyrazolyl)borate, dmso = dimthylsulfoxide, dmf = dimethylformamide; ([c]) relaxation mechanism of the magnetization: O = Orbach, R = Raman, QT = quantum tunnelling, D = direct ([d]) Eu (98%)/Dy (2%); ([e]) data with the anilato bridge reduced.

4. Optical Properties

Besides magnetic properties, all these Ln-anilato compounds may also show interesting optical properties, such as luminescence, very common in many Ln-containing compounds [66]. Furthermore, some anilato ligands such as chlorocyananilato and nitranilato, may also show luminescence in solid state [26,67] and in solution [68,69], even when they are not coordinated. Table 29 shows all the structurally characterized Ln-anilato compounds showing luminescence with the corresponding ligand- and lanthanoid-based emission bands.

The first luminescence study on a Ln-anilato compound (and the only one with chloranilato) dates back to 2004 when Kaizaki et al. [25] performed a study of the Yb(III) dimer: $[(YbTp)_2(C_6O_4Cl_2)]\cdot 2CH_2Cl_2$ (**28**). This compound shows a strong 4f-4f emission at ca. 1000 nm attributed to ligand-to-metal energy transfer from the triplet state of the chloranilato ligand to the excited 4f state of the Yb(III) ion [25]. The strong absorption band at 560 nm observed in this compound was attributed to the chloranilato ligand. In contrast, the analogue dimers with Tb(III) or Eu(III) did not show any emission, suggesting the presence of a back-transfer from the Ln(III) ions to the chloranilato ligand [25].

The other dimers showing luminescence, $[Ln_2(C_6O_4(NO_2))_3(H_2O)_{10}]\cdot 6H_2O$ with Ln = Gd (**13**), Tb (**14**), Dy (**15**), Ho (**16**) and Sm (**17**) were reported in 2016 [26]. These dimers show the emission of the nitranilato ligand, centered at ca. 590 nm. In contrast to compounds **13-15** and **17**, where the anilato ligand does not sensitize the emission of the Ln(III) ions, in compound **16** there are two emission bands from the Ho(III) ions at 531 and 643 nm, attributed to the $^5F_4 \rightarrow {}^5I_8$ and $^5F_5 \rightarrow {}^5I_8$ transitions, respectively [26]. Besides dimers, luminescence has also been very recently observed in some 2D Ln-anilato lattices. The first observation of luminescence in 2D lattices was reported in a chlorocyananilato lattice with Yb(III): $[Yb_2(C_6O_4(CN)Cl)_3(dmso)_4]\cdot 2H_2O$ (**87**) [46]. This compound shows the emission of the chlorocyananilato ligand at around 700 nm (Figure 23a), with a red shift of ca. 25 nm when compared with the free ligand in the solid $K_2(C_6O_4(CN)Cl)$ salt. Besides the ligand emission, compound **87** shows the typical emission in the NIR, at ca. 980 nm, corresponding to the $^2F_{5/2} \rightarrow {}^2F_{7/2}$

transition of the Yb(III) ion (Figure 23b) [46]. The related 2D lattices $[Pr_2(C_6O_4(CN)Cl)_3(dmso)_6]$ (**104**) and $[Pr_2(C_6O_4(CN)Cl)_3(dmf)_6]$ (**126**) also show the ligand emission at ca. 700 and 680 nm, respectively (although much weaker in **104**), but no emission from the Ln(III) ions could be observed [46].

Table 29. Ln-anilato complexes and lattices with anilato-based and/or Ln-based luminescence.

#	CCDC	Structure	Ln	X	Anilato (nm)	Ln(III) (nm)	Reference
13	EDEZAR	Dimer	Gd	NO_2	≈590	–	[26]
14	EDEZEV	Dimer	Tb	NO_2	≈590	–	[26]
15	EDEZIZ	Dimer	Dy	NO_2	≈590	–	[26]
16	EDEZOF	Dimer	Ho	NO_2	596	531, 643	[26]
17	EDEZUL	Dimer	Sm	NO_2	≈590	–	[26]
28	OBIBEH	Dimer	Yb	Cl	560	≈1000	[25]
53	XIKNOX	2D-hex	Nd	Cl/CN	≈650 ≈460 [a] 680–720 [b]	900, 1070, 1350	[48]
54	XIKPAL	2D-hex	Er	Cl/CN	≈650 ≈460 [a] 680–720 [b]	≈1550	[48]
80	1565279	2D-hex	Dy	Br	–	≈500	[55]
83	NIDFUE	2D-hex	Dy	Br	–	≈500	[55]
87	DIFLUC	Distorted 2D-hex	Yb	Cl/CN	≈700	980	[46]
88	POMTUJ	Distorted 2D-hex	Yb	Cl/CN	–	980	[37]
89	POMVAR	Distorted 2D-hex	Yb/Er	Cl/CN	–	980 1530	[37]
104	DIFLOW	2D-brick wall	Pr	Cl/CN	≈680	–	[46]
111	QOVJUJ	2D-brick wall	Yb	Cl/CN	650–900	≈1000	[56]
112	QOVJOD	2D-brick wall	Yb	Cl/CN	650–900	≈1000	[56]
125	LUTROK	2D-herr	Dy	Br	–	≈500	[55]
126	DIFLIQ	2D-herringbone	Pr	Cl/CN	≈680	–	[46]
127	XIKNUD	2D-herringbone	Yb	Cl/CN	≈650 ≈460 [a] 680–720 [b]	≈980	[48]
149	POMVIZ	2D-(3,4)+(3,8)	Er	Cl/CN	710	1530	[37]

([a]) Nanosheets suspension; ([b]) drop-casted nanosheets.

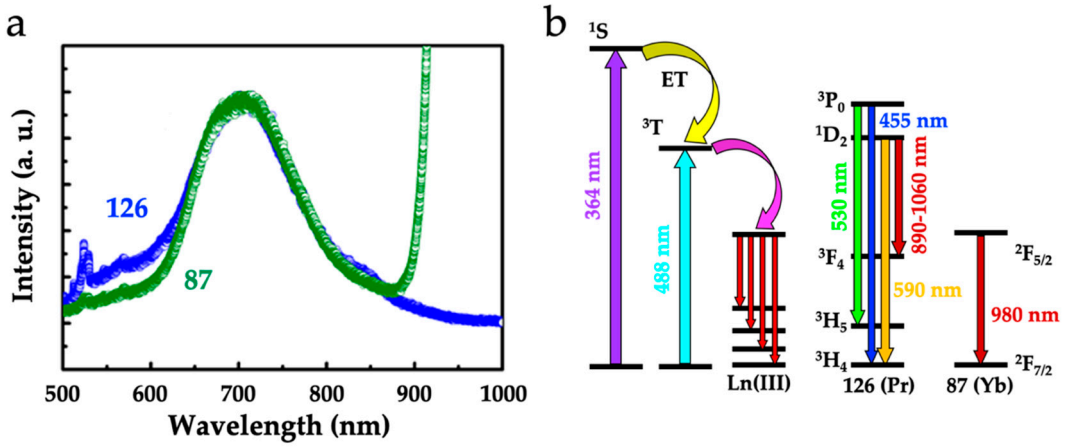

Figure 23. (**a**) Emission spectra of compounds **87** and **126** with an excitation wavelength of 364 nm. (**b**) Energy diagram with the main energy transfer and sensitization pathways in compounds **87** and **126**.

A recent study by Mercuri et al. [37] of two related series, also with the ligand chlorocyananilato and dmso as solvent, formulated as $[Ln_2(C_6O_4(CN)Cl)_3(dmso)_4]\cdot dmso$, with Ln = Yb (**88**), Yb/Er (**89**) and $[Er_2(C_6O_4(CN)Cl)_3(dmso)_6]$ (**149**) [37], showed similar results, further confirming the antenna effect of the chlorocyananilato ligand and the Ln-based emission in the NIR region. Thus, compounds **88** and **89** show an emission band at 980 nm, corresponding to the $^2F_{5/2} \rightarrow {}^2F_{7/2}$ transition in the Yb(III) ions and compounds **89** and **149** show an emission band at 1530 nm, corresponding to the $^4I_{13/2} \rightarrow {}^4I_{15/2}$ transition in the Er(III) ions [37]. These compounds show high quantum yields of 15.6% for the Yb(III) compound and 0.16% for the Er(III) one, the highest reported for coordination compounds to date. Remarkably, these properties are retained in dmso solutions and in drop-casted films [37].

A very interesting report also by Mercuri et al. [48] showed NIR emission in a family of three 2D lattices formulated as $[Ln_2(C_6O_4(CN)Cl)_3(dmf)_6]\cdot G$ with Ln/G = Nd/$2CH_2Cl_2$ (**53**), Er/$2CH_2Cl_2$ (**54**) and Yb/- (**127**). These layered compounds show the emission of the chlorocyananilato ligand at around 650 nm (with a red shift of ca. 50 nm when compared with the free ligand in the solid $KH(C_6O_4(CN)Cl)$ salt). Besides the ligand emission, the three compounds show the Ln(III) emission at ca. 900, 1070 and 1350 nm in **53**, ca. 1550 nm in **54** and ca. 980 nm in **127**, showing the antenna effect of the chlorocyananilato ligand [48]. The measurements performed on suspensions of nanosheets of these compounds show that the emission of the Ln(III) ions are similar to those of the crystals but the ligand emission appears blue-shifted at ca. 460 nm, close to the value observed for the free ligand in dilute solution. When these nanosheets are drop-casted, the Ln(III) emission remains unchanged but the ligand emission appears at ca. 680-720 nm, close to the value observed in the crystals [48].

A similar study has very recently been performed by the same team on two original Ln-anilato 2D lattices including additional coligands such as the dianion of 2,5-dihydroxybenzene-1,4-dicarboxylic acid (H_2dobdc): $[Yb_4(C_6O_4(CN)Cl)_5(dobdc)(dmso)_{10}]\cdot 2dmso$ (**111**) and the dianion of 2,3,5,6-tetrafluorobenzene-1,4-dicarboxylic acid (H_2F_4bdc): $[Yb_2(C_6O_4(CN)Cl)_2(F_4bdc)(dmso)_6]$ (**112**) [56]. These two compounds show a very broad emission from ca. 650 nm to more than 900 nm attributed to the chlorocyananilato ligand together with a much stronger emission at ca. 1000 nm from the Yb(III) ions, showing once more the antenna effect of the ligand. Studies performed on nanosheets of compounds **111** and **112** show similar photoluminescence spectra although with much weaker signals [56].

Finally, luminescence has also been reported [55] in three related 2D latices formulated as $[Dy_2(C_6O_4Br_2)_3(H_2O)_6]\cdot 8H_2O$ (**80**), $[Dy_2(C_6O_4Br_2)_3(dmso)_4]\cdot 2dmso\cdot 2H_2O$ (**83**) and $[Dy_2(C_6O_4Br_2)_3(dmf)_6]$ (**125**) that can be easily interconverted by solvent exchange and that also show FI-SMM behaviour (see above). These three compounds show an increase in the emission of the Dy(III) ion when changing the solvent from dmf (where the emission is almost completely quenched) to H_2O and dmso [55].

5. Gas/Solvent Adsorption/Absorption and Solvent Exchange

Very recently, gas and solvent adsorption and even solvent exchange have been reported in some Ln-anilato compounds (Table 30). The first observation of gas adsorption in a Ln-anilato compound was reported in the series $[Ln_2(dhbq)_3(H_2O)_6]\cdot 18H_2O$ with Ln(III) = Ho (**35**), La (**36**), Gd (**37**), Yb (**38**), Lu (**39**), Y (**40**), Er (**41**), Ce (**42**), Pr (**43**), Nd (**44**), Sm (**45**), Eu (**46**), Tb (**47**), Dy (**48**) and Tm (**49**) [45]. As described above (Figure 6d), this series contains a cluster of 18 water molecules, plus six crystallization extra water molecules, that can be easily removed when the samples are heated to 80 °C or simply under vacuum at room temperature (the total number of removed water molecules oscillates between 18 and 22) [45]. The removal of the water molecules leads to a colour change of the samples and to an almost complete collapse of the structure, as shown by the X-ray powder diffraction of the evacuated samples (Figure 24a). Studies of the reversibility of this process showed that it is fully reversible and when the dehydrated samples are immersed in water, they recover the original structure (Figure 24a). Moreover, when the dehydrated samples are immersed in different solvents, these solvents enter in the

interlayer space and, in some cases, the samples recover the crystallinity, although the new structure is not the same as the hydrated pristine sample (Figure 24b).

Table 30. Ln-anilato compounds with gas/solvent adsorption or solvent exchange capacity.

#	Formula	Ln	Structure	Properties	Reference
35–38 **41–49**	$[Ln_2(dhbq)_3(H_2O)_6]\cdot 18H_2O$	La, Ce, Pr, Nd, Sm, Eu, Gd, Tb, Dy, Ho, Er, Tm, Yb	2D-hexagonal	$-H_2O/+H_2O$ $-H_2O/+$Guess CO_2 adsorption	[45]
58–60 **62,** **64–70**	$[Ln_2(C_6O_4Cl_2)_3(H_2O)_6]\cdot nH_2O$	La, Ce, Pr, Nd, Sm, Eu, Gd, Tb, Dy, Ho, Er	Distorted 2D-hex.	$-H_2O/+H_2O$ $-H_2O/+$Guess CO_2 adsorption	[45]
71–81	$[Ln_2(C_6O_4Br_2)_3(H_2O)_6]\cdot nH_2O$	La, Ce, Pr, Nd, Sm, Eu, Gd, Tb, Dy, Ho, Er	Distorted 2D-hex.	$-H_2O/+H_2O$ $-H_2O/+$Guess CO_2 adsorption	[45]
80	$[Dy_2(C_6O_4Br_2)_3(H_2O)_6]\cdot 8H_2O$	Dy	2D-brickwall	Solv Exch.	[55]
83	$[Dy_2(C_6O_4Br_2)_3(dmso)_6]\cdot 2dmso$	Dy	Distorted 2D-hex.	Solv Exch.	[55]
125	$[Dy_2(C_6O_4Br_2)_3(dmf)_6]$	Dy	2D-herringbone	Solv Exch.	[55]
92	$[La_2(C_6O_4(t\text{-}Bu)_2)_3(dma)_4]$	La	Distorted 2D-hex.	CO_2 abs	[52]
93	$[Pr_2(C_6O_4(t\text{-}Bu)_2)_3(dma)_4]$	Pr	Distorted 2D-hex.	CO_2 abs	[52]
94	$[Nd_2(C_6O_4(t\text{-}Bu)_2)_3(dma)_4]$	Nd	Distorted 2D-hex.	CO_2 abs	[52]
99–100	$[Ln_2(C_6O_4Cl_2)_3(H_2O)_6]\cdot nH_2O$	Tm, Yb	2D-brickwall	$-H_2O/+H_2O$ $-H_2O/+$Guess	[45]
102–103	$[Ln_2(C_6O_4Br_2)_3(H_2O)_6]\cdot nH_2O$	Tm, Yb	2D-brickwall	$-H_2O/+H_2O$ $-H_2O/+$Guess	[45]
131	$(NEt_4)[Y(C_6O_4Cl_2)_2]\cdot 1.4CS_2$	Y	2D-4,4	1.4 CS_2 abs	[57]
132	$(NEt_4)[Y(C_6O_4Cl_2)_2]$	Y	2D-4,4	$N_2/H_2/CO_2/CH_4$	[57]
133	$(NEt_4)[Y(C_6O_4Cl_2)_2]\cdot 1.9I_2$	Y	2D-4,4	1.9 I_2 abs	[57]
134	$(NEt_4)[Y(C_6O_4Cl_2)_2]\cdot 0.9Br_2$	Y	2D-4,4	0.9 Br_2 abs	[57]

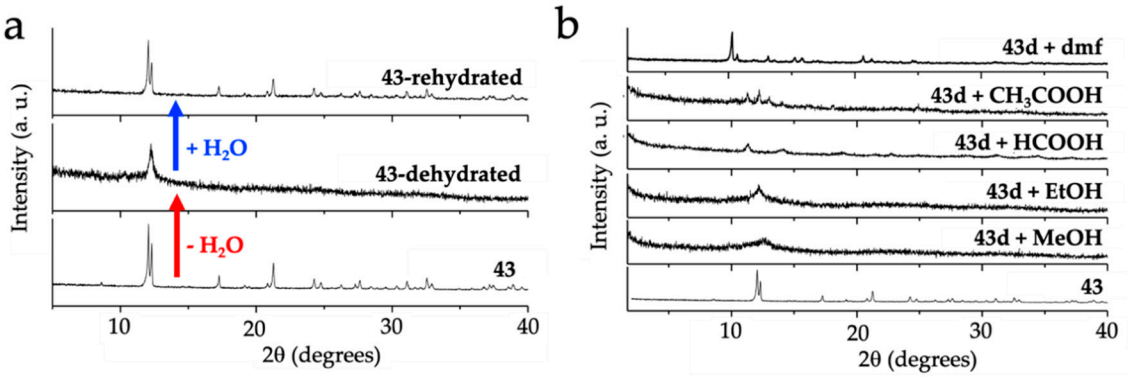

Figure 24. (**a**) X-ray powder diffractogram of compound $(Pr_2(dhbq)_3(H_2O)_6)\cdot 18H_2O$ (**43**), its dehydrated form and the rehydrated one, showing the collapse of the structure upon dehydration and the reversibility of the process. (**b**) X-ray powder diffractogram of compound **43** and the solvated compounds obtained from the dehydrated compound (**43d**) by immersion in different solvents.

The evacuation of the water molecules in compounds **35-38** and **41-49** leaves empty hexagonal cavities where, besides other solvents, it is also possible to insert gases (Figure 25a). Thus, the dehydrated compounds show CO_2 uptake with a maximum of ca. one CO_2 molecule per hexagonal cavity at 0 °C and 100 kPa (Figure 25b) [45].

Similar results have also been observed in the corresponding series with chloranilato, formulated as $[Ln_2(C_6O_4Cl_2)_3(H_2O)_6]\cdot nH_2O$, with Ln(III) = Pr (**58**), Nd (**59**), Tb (**60**), Ce (**61** and **62**), Y (**63**), Gd (**64**), Eu (**65**), Er (**66**), La (**67**), Sm (**68**), Dy (**69**), Ho (**70**), Tm (**99**) and Yb (**100**) [45] and with bromanilato, formulated as $[Ln_2(C_6O_4Br_2)_3(H_2O)_6]\cdot nH_2O$ with Ln/n = La/9 (**72**), Ce/8 (**73**), Pr/11 (**74**), Nd/7 (**75**), Sm/10 (**76**), Eu/6 (**77**), Gd/8 (**78**), Tb/10 (**79**), Dy/8 (**80**), Ho/10 (**81**), Er/7 (**71**), Tm/5.5 (**102**) and Yb/3.5 (**103**) [45]. The main difference is that in these two series, the structure does not collapse upon dehydration (only some reflections are lost), probably because now, in contrast with the $dhbq^{2-}$ series, the water molecules do not play any structural role since they are located in the distorted hexagonal or rectangular cavities and in the interlayer space.

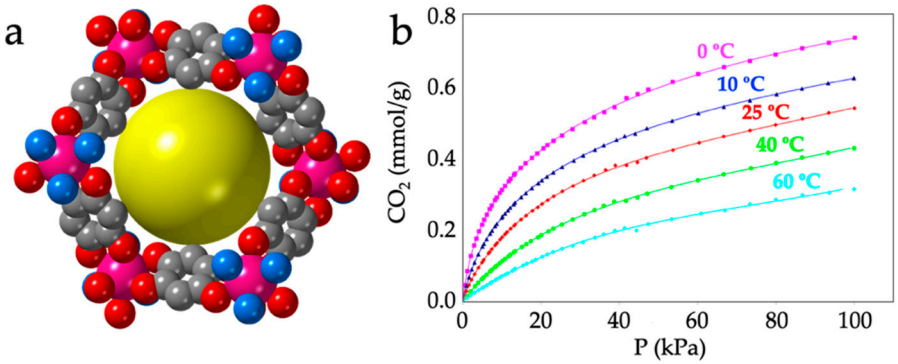

Figure 25. (**a**) View of an empty hexagonal cavity in compounds **35**-**49**. (**b**) Adsorption isothermal for CO_2 uptake at different temperatures for compound **43**.

There are two other very recently published studies showing gas/solvent uptake in Ln-anilato compounds [52,57]. The first one is a very interesting study performed on compound $(NEt_4)[Y(C_6O_4Cl_2)_2]$ (**132**), a square 2D-4,4 anionic lattice (Figure 16f) that shows reversible CS_2, I_2 and Br_2 uptake, while keeping the crystallinity [57]. This uptake capacity has allowed the synthesis of compounds $(NEt_4)[Y(C_6O_4Cl_2)_2]\cdot nG$ with nG = 1.43 CS_2 (**131**), 1.87 I_2 (**133**) and 0.91 Br_2 (**134**) [57]. Additionally, compound **132** can also uptake N_2, H_2, CO_2 and CH_4 in its square channels, with high binding enthalpies, among the highest reported for porous coordination polymers, as clearly evidenced by the corresponding adsorption isotherms and by a neutron diffraction study that allowed to determine the location of the adsorbed molecules and their interactions with the lattice [57].

The second study has been published very recently for compounds $[Ln_2(C_6O_4(t\text{-}Bu)_2)_3(dma)_4]$ with Ln = La (**92**), Pr (**93**) and Nd (**94**) (Figure 11c). As expected, given the bulky *t*-Bu groups in the anilato ligands, this study has shown a low porosity with CO_2 adsorption isotherms typical of microporous materials [52].

Finally, we have very recently reported three examples of direct solvent exchange without the need to evacuate the pristine compounds [55]. This study shows that it is possible to exchange the solvent molecules, even the coordinated ones, by immersing compounds $[Dy_2(C_6O_4Br_2)_3(H_2O)_6]\cdot 8H_2O$ (**80**), $[Dy_2(C_6O_4Br_2)_3(dmf)_6]$ (**83**), or $[Dy_2(C_6O_4Br_2)_3(dmso)_4]\cdot 2dmso\cdot 2H_2O$ (**125**) in any of the two other solvents (Figure 26). Interestingly, the three compounds present slow relaxation of the magnetization with different relaxation mechanisms and relaxation times (Table 28) that can be easily modified by simple immersion in the desired solvent [55].

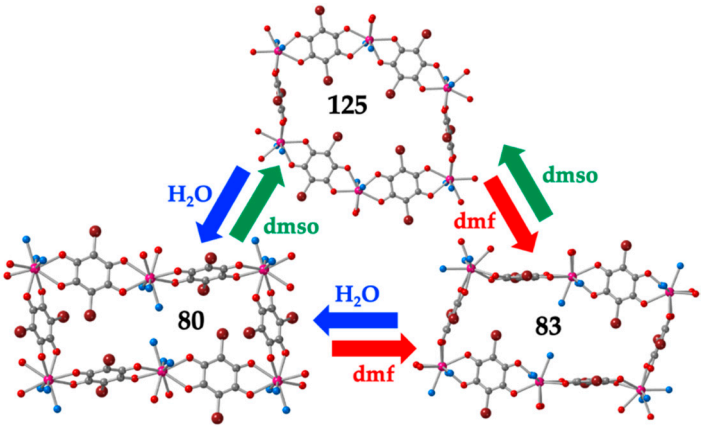

Figure 26. Solvent exchange scheme between compounds $[Dy_2(C_6O_4Br_2)_3(H_2O)_6]\cdot 8H_2O$ (**80**), $[Dy_2(C_6O_4Br_2)_3(dmf)_6]$ (**83**) and $[Dy_2(C_6O_4Br_2)_3(dmso)_4]\cdot 2dmso\cdot 2H_2O$ (**125**).

6. Redox Studies

An additional interesting aspect of the anilato ligands is the possibility to be chemically or electrochemically reduced by one or two electrons to form the semiquinoid and cathecolato forms, respectively (Scheme 1b). This possibility has been studied in several of the reported dimers in order to try to increase the magnetic exchange through the anilato bridge and to improve the SMM properties of these dimers. Interestingly, all the reported compounds with reduced anilato bridges are dimers and have been reported in the last three years (Table 31).

The first reduction study was performed by Molainen et al. [21] in compounds $[Ln_2(C_6O_4H_2)(thf)_6Cl_4]$; Ln = Dy (**2**) and Y (**3**) (Figure 2a). This study showed a one electron reduction process in the $dhbq^{2-}$ bridge in both compounds to generate the radical $(dhbq^{3-})\cdot$ that could be easily detected with electron paramagnetic resonance (EPR) spectroscopy. In this report, both compounds could be reduced electrochemically and chemically using tetrakis-(dimethylamino)ethylene (TDAE) as reducing agent [21].

A second study, published almost simultaneously, by Boskovic et al. [20] on compounds $[(LnTp)_2(C_6O_4X_2)]\cdot G$ with Ln/X/G = Dy/Cl/$2CH_2Cl_2$ (**4**), Y/Cl/$2CH_2Cl_2$ (**7**), Y/Cl/$2Me_2CO$ (**9**), Y/CH_3/$1.2CH_2Cl_2$ (**11**) and Y/CH_3/4.5MeOH (**12**) shows two reduction processes (one reversible and one quasi-reversible) and one oxidation irreversible process in the cyclic voltammetry. Attempts to chemically reduce the chloranilate derivatives **4**, **7** and **9** with cobaltocene in anaerobic and anhydrous conditions led to a colour change from purple to green, indicative of a chemical reduction, but the reduced compounds could not be isolated [20].

A third study, published a few months later on the closely related compounds $[(LnTp)_2(C_6O_4X_2)]\cdot G$ with Ln/X/G = Dy/Cl/$2CH_2Cl_2$ (**5**), Y/Cl/$2CH_2Cl_2$ (**8**), Tb/Cl/$2CH_2Cl_2$ (**24**) and Gd/Cl/$2CH_2Cl_2$ (**26**) [22] showed very similar results to those previously reported on the same series of compounds although now, the authors were able to prepare the reduced products with cobaltocene as cation and could measure an antiferromagnetic coupling of -4.17 cm^{-1} in the Gd(III) derivative, confirming that the magnetic coupling is much higher when the anilato bridge is in its radical semiquinone form [22].

Finally, a more recent cyclic voltammetry study performed on the series of dimers $[(LnTp)_2(C_6O_4Br_2)]\cdot 2CH_2Cl_2$ with Ln = Dy (**18**) and Y (**21**) [23] also shows the presence of one reversible and one quasi-reversible reduction processes and one irreversible oxidation process in both compounds. As in other similar examples, compounds **18** and **21** could also be reduced chemically with cobaltocene, although only amorphous solids could be isolated [23].

Table 31. Ln-anilato compounds with reduced anilato ligands.

#	CCDC	Structure	Ln	X	Redox processes	Reductant [a]	Reference
2	DEHQUF	Dimer	Dy	H	1 red.	Electrochem/TDAE	[21]
3	DEHRAM	Dimer	Y	H	1 red.	Electrochem/TDAE	[21]
4	DEKTOF	Dimer	Dy	Cl	2 red./1 oxid.	Electrochem/$Co(Cp)_2$	[20]
5	DEKTOF01	Dimer	Dy	Cl	2 red.	Electrochem/$Co(Cp)_2$	[22]
7	DEKTUL	Dimer	Y	Cl	2 red./1 oxid.	Electrochem/$Co(Cp)_2$	[20]
8	DEKTUL01	Dimer	Y	Cl	2 red.	Electrochem/$Co(Cp)_2$	[22]
9	DEKVAT	Dimer	Y	Cl	2 red./1 oxid.	Electrochem/$Co(Cp)_2$	[20]
11	DEKVIB	Dimer	Y	CH_3	2 red./1 oxid.	Electrochem.	[20]
12	DEKVOH	Dimer	Y	CH_3	2 red./1 oxid.	Electrochem.	[20]
18	JOQSEQ	Dimer	Dy	Br	2 red./1 oxid.	Electrochem/$Co(Cp)_2$	[23]
21	JOQSUG	Dimer	Y	Br	2 red./1 oxid.	Electrochem/$Co(Cp)_2$	[23]
24	LEPNIG	Dimer	Tb	Cl	2 red.	Electrochem/$Co(Cp)_2$	[22]
26	LEPNOM	Dimer	Gd	Cl	2 red.	Electrochem/$Co(Cp)_2$	[22]

([a]) TDAE = tetrakis-(dimethylamino)ethylene; $Co(Cp)_2$ = cobaltocene.

7. Thin Films

Since most of the Ln-anilato compounds crystallize as neutral layers, with general formula $[Ln_2(C_6O_4X_2)_3(L)_n]$, several recent attempts to delaminate these 2D materials in thin films with nanometric dimensions have been performed (Table 32). The aim is to prepare crystalline thin films with a few monolayers showing properties such as luminescence, gas adsorption, or solvent exchange, in order to prepare thin film devices with potential applications as sensors.

The first compounds that have been delaminated as nanometric thin films are the series $[Ln_2(dhbq)_3(H_2O)_6]\cdot 18H_2O$ with Ln(III) = Ce (**42**), Nd (**44**), Eu (**46**) and Dy (**48**) [45]. These compounds were dispersed in different solvents such as acetone, methanol and ethanol and sonicated during ten minuntes to obtain suspensions with nanosheets showing the Tyndall effect that confirms the presence of nanosheets in the suspensions (Figure 27a). By simply drop-casting these suspensions, it was possible to prepare nanosheets with lateral dimensions of a few microns (Figure 27b) and thickness of a few nanometers, corresponding to a few monolayers (Figure 27c).

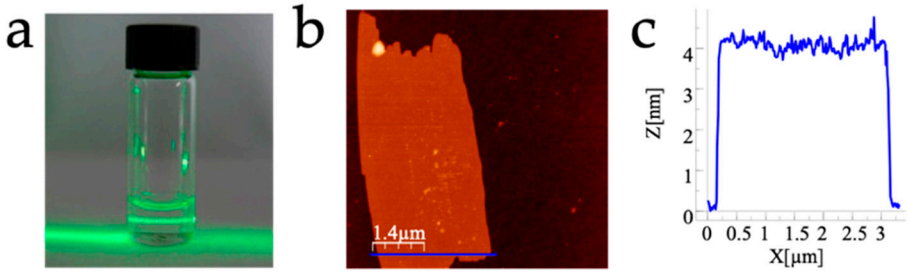

Figure 27. (**a**) Tyndall effect in compound **42**. (**b**) AFM image of a drop-casted thin film of compound **42**. (**c**) Height profile of the thin film showed in (**b**).

A similar procedure allowed the preparation of thin films with a few monolayers of one chloranilato: $[Tm_2(C_6O_4Cl_2)_3(H_2O)_6]\cdot 8H_2O$ (**99**) and two bromanilato: $[Ln_2(C_6O_4Br_2)_3(H_2O)_6]\cdot nH_2O$ with Ln/n = Er/7 (**71**) and Sm/10 (**76**) compounds [45].

Table 32. Ln-anilato compounds prepared as thin films.

#	CCDC	Compound	Ln	X	Film thickness	Reference
42	ZOTTAD	$[Ce_2(dhbq)_3(H_2O)_6]\cdot 18H_2O$	Ce	H	3–4 monolayers	[45]
44	1944110	$[Nd_2(dhbq)_3(H_2O)_6]\cdot 18H_2O$	Nd	H	3–4 monolayers	[45]
46	1944112	$[Eu_2(dhbq)_3(H_2O)_6]\cdot 18H_2O$	Eu	H	5–6 monolayers	[45]
48	1944114	$[Dy_2(dhbq)_3(H_2O)_6]\cdot 18H_2O$	Dy	H	4–5 monolayers	[45]
99	1944126	$[Tm_2(C_6O_4Cl_2)_3(H_2O)_6]\cdot 8H_2O$	Tm	Cl	3–4 monolayers	[45]
71	XAWZUT	$[Er_2(C_6O_4Br_2)_3(H_2O)_6]\cdot 7H_2O$	Er	Br	6–7 monolayers	[45]
76	1565275	$[Sm_2(C_6O_4Br_2)_3(H_2O)_6]\cdot 10H_2O$	Sm	Br	4–5 monolayers	[45]
53	XIKNOX	$[Nd_2(C_6O_4(CN)Cl)_3(dmf)_6]\cdot 2CH_2Cl_2$	Nd	Cl/CN	1–4 monolayers	[48]
54	XIKPAL	$[Er_2(C_6O_4(CN)Cl)_3(dmf)_6]\cdot 2CH_2Cl_2$	Er	Cl/CN	1–4 monolayers	[48]
88	POMTUJ	$[Yb_2(C_6O_4(CN)Cl)_3(dmso)_4]\cdot dmso$	Yb	Cl/CN	–	[37]
89	POMVAR	$[YbEr_2(C_6O_4(CN)Cl)_3(dmso)_4]\cdot dmso$	Yb/Er	Cl/CN	–	[37]
111	QOVJUJ	$[Yb_4(C_6O_4(CN)Cl)_5(dobdc)(dmso)_{10}]\cdot 2dmso$ [a]	Yb	Cl/CN	1-5 monolayers	[56]
112	QOVJOD	$[Yb_2(C_6O_4(CN)Cl)_2(F_4bdc)(dmso)_6]$ [b]	Yb	Cl/CN	1-5 monolayers	[56]
127	XIKNUD	$[Yb_2(C_6O_4(CN)Cl)_3(dmf)_6]$	Yb	Cl/CN	1–4 monolayers	[48]
149	POMVIZ	$[Er_2(C_6O_4(CN)Cl)_3(dmso)_6]$	Er	Cl/CN	–	[37]

([a]) $dobdc^{2-}$ = dianion of 2,5-dihydroxybenzene-1,4-dicarboxylic acid; ([b]) the dianion of 2,3,5,6-tetrafluorobenzene-1, 4-dicarboxylic acid (H_2F_4bdc).

The series $[Ln_2(C_6O_4(CN)Cl)_3(dmf)_6]\cdot G$ with Ln/G = Nd/$2CH_2Cl_2$ (**53**), Er/$2CH_2Cl_2$ (**54**) and Yb/- (**127**) has also been prepared as thin films, with a thickness of 1-4 monolayers and a few microns lateral dimensions, using the same wet sonication and drop-casting method [48]. This method has also recently been used to prepare thin films of compounds $[Ln_2(C_6O_4(CN)Cl)_3(dmso)_4]\cdot dmso$, with Ln = Yb (**88**), Yb/Er (**89**) and $[Er_2(C_6O_4(CN)Cl)_3(dmso)_6]$ (**149**), although the thickness of the drop-casted films was not reported [37].

Finally, there are two more Ln-anilato compounds that have been prepared as thin films: $[Yb_4(C_6O_4(CN)Cl)_5(dobdc)(dmso)_{10}]\cdot 2dmso$ (**111**) and $[Yb_2(C_6O_4(CN)Cl)_2(F_4bdc)(dmso)_6]$ (**112**). Nanosheets with 1-5 monolayers thickness and a few microns lateral dimensions of these compounds, prepared with the same sonication plus drop-casting method, have been very recently reported [56].

8. Conclusions

The rich coordination chemistry of anilato-type ligands when combined with Ln(III) ions, including La, Y and Lu, has produced in the last two decades around 150 different complexes and coordination polymers. In all these compounds, the anilato ligands act as bidentate or bis-bidentate, connecting two Ln(III) ions to generate monomers, dimers, tetramers, chains, layers, or 3D structures. These Ln-anilato compounds can be classified according to the dimensionality, nuclearity and topology into: (i) monomers (only two reported compounds); (ii) dimers (twenty-five reported compounds); (iii) tetramers (only one reported compound); (iv) chains (only two reported examples: a zigzag and a ladder chain); (v) regular hexagonal honeycomb layers (twenty-two prepared compounds); (vi) distorted hexagonal layers (thirty-nine prepared compounds); (vii) rectangular brick-wall type layers (seventeen known examples); (viii) rectangular herringbone type layers (fifteen reported cases); (ix) other 2D structures, including one (3,4)-gon lattice, twenty (4,4)-gon lattices and two mixed (3,4)+(3,8)-gon lattices and (x) 3D structures, including five adamantane, one 3D-noq and one 3D-4,4-c lattices.

These more than one hundred and fifty Ln-anilato compounds prepared to date include sixty-three examples with chloranilato (X = Cl), thirty-one with bromanilato (X = Br), twenty-five with the asymmetric chlorocyananilato (X = Cl and CN), nineteen with $dhbq^{2-}$ (X = H), five with nitranilato (X = NO_2), three with methylanilato (X = CH_3), three with tert-butylanilato (X = *t*-Bu) and two with fluoranilato.

If we look at the Ln(III) ions combined with anilato ligands, we can see that Y(III), Dy(III) and Er(III) are the most used lanthanoids, with eighteen compounds of each. There are twelve compounds with Ce(III) and Yb(III), ten compounds with Nd(III), Eu(III) and Gd(III); eight compounds with Pr(III), Tb(III) and Ho(III); seven with La(III); and three with Tm(III) and Lu(III). That Dy(III), Er(III) and Y(III) are the most used ones to date is not casual. Y(III) was largely used in the first studies since it crystallizes very easily, whereas Dy(III) and Er(III) are being used more recently in the search of SMMs and SIMs.

The good magnetic isolation provided by the anilato ligands constitutes an advantage to obtain slow relaxation of the magnetization of the Ln(III) ions. Thus, a total of fourteen single-molecule and single-ion magnets have been prepared to date with Ln(III) and anilato ligands. These fourteen examples include one monomer, seven dimers and six 2D lattices (two hexagonal 3,6-gon, two herringbone 3,6-gon and two square 4,4-gon lattices). In most cases, these compounds behave as field-induced-SMM or SIM since the application of a DC field (usually around 1000 Oe) is needed to suppress the fast relaxation of the magnetization through a quantum tunnelling mechanism. In a few dimers, the anilato bridge has been reduced, increasing the magnetic coupling and giving rise to SMM with no DC field applied. Doping an Eu layer with 2% of Dy(III) also results in a SMM behaviour with no applied DC field. As expected, most of these SMMs and SIMs have been prepared with Dy(III) ions, although there is one example with Yb(III), one with Er(III) and even one with the isotropic Gd(III) ion.

Given the well-known luminescence on many Ln(III) compounds and the, less known, luminescence shown by some anilato ligands, in the last three years a total of seventeen Ln-anilato compounds have been reported to present luminescence either from the ligand, from the Ln(III) ion, or from both. In most cases, the emission from the ligand, centred at around 590–720 nm, coexist with the NIR emission of the Ln(III) ions (in the Yb, Er, Ho and Nd compounds). Interestingly, the luminescence is essentially maintained (although with slight shifts in the emission bands) when the compounds are delaminated and prepared as drop-casted thin films.

Also, recently, some of these layered coordination polymers have shown a remarkable capacity to release the solvent molecules (usually water) located between the layers by gentle heating or under vacuum at room temperature. This dehydration results in a collapse of the crystal structure that can be easily fully recovered by immersing the dehydrated compounds in water. Furthermore, besides this reversible water release/uptake, some dehydrated compounds also show the capacity to adsorb other solvents, keeping the original structure or giving rise to novel crystal structures. Interestingly, the dehydrated compounds can also adsorb gas molecules such as H_2, N_2, CH_4 and CO_2.

A very recent study has also shown a remarkable solvent exchange capacity in three layered compounds without the need to previously evacuate the original solvent molecules. This result opens the way to the synthesis of different solvates starting from one on them.

The capacity of the anilato ligands to be reduced to the corresponding semiquinone and cathecolato forms has also been checked in some Ln-anilato dimers, electrochemically and chemically, resulting in an increase of the magnetic coupling between the Ln(III) ions and in the observation of slow relaxation of the magnetization even with zero applied DC field.

Last, but not least, these layered materials can be easily delaminated and drop-casted in thin films with a few monolayers thickness and micrometric lateral dimensions. Interestingly, the optical properties are retained in these thin films.

The future directions of these Ln-anilato based materials are many and very promising. Thus, the great variety of structures will soon increase with the synthesis of novel compounds with other coordinating solvents and coligands, specially, with bridging ones. Furthermore, some very recent results have shown the possibility to modulate, at will, the dimensionality of these, in some cases, porous materials. This capacity may lead to the synthesis of 2D and 3D structures with predetermined porous sizes and dimensionalities. The use of different X groups in the anilato rings will allow a modulation not only of the size but also the nucleophilicity and hydrophilicity of the cavities, channels and interlaminar spaces created in these structures. The use of different templating cations in

the anionic Ln-anilato lattices, constitute another very interesting tool to control the dimensionality and properties of these materials.

Besides the structural aspects, the magnetic properties of these materials constitute a second interesting aspect worth to investigate. The use of different very asymmetric coligands may lead to an increase in the anisotropy of the Ln(III) coordination geometry that may result in an increase in the energy barriers and blocking temperatures of these SMMs and SIMs.

The luminescence displayed by many Ln(III) ions and their sensitivity to changes in their coordination environments is another important aspect to exploit and develop. Furthermore, given the gas absorption capacity and solvent or ligand exchange ability shown by some of these materials, they are promising candidates to prepare devices with sensing capacity towards different gas, solvent and ionic species. The capacity to be delaminated into large thin films with a few nanometers thickness represents an additional advantage for this purpose.

Finally, the redox activity of the anilato ligand adds additional potentialities to these materials since the reduced materials might be good electronic conductors or semiconductors (specially, if combined with Ce(III), Eu(III) or Yb(III) that have two accessible oxidation states) [70] and may also show promising magnetic properties as already shown by some Ln(III)-anilato-Ln(III) dimers with reduced anilato bridges. Finally, they may also find applications as redox/luminescent sensors since their electronic and optical properties change dramatically upon reduction of the anilato ligands.

In summary, all the above-mentioned properties in these Ln-anilato compounds render them as good candidates to prepare devices with potential applications.

CCDC-1944109-14, 1944117, 1944118, 1944120, 1944123, 1944124, 1565271-80, 1944126, 1944127 and 1565282 contain the crystallographic data for compounds **43-48**, **49**, **67**, **68**, **69**, **70**, **72-81**, **99**, **100** and **102**, respectively. These data can be obtained free of charge from The Cambridge Crystallographic Data Centre at www.ccdc.cam.ac.uk/data_request/cif.

Author Contributions: Both authors contributed equally to the manuscript. All authors have read and agreed to the published version of the manuscript.

Funding: This research was founded by the Spanish MINECO (project CTQ2017-87201-P AEI/FEDER, UE) and the Generalidad Valenciana (project PrometeoIII/2019/076) for financial support.

Acknowledgments: We also thank all the coauthors that appear in our contributions in this field.

Conflicts of Interest: The authors declare no conflict of interest.

References

1. Fordham, S.; Wang, X.; Bosch, M.; Zhou, H. Lanthanide Metal-Organic Frameworks: Syntheses, Properties and Potential Applications. *Struct. Bond.* **2015**, *163*, 1–27.
2. Wang, C.; Liu, X.; Keser Demir, N.; Chen, J.P.; Li, K. Applications of Water Stable Metal-Organic Frameworks. *Chem. Soc. Rev.* **2016**, *45*, 5107–5134. [CrossRef] [PubMed]
3. Liu, X.; Fu, W.; Bouwman, E. One-Step Growth of Lanthanoid Metal-Organic Framework (MOF) Films Under Solvothermal Conditions for Temperature Sensing. *Chem. Commun.* **2016**, *52*, 6926–6929. [CrossRef] [PubMed]
4. Kitagawa, S.; Kawata, S. Coordination Compounds of 1,4-Dihydroxybenzoquinone and its Homologues. Structures and Properties. *Coord. Chem. Rev.* **2002**, *224*, 11–34. [CrossRef]
5. Benmansour, S.; Vallés-García, C.; Gómez-Claramunt, P.; Mínguez Espallargas, G.; Gómez-García, C.J. 2D and 3D Anilato-Based Heterometallic M(I)M(III) Lattices: The Missing Link. *Inorg. Chem.* **2015**, *54*, 5410–5418. [CrossRef] [PubMed]
6. Atzori, M.; Benmansour, S.; Mínguez Espallargas, G.; Clemente-León, M.; Abhervé, A.; Gómez-Claramunt, P.; Coronado, E.; Artizzu, F.; Sessini, E.; Deplano, P.; et al. A Family of Layered Chiral Porous Magnets Exhibiting Tunable Ordering Temperatures. *Inorg. Chem.* **2013**, *52*, 10031–10040. [CrossRef]
7. Jeon, I.; Negru, B.; Duyne, R.P.V.; Harris, T.D. A 2D Semiquinone Radical-Containing Microporous Magnet with Solvent-Induced Switching from T_c = 26 to 80 K. *J. Am. Chem. Soc.* **2015**, *137*, 15699–15702. [CrossRef]

8. Atzori, M.; Artizzu, F.; Sessini, E.; Marchio, L.; Loche, D.; Serpe, A.; Deplano, P.; Concas, G.; Pop, F.; Avarvari, N.; et al. Halogen-Bonding in a New Family of Tris(Haloanilato)Metallate(III) Magnetic Molecular Building Blocks. *Dalton Trans.* **2014**, *43*, 7006–7019. [CrossRef]
9. Benmansour, S.; Gómez-Claramunt, P.; Vallés-García, C.; Mínguez Espallargas, G.; Gómez García, C.J. Key Role of the Cation in the Crystallization of Chiral Tris(Anilato)Metalate Magnetic Anions. *Cryst. Growth Des.* **2016**, *16*, 518–526. [CrossRef]
10. Abrahams, B.F.; Grannas, M.J.; Hudson, T.A.; Hughes, S.A.; Pranoto, N.H.; Robson, R. Synthesis, Structure and Host-Guest Properties of $(Et_4N)_2[Sn^{IV}Ca^{II}(Chloranilate)_4]$, a New Type of Robust Microporous Coordination Polymer with a 2D Square Grid Structure. *Dalton Trans.* **2011**, *40*, 12242–12247. [CrossRef]
11. Benmansour, S.; Gómez-García, C.J. A Heterobimetallic Anionic 3,6-Connected 2D Coordination Polymer Based on Nitranilate as Ligand. *Polymers* **2016**, *8*, 89. [CrossRef] [PubMed]
12. Kanda, S.; Saito, Y. Synthesis of Co-Ordination Compounds of High Molecular Weight. *Bull. Chem. Soc. Jpn.* **1957**, *30*, 192–193. [CrossRef]
13. Riley, P.E.; Haddad, S.F.; Raymond, K.N. Preparation of Praseodymium(III) Chloranilate and the Crystal Structures of $Pr_2(C_6Cl_2O_4)_3.8C_2H_5OH$ and $Na_3[C_6H_2O(OH)(SO_3)_2].H_2O$. *Inorg. Chem.* **1983**, *22*, 3090–3096. [CrossRef]
14. Christian, R. Complexes with Substituted 2,5-Dihydroxy-p-Benzoquinones: The Inclusion Compounds $[Y(H_2O)_3]_2$ $(C_6Cl_2O_4)_3{\cdot}6.6H_2O$ and $[Y(H_2O)_3]_2$ $(C_6Br_2O_4)_3{\cdot}6H_2O$. *Mater. Res. Bull.* **1987**, *22*, 1483–1491.
15. Abrahams, B.F.; Coleiro, J.; Hoskins, B.F.; Robson, R. Gas Hydrate-Like Pentagonal Dodecahedral $M_2(H_2O)_{18}$ Cages (M = Lanthanide or Y) in 2,5-Dihydroxybenzoquinone-Derived Coordination Polymers. *Chem. Commun.* **1996**, 603–604. [CrossRef]
16. Abrahams, B.F.; Coleiro, J.; Ha, K.; Hoskins, B.F.; Orchard, S.D.; Robson, R. Dihydroxybenzoquinone and Chloranilic Acid Derivatives of Rare Earth Metals. *J. Chem. Soc. Dalton Trans.* **2002**, 1586–1594. [CrossRef]
17. Mercuri, M.L.; Congiu, F.; Concas, G.; Sahadevan, S.A. Recent Advances on Anilato-Based Molecular Materials with Magnetic and/or Conducting Properties. *Magnetochemistry* **2017**, *3*, 17. [CrossRef]
18. Benmansour, S.; Gómez-García, C.J. Heterometallic Anilato-Based Layered Magnets. *Gen. Chem.* **2020**, *6*, 190033. [CrossRef]
19. Ishikawa, R.; Michiwaki, S.; Noda, T.; Katoh, K.; Yamashita, M.; Matsubara, K.; Kawata, S. Field-Induced Slow Magnetic Relaxation of Mono- and Dinuclear Dysprosium(III) Complexes Coordinated by a Chloranilate with Different Resonance Forms. *Inorganics* **2018**, *6*, 7. [CrossRef]
20. Dunstan, M.A.; Rousset, E.; Boulon, M.; Gable, R.W.; Sorace, L.; Boskovic, C. Slow Magnetisation Relaxation in Tetraoxolene-Bridged Rare Earth Complexes. *Dalton Trans.* **2017**, *46*, 13756–13767. [CrossRef]
21. Moilanen, J.O.; MansikkamÃ¤ki, A.; Lahtinen, M.; Guo, F.; Kalenius, E.; Layfield, R.A.; Chibotaru, L.F. Thermal Expansion and Magnetic Properties of Benzoquinone-Bridged Dinuclear Rare-Earth Complexes. *Dalton Trans.* **2017**, *46*, 13582–13589. [CrossRef] [PubMed]
22. Zhang, P.; Perfetti, M.; Kern, M.; Hallmen, P.P.; Ungur, L.; Lenz, S.; Ringenberg, M.R.; Frey, W.; Stoll, H.; Rauhut, G.; et al. Exchange Coupling and Single-Molecule Magnetism in Redox-Active Tetraoxolene-Bridged Dilanthanide Complexes. *Chem. Sci.* **2018**, *9*, 1221–1230. [CrossRef] [PubMed]
23. Reed, W.R.; Dunstan, M.A.; Gable, R.W.; Phonsri, W.; Murray, K.S.; Mole, R.A.; Boskovic, C. Tetraoxolene-Bridged Rare-Earth Complexes: A Radical-Bridged Dinuclear Dy Single-Molecule Magnet. *Dalton Trans.* **2019**, *48*, 15635–15645. [CrossRef]
24. Ishikawa, R.; Michiwaki, S.; Noda, T.; Katoh, K.; Yamashita, M.; Kawata, S. Series of Chloranilate-Bridged Dinuclear Lanthanide Complexes: Kramers Systems Showing Field-Induced Slow Magnetic Relaxation. *Magnetochemistry* **2019**, *5*, 30. [CrossRef]
25. Abdus Subhan, M.; Kawahata, R.; Nakata, H.; Fuyuhiro, A.; Tsukuda, T.; Kaizaki, S. Synthesis, Structure and Spectroscopic Properties of Chloranilate-Bridged 4f–4f Dinuclear Complexes: A Comparative Study of the Emission Properties with Cr-Ln Complexes. *Inorg. Chim. Acta* **2004**, *357*, 3139–3146. [CrossRef]
26. Benmansour, S.; López-Martínez, G.; Canet-Ferrer, J.; Gómez-García, C.J. A Family of Lanthanoid Dimers with Nitroanilato Bridges. *Magnetochemistry* **2016**, *2*, 32. [CrossRef]
27. Hernández-Paredes, A.; Cerezo-Navarrete, C.; Gómez García, C.J.; Benmansour, S. Slow Relaxation in Doped Coordination Polymers and Dimers Based on Lanthanoids and Anilato Ligands. *Polyhedron* **2019**, *170*, 476–485. [CrossRef]

28. Benmansour, S.; Pérez-Herráez, I.; Cerezo-Navarrete, C.; López-Martínez, G.; Martínez Hernandez, C.; Gómez-García, C.J. Solvent-Modulation of the Structure and Dimensionality in Lanthanoid-Anilato Coordination Polymers. *Dalton Trans.* **2018**, *47*, 6729–6741. [CrossRef]
29. Llunell, M.; Casanova, D.; Cirera, J.; Bofill, J.M.; Alemany, P.; Alvarez, S.; Pinsky, M.; Avnir, D. SHAPE. 2013. v 2.1. Available online: http://www.ee.ub.edu/index.php?option=com_jdownloads&view=viewcategories&Itemid=529.
30. Pinsky, M.; Avnir, D. Continuous Symmetry Measures. 5. The Classical Polyhedra. *Inorg. Chem.* **1998**, *37*, 5575–5582. [CrossRef]
31. Casanova, D.; Cirera, J.; Llunell, M.; Alemany, P.; Avnir, D.; Alvarez, S. Minimal Distortion Pathways in Polyhedral Rearrangements. *J. Am. Chem. Soc.* **2004**, *126*, 1755–1763. [CrossRef]
32. Alvarez, S. Distortion Pathways of Transition Metal Coordination Polyhedra Induced by Chelating Topology. *Chem. Rev.* **2015**, *115*, 13447–13483. [CrossRef] [PubMed]
33. Casanova, D.; Alemany, P.; Bofill, J.M.; Alvarez, S. Shape and Symmetry of Heptacoordinate Transition-Metal Complexes: Structural Trends. *Chem. Eur. J.* **2003**, *9*, 1281–1295. [CrossRef] [PubMed]
34. Casanova, D.; Llunell, M.; Alemany, P.; Alvarez, S. The Rich Stereochemistry of Eight-Vertex Polyhedra: A Continuous Shape Measures Study. *Chem. Eur. J.* **2005**, *11*, 1479–1494. [CrossRef]
35. Ruiz-Martínez, A.; Casanova, D.; Alvarez, S. Polyhedral Structures with an Odd Number of Vertices: Nine-Coordinate Metal Compounds. *Chem. Eur. J.* **2008**, *14*, 1291–1303. [CrossRef] [PubMed]
36. Ruiz-Martínez, A.; Alvarez, S. Stereochemistry of Compounds with Coordination Number Ten. *Chem. Eur. J.* **2009**, *15*, 7470–7480. [CrossRef] [PubMed]
37. Artizzu, F.; Atzori, M.; Liu, J.; Mara, D.; Van Hecke, K.; Van Deun, R. Solution-Processable Yb/Er 2D-Layered Metallorganic Frameworks with High NIR-Emission Quantum Yields. *J. Mater. Chem. C* **2019**, *7*, 11207–11214. [CrossRef]
38. Sahadevan, S.A.; Monni, N.; Abhervé, A.; Cosquer, G.; Oggianu, M.; Ennas, G.; Yamashita, M.; Avarvari, N.; Mercuri, M.L. Dysprosium Chlorocyanoanilate-Based 2D-Layered Coordination Polymers. *Inorg. Chem.* **2019**, *58*, 13988–13998. [CrossRef]
39. Weiss, A.; Riegler, E.; Robl, C. Polymeric 2,5-Dihydroxy-1,4-Benzoquinone Transition-Metal Complexes $Na_2(H_2O)_{24}[M_2(C_6H_2O_4)_3]$ (M = Mn^{2+}, Cd^{2+}). *Z. Naturforsch. B Chem. Sci.* **1986**, *41*, 1501–1505. [CrossRef]
40. Luo, T.; Liu, Y.; Tsai, H.; Su, C.; Ueng, C.; Lu, K. A Novel Hybrid Supramolecular Network Assembled from Perfect Stacking of an Anionic Inorganic Layer and a Cationic Hydronium-Ion-Mediated Organic Layer. *Eur. J. Inorg. Chem.* **2004**, 4253–4258. [CrossRef]
41. Diaz-Torres, R.; Alvarez, S. Coordinating Ability of Anions and Solvents Towards Transition Metals and Lanthanides. *Dalton Trans.* **2011**, *40*, 10742–10750. [CrossRef]
42. Alvarez, S. Coordinating Ability of Anions, Solvents, Amino Acids and Gases towards Alkaline and Alkaline-Earth Elements, Transition Metals and Lanthanides. *Chem. Eur. J.* **2020**, *26*, 8663. [CrossRef]
43. Nakabayashi, K.; Ohkoshi, S. Poly[hexa-aqua-tris-[m_2-2,5-dihydroxy-1,4-benzoquinonato(2-)] diholmium(III)] Octa-Deca-Hydrate. *Acta Cryst. E* **2010**, *66*, m1300. [CrossRef] [PubMed]
44. Ponjan, N.; Kodchasanthong, K.; Jiajaroen, S.; Chainok, K. Crystal Structure of poly[[hexa-aqua-tris-(m-3,6-di-oxo-cyclo-hexa-1,4-diene-1,4-diolato)dierbium(III)] octa-deca-hydrate]. *Acta Cryst. E* **2019**, *75*, 64–67. [CrossRef] [PubMed]
45. López-Martínez, G. Multifunctionality in Molecular Materials Based on Anilato-Type Ligands. PhD. Thesis, University of Valencia, Valencia, Spain, 2017.
46. Gómez-Claramunt, P.; Benmansour, S.; Hernández-Paredes, A.; Cerezo-Navarrete, C.; Rodríguez-Fernández, C.; Canet-Ferrer, J.; Cantarero, A.; Gómez-García, C.J. Tuning the Structure and Properties of Lanthanoid Coordination Polymers with an Asymmetric Anilato Ligand. *Magnetochemistry* **2018**, *4*, 6.
47. Benmansour, S.; Hernández-Paredes, A.; Gómez-García, C.J. Two-Dimensional Magnetic Coordination Polymers Formed by Lanthanoids and Chlorocyananilato. *Magnetochemistry* **2018**, *4*, 58. [CrossRef]
48. Ashoka Sahadevan, S.; Monni, N.; Abhervé, A.; Marongiu, D.; Sarritzu, V.; Sestu, N.; Saba, M.; Mura, A.; Bongiovanni, G.; Cannas, C.; et al. Nanosheets of Two-Dimensional Neutral Coordination Polymers Based on Near-Infrared-Emitting Lanthanides and a Chlorocyananilate Ligand. *Chem. Mater.* **2018**, *30*, 6575–6586. [CrossRef]
49. Zucchi, G.; Thuery, P.; Ephritikhine, M. CSD Communication. 2012.

50. Benmansour, S.; Pérez-Herráez, I.; López-Martínez, G.; Gómez García, C.J. Solvent-Modulated Structures in Anilato-Based 2D Coordination Polymers. *Polyhedron* **2017**, *135*, 17–25. [CrossRef]
51. Benmansour, S.; Hernández-Paredes, A.; Gómez-García, C.J. Effect of the Lanthanoid-Size on the Structure of a Series of Lanthanoid-Anilato 2-D Lattices. *J. Coord. Chem.* **2018**, *71*, 845–863. [CrossRef]
52. Kharitonov, A.D.; Trofimova, O.Y.; Meshcheryakova, I.N.; Fukin, G.K.; Khrizanforov, M.N.; Budnikova, Y.H.; Bogomyakov, A.S.; Aysin, R.R.; Kovalenko, K.A.; Piskunov, A.V. 2D-metal–organic Coordination Polymers of Lanthanides (La(III), Pr(III) and Nd(III)) with Redox-Active Dioxolene Bridging Ligands. *CrystEngComm* **2020**, *22*, 4675–4679. [CrossRef]
53. Demars, T.; Boltoeva, M.; Vigier, N.; Maynadié, J.; Ravaux, J.; Genre, C.; Meyer, D. From Coordination Polymers to Doped Rare-Earth Oxides. *Eur. J. Inorg. Chem.* **2012**, *2012*, 3875–3884. [CrossRef]
54. Bondaruk, K.; Hua, C. Effect of Counterions on the Formation and Structures of Ce(III) and Er(III) Chloranilate Frameworks. *Cryst. Growth Des.* **2019**, *19*, 3338–3347. [CrossRef]
55. Benmansour, S.; Hernández-Paredes, A.; Mondal, A.; López Martínez, G.; Canet-Ferrer, J.; Konar, S.; Gómez-García, C.J. Slow Relaxation of the Magnetization, Reversible Solvent Exchange and Luminescence in 2D Anilato-Based Frameworks. *Chem. Commun.* **2020**, *56*, 9862–9865. [CrossRef] [PubMed]
56. Ashoka Sahadevan, S.; Monni, N.; Oggianu, M.; Abhervé, A.; Marongiu, D.; Saba, M.; Mura, A.; Bongiovanni, G.; Mameli, V.; Cannas, C.; et al. Heteroleptic NIR-Emitting Yb^{III}/Anilate-Based Neutral Coordination Polymer Nanosheets for Solvent Sensing. *ACS Appl. Nano Mater.* **2020**, *3*, 94–104. [CrossRef]
57. Kingsbury, C.J.; Abrahams, B.F.; Auckett, J.E.; Chevreau, H.; Dharma, A.D.; Duyker, S.; He, Q.; Hua, C.; Hudson, T.A.; Murray, K.S.; et al. Square Grid Metal-Chloranilate Networks as Robust Host Systems for Guest Sorption. *Chem. Eur. J.* **2019**, *25*, 5222–5234. [CrossRef] [PubMed]
58. Hua, C.; Tay, H.M.; He, Q.; Harris, T.D. A Series of Early Lanthanide Chloranilate Frameworks with a Square Grid Topology. *Aust. J. Chem.* **2019**, *72*, 778–785. [CrossRef]
59. Robson, R. A Net-Based Approach to Coordination Polymers. *J. Chem. Soc. Dalton Trans.* **2000**, 3735–3744. [CrossRef]
60. Wang, Y.; Liu, X.; Li, X.; Zhai, F.; Yan, S.; Liu, N.; Chai, Z.; Xu, Y.; Ouyang, X.; Wang, S. Direct Radiation Detection by a Semiconductive Metal-Organic Framework. *J. Am. Chem. Soc.* **2019**, *141*, 8030–8034. [CrossRef]
61. Schweinfurth, D.; Khusniyarov, M.M.; Bubrin, D.; Hohloch, S.; Su, C.; Sarkar, B. Tuning Spin–Spin Coupling in Quinonoid-Bridged Dicopper(II) Complexes through Rational Bridge Variation. *Inorg. Chem.* **2013**, *52*, 10332–10339. [CrossRef]
62. Liddle, S.T.; van Slageren, J. Improving f-Element Single-Molecule Magnets. *Chem. Soc. Rev.* **2015**, *44*, 6655–6669. [CrossRef]
63. Liu, J.L.; Chen, Y.C.; Tong, M.L. Symmetry Strategies for High Performance Lanthanide-Based Single-Molecule Magnets. *Chem. Soc. Rev.* **2018**, *47*, 2431–2453. [CrossRef]
64. Goodwin, C.A.P. Blocking Like it's Hot: A Synthetic Chemists' Path to High-Temperature Lanthanide Single Molecule Magnets. *Dalton Trans.* **2020**, *49*, 14320–14337. [CrossRef] [PubMed]
65. Holmberg, R.J.; Ho, L.T.A.; Ungur, L.; Korobkov, I.; Chibotaru, L.F.; Murugesu, M. Observation of Unusual Slow-Relaxation of the Magnetisation in a Gd-EDTA Chelate. *Dalton Trans.* **2015**, *44*, 20321–20325. [CrossRef] [PubMed]
66. Armelao, L.; Quici, S.; Barigelletti, F.; Accorsi, G.; Bottaro, G. Design of Luminescent Lanthanide Complexes: From Molecules to Highly Efficient Photo-Emitting Materials. *Coord. Chem. Rev.* **2010**, *254*, 487–505. [CrossRef]
67. Rehwoldt, R.E.; Chasen, B.; Li, J. 2-chloro-5-cyano-3,6-dihydroxybenzoquinone, a New Analytical Reagent for the Spectrophotometric Determination of Calcium(II). *Anal. Chem.* **1966**, *38*, 1018–1019. [CrossRef]
68. Szostak, M.M.; Kozankiewicz, B.; Lipinski, J. Low-Temperature Photoluminescence of p-Nitroaniline and o-Methyl-p-Nitroaniline Crystals. *Spectrochim. Acta Part A Mol. Biomol. Spectrosc.* **2007**, *67*, 1412–1416. [CrossRef]
69. Atzori, M.; Artizzu, F.; Marchio, L.; Loche, D.; Caneschi, A.; Serpe, A.; Delano, P.; Avarvari, N.; Mercuri, M.L. Switching-on Luminescence in Anilate-Based Molecular Materials. *Dalton Trans.* **2015**, *44*, 15786–15802. [CrossRef]
70. Boskovic, C.; Hay, M. Lanthanoid Complexes as Molecular Materials: The Redox Approach. *Chem. Eur. J.* **2020**. [CrossRef]